IDENTIFICATION OF NEUROGENIC FATE DETERMINANTS AIMING TO PROLONG CORTICAL NEUROGENESIS

Franziska Vierl

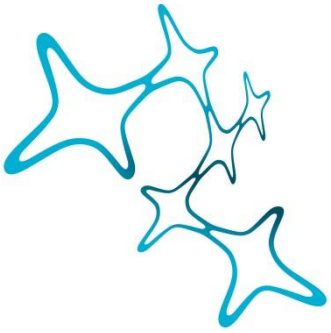

Graduate School of
Systemic Neurosciences

LMU Munich

Dissertation at the Graduate School of Systemic Neurosciences
Ludwig-Maximilians-Universität München

March 2021

Supervisor

Prof. Dr. Magdalena Götz

Institute of Stem Cell Research
Helmholtz Zentrum München

Department of Physiological Genomics
Ludwig-Maximilians-Universität München

First Reviewer: Prof. Dr. Magdalena Götz
Second Reviewer: Prof. Dr. Wolfgang Wurst
External Reviewer: Prof. Dr. Federico Calegari

Date of Submission: 30. March 2021
Date of Defense: 08. September 2021

ACKNOWLEDGEMENTS

First and foremost, I want to thank Magdalena for giving me the opportunity to work on such exciting projects for my thesis. I also want to thank her for her guidance in the last years, for all her feedback, ideas and discussions, her patience and advice, and her support which have brought me this far.

I also want to thank Stefan and my TAC members Wolfgang and Gunnar for their co-supervision and their advice on my projects, and my graduate schools GSN and HELENA for their support.

There are several lab members whose invaluable help was essential for the success of my work. Pawel, without whom my sequencing data would just be a string of numbers; Chris, who masterminded the design of the piggyBac delivery system and gRNAs; Nancy, my student, who worked with great patience and effort on establishing and testing these systems – a big and well-deserved thanks to every one! I also want to thank Alessandro and Tjaša for teaching me the art of preparing RNA and ATAC libraries, and Maxi for his help with mNPC cultures.

My heartfelt thanks also go out to all current and former members of the embryo lab – Sven, Miriam, Kalina, Germán, Adam, Giulia, Florencia and Fatma – who not only have been wonderful office mates and great to work and collaborate with, but whose ideas and discussions inspired me daily. I learned a lot from each and every one of them.

Of course, no lab work would be possible without our wonderful technicians. Here especially I want to thank Andrea for her amazing help in establishing the FACS protocol and with so many other things; Edina, Flo and Ines for their help and advice in cloning; and Gabi for her great help with cryosectioning. A big thank you also to Tatiana and Manja for their support with everything day-to-day, and Detlef and Gül for their help in genotyping mice.

I also thank the staff of both our animal facilities, Dani, Nici and Benny. My greatest thanks go out to Anja, whose wonderful management of our enormous plug mating colony has made all this work much easier, or even possible.

I also want to thank Judith for her help in all things animal license related, and Elsa for her wonderful and very patient support in all administrative matters.

I want to also thank all the current and former lab members I did not mention by name for making the work on this thesis an enjoyable one. I really appreciate the collaborative and supportive atmosphere of our group, and each and every one has surely helped me along the way.

Of course I would not be where I am without the support of my family. I thank my parents, sisters, grandparents, and everybody else for their encouragement and support. I want to especially thank my late grandmother, whose lifelong passion for learning and exploring influenced me greatly, and who I like to think would have been very proud of me now.

And last, but certainly not least, I want to thank my wonderful husband Nico for his support, patience and encouragement and for just being an amazing person – you really are the best, and I could have done none of this without you. Thank you for being by my side.

INDEX

1 ABSTRACT

During neocortical development, neural stem cells undergo several fate switches necessary for a proper sequential progression through a proliferative, neurogenic and finally gliogenic phase. While some of the fate determining factors have already been examined, others are poorly described, and many may not have been identified as such yet at all. In this thesis, I propose a role of the NuRD complex subunit MTA3 in cortical neurogenesis similar to that reported of other NuRD subunits, in which depletion during neurogenic stages leads to premature differentiation or impaired migration. Furthermore, I applied a genome-wide approach, in which I analyzed the transcriptome of different telencephalic regions, developmental time points and cell types in the murine embryonic brain, to identify key fate determinants of neurogenesis. I found that chromatin remodelers likely play a role in maintaining plasticity, and maintenance of neurogenesis is determined by region-specific gene expression. In evaluating the piggyBac transposon system for genomic integration of expression constructs in mouse neurogenic stem cells *in vivo*, I uncovered a phenotype of progenitor cell ectopia and cortical folding, reminiscent of basal progenitor amplification in gyrencephalic species, which is likely elicited by transposition itself. Finally, I evaluated the concurrent activation of several neurogenic determinant candidates into early gliogenic stages, and found a possible effect of prolonging neocortical neurogenesis by the simultaneous activation of 15 genes, in which the proportion of cells in the ventricular zone, as well as their expression of stem cell and progenitor markers, were increased.

2 INTRODUCTION

The brain is quite possibly the most complex organ in most organisms, and this holds especially true for mammalian and human systems with their plethora of different cell types, regional and temporal patterning, and an unfathomable amount of connections between those. Here, the overwhelming majority of brain development takes place before or shortly after birth, with very little neurons still being generated in the adult brain (see Chapter 2.2).

It is thus not surprising that neurons lost due to disease or injury are not replaced by endogenous means. Some strategies are being developed or are already being applied in clinical practice, such as the transplantation of fetal allografts, or neurons and stem cells derived from embryonic or induced pluripotent stem cells. One of the most promising approaches may to be to utilize and modify endogenous sources, either recruiting the few neurons produced in the adult brain to the desired target site, or reprogramming local glial cells to the desired neuronal subtype (Barker et al. 2018; Grade and Götz 2017).

Along this line, the establishment of an adult neurogenic niche in the cerebral cortex would be a promising approach to facilitate replacement of lost neurons in this otherwise postmitotic area. However, to efficiently employ strategies targeting the endogenous system by replicating aspects of developmental neurogenesis, it is imperative to understand the initial neurogenic process, its progression and eventual termination.

2.1 DEVELOPMENT OF THE EMBRYONIC CORTEX IN MOUSE AND HUMAN

Although the term “stem cell” is difficult to define, usually it describes a cell that has the capacity to (indefinitely) proliferate without changes to its cellular identity, thus maintaining self-renewal, but at the same time is able to produce more specialized daughter cells that shift their cell identity in a differentiation process (Götz et al. 2015).

During development, all cell types of the brain – neurons, macroglia (astrocytes and oligodendrocytes) and adult neural stem cells – are created by the progeny of a single type

of stem cells, the neuroepithelial cells (NEC) (Merkle et al. 2004). This is achieved by several stages of progenitors and different fate switches, which will be elucidated in the following chapters.

2.1.1 Neuroepithelial cells: initial expansion

The entire brain is derived from the neural tube, which divides into three vesicles shortly after its closure. These develop into the forebrain, midbrain and hindbrain, and the forebrain vesicle further divides into the telencephalon and diencephalon to generate distinct brain regions. The cerebral cortex is mainly derived from the dorsal telencephalon, with the addition of interneurons migrating into the cortex from the ventral telencephalon-derived ganglionic eminences (GE) (Agirman et al. 2017).

The first cell type to emerge in the developing brain, and at the same time the cell type from which all neurons, macroglia and ependymal cells will derive, are the NEC. They emerge in the murine brain around embryonic day nine (E9) and rapidly increase their abundance by proliferating for a defined number of approximately two to four symmetrical, self-renewing divisions (Gao et al. 2014), generating new NEC as both daughter cells in a lateral expansion (Agirman et al. 2017; Namba and Huttner 2017; Llorca and Marín 2021).

NEC show epithelial features and have a distinct apical-basal polarity, a basal process contacting the pial surface and an apical endfoot that contacts the lumen of the ventricle, and extends a non-motile primary cilium into the cerebrospinal fluid (CSF). During mitosis, the NEC undergo interkinetic nuclear migration (INM), in which the cell body containing the nucleus moves along the entire apical-basal axis. Cells reside more basally during S phase, then migrate to the apical membrane during G1, divide at the ventricle and return to the basal position during G2. This different localization of cell somata is the cause for the pseudostratified appearance of the neuroepithelium (Namba and Huttner 2017; Agirman et al. 2017; Uzquiano et al. 2018).

One reason for this behavior could be spatial restrictions of the apical membrane influencing the division symmetry, as contact with only the endfoot occupies a much smaller area than the cell body and permits increased NEC density. Indeed, when INM is inhibited, NEC delaminate during mitosis (Namba and Huttner 2017).

After the initial amplifications, between E10 and E12, NEC slow down their cell cycle by increasing the duration of G1 phase, and start to divide asymmetrically, generating a neuronal cell in addition to the self-renewed NEC. Concurrently, they start to produce (apical) radial glial cells ([a]RGC) in symmetrical or asymmetrical divisions (Mukhtar and Taylor 2018).

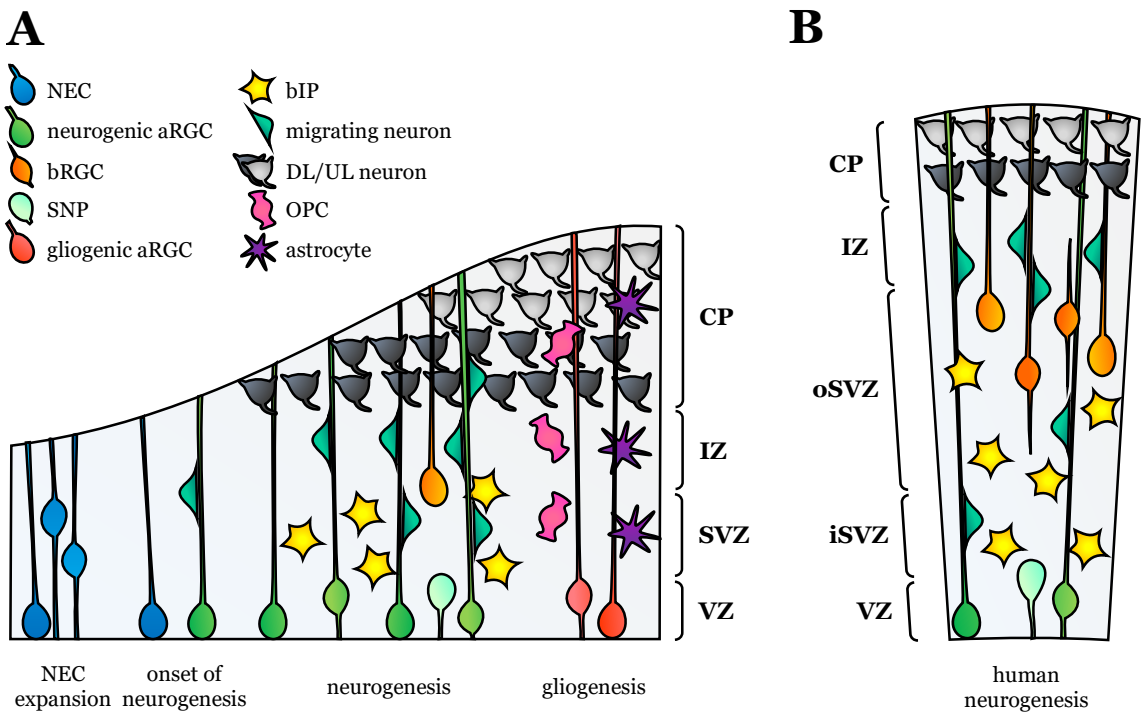

Figure 1: Cortical neurogenesis and cellular subtypes in mouse and human

A. *Progenitor types in murine embryonic corticogenesis from initial expansion of NEC to the onset of gliogenesis.* ***B.*** *Basal progenitor subtypes are much more abundant in gyrencephalic species, such as human, forming the oSVZ. (NEC: neuroepithelial cell, aRGC: apical radial glial cell, bRGC: basal radial glial cell, SNP: short neural precursor, bIP: basal intermediate progenitor, DL: deep layer, UL: upper layer, OPC: oligodendrocyte progenitor cell; VZ: ventricular zone, SVZ/iSVZ/oSVZ: inner/outer subventricular zone, IZ: intermediate zone, CP: cortical plate.)*

2.1.2 Radial glial cells: the importance of (a)symmetry

After their initial identification as stem cells (Malatesta et al. 2000), RGC are now known to be the predominant type of neuronal progenitor cell in the developing cerebral cortex, creating both glutamatergic projection neurons as well as macroglia (Namba and Huttner 2017; Uzquiano et al. 2018).

These cells are similar to NEC in that they maintain apical-basal polarity, with a basal process extended towards the basal lamina/pial surface, and the prominin-expressing primary cilium at the apical surface contacting the CSF to convey signaling by soluble morphogens (see also Chapter 2.3.1), such as fibroblast growth factor (FGF), insulin-like growth factor (IGF), sonic hedgehog (Shh), retinoic acid, bone morphogenic protein (BMP) and Wingless-related integration site proteins (Wnt) (Agirman et al. 2017).

RGC continue to undergo INM. In contrast to NECs, however, the INM does not occur along the entire apical-basal extension, but is limited to a short distance basal from the apical endfoot. The cell bodies thus remain in a defined zone adjacent to the ventricle and apical membrane, defining the ventricular zone (VZ). In addition to neuroepithelial markers like NESTIN, RGC acquire the expression of astroglial genes, such as brain lipid-binding protein (BLBP), sodium-dependent glutamate/aspartate transporter (GLAST), glial fibrillary acidic protein (GFAP) and S 100 calcium binding protein B (S100β) (Namba and Huttner 2017; Uzquiano et al. 2018; Llorca and Marín 2021). A characteristic marker of neurogenic cortical aRGC is paired box 6 (PAX6) (Englund et al. 2005; Götz et al. 1998).

Despite a contribution from NEC-derived neurons, the vast majority of neuronal cells in the cortex is generated directly or indirectly by RGC. These cells can, in addition to a self-renewing, symmetrical division, and the symmetrical or asymmetrical generation of neurons, divide symmetrically or asymmetrically to produce another RGC and an basal intermediate progenitor cell (bIP) or two bIP. Similar to the NEC, proliferative divisions have a shorter G1 phase than neurogenic divisions (Uzquiano et al. 2018).

The resulting cell types after a division of the aRGC are decided by the orientation of the mitotic spindle, which defines the cleavage plane. One determinant is the inheritance of the basal process, as local translation of cyclin D2 at the basal endfoot promotes proliferative capacity. In general, upon asymmetric inheritance of the basal process, the receiving daughter cell retains proliferative capacity (Tsunekawa et al. 2012).

In early neurogenesis, the cleavage plane is often perpendicular to the apical surface, leading to the inheritance of apical features by both daughter cells. While this was initially thought to represent symmetric self-renewing divisions, it has now been shown that progeny which inherited apical features might still lose aRGC identity (Uzquiano et al.

2018). Later in development, the cleavage plane tends to be more oblique or even horizontal, leading to asymmetric division by unequal inheritance of fate determinants like proteins and signaling molecules (Mukhtar and Taylor 2018; Uzquiano et al. 2018). Both the inheritance of apical and basal epithelial features are thus defining for the progeny of dividing aRGC (Uzquiano et al. 2018).

2.1.3 Basal progenitors: the bulk of neurogenesis, and a facilitator of evolutionary cortical expansion

While neuronal cells can directly be generated by NEC as well as aRGC, the majority of cortical neurons is generated over the course of the neurogenic period by aRGC through indirect neurogenesis via different kinds of basal progenitors, which is especially important in gyrified species such as human (Uzquiano et al. 2018; Namba and Huttner 2017).

In mice, the predominant type of basal progenitor, and the main contributor to the neurogenic output, is the bIP (Namba and Huttner 2017; Uzquiano et al. 2018; Hevner 2019). These cells lose PAX6 expression, but acquire T-box brain protein 2 (TBR2, also known as Eomesodermin [EOMES]) and delaminate after mitosis, after which they are located more basally than the VZ, in the subventricular zone (SVZ), where they establish a second zone of mitosis and neurogenesis (Englund et al. 2005; Haubensak et al. 2004; Miyata et al. 2004; Noctor et al. 2004). When moving to the SVZ, bIP lose the bipolarity and exhibit a multipolar morphology with dynamically extending and retracting processes, that however yield little to no net migration (Kriegstein and Alvarez-Buylla 2009; Hevner 2019).

There are several subtypes of bIP: most abundant in mice are the neurogenic bIP (nbIP), which are multipolar and usually, in rare cases preceded by one self-renewing division, perform one consumptive division, generating two neurons and thus increasing the neuronal output for each aRGC mitosis (Namba and Huttner 2017; Uzquiano et al. 2018). This increase in neuronal output is important, as aRGC are limited to six to eight divisions in the mouse brain (Gao et al. 2014).

While the general cortical layout and embryonic cell types present in mouse are conserved in the human embryo (Figure 1), the requirement for neuronal output is greatly

increased, as the human neocortex contains more than thousand-fold the number of neurons than the murine one due to the increase of pial surface. To achieve this level of neurogenesis, not only is the starting pool of aRGC increased and the neurogenic period considerably longer, but the indirect neurogenesis via intermediate progenitors is emphasized compared to mice (Namba and Huttner 2017; Agirman et al. 2017).

One such specialized progenitor type of the gyrified brain, which is rare in the murine brain, are the proliferating bIP (pbIP), which divide several times to increase the progenitor pool and, corresponding to this proliferation potential, some retain PAX6 expression along with TBR2 (Namba and Huttner 2017).

However, the most characteristic feature for the expansion of the gyrified, compared to the lissencephalic, brain are the basal RGC (bRGC), which are rare in mice, but abundant in human embryonic cortex. These cells derive from aRGC during early corticogenesis by a shift to more oblique divisions (Uzquiano et al. 2018), but lose the apical endfoot – and thus the lumenal contact and prominin expression – and only maintain their process and connection towards the basal lamina. Due to the loss of apical connection, they move into the SVZ, which is greatly expanded and can be divided into the inner (iSVZ) and outer SVZ (oSVZ) in gyrencephalic species (Mukhtar and Taylor 2018; Namba and Huttner 2017; Uzquiano et al. 2018).

While pbIP are found both in the iSVZ and oSVZ, bRGC populate and expand especially the oSVZ, making it the most proliferative neurogenic zone in primate and human cortex. They maintain the basal process during mitosis, when they undergo mitotic somal translocation, a rapid movement of the cell body towards the apical or basal surface that is assumed to aid in radial expansion of the oSVZ (Namba and Huttner 2017; Uzquiano et al. 2018).

Both in mouse and in human, bRGC retain aRGC characteristics, such as PAX6 expression. However, murine bRGC are transcriptionally similar to bIP, often express TBR2 and mainly undergo one exhaustive neurogenic division (Namba and Huttner 2017; Uzquiano et al. 2018). In contrast, human bRGC more resemble aRGC (Namba and Huttner 2017) and undergo mostly asymmetrical self-renewing divisions, generating both neurons and bIP, to dramatically increase the progenitor pool and neurogenic output (Mukhtar and Taylor 2018; Uzquiano et al. 2018; Llorca and Marín 2021).

However, the populations of basal progenitor types in humans are complex and the definitions quite blurred: bRGC can assume many different morphologies, with or without apical and basal processes (Figure 1B), and a fraction of them also express TBR2 – indeed, all basal progenitor types (bIP and bRGC) can convert into each other, and all are able to generate neurons (Namba and Huttner 2017).

An intermediate between apical and basal progenitor cell types is the short neural precursor cell (SNP), which is located in the VZ and maintains an apical endfoot and prominin$^+$ primary cilium, but has lost the basal connection. These cells are similar to aRGC in that they express PAX6, and undergo INM, but transcriptionally different from both aRGC in that they do not express glial markers, and bIP as they do not express TBR2. These progenitors undergo one more symmetrical consumptive division into two neurons (Agirman et al. 2017; Namba and Huttner 2017). A molecularly less differentiated subtype of SNP are TBR2$^+$ pin-like bIP, that contact the apical surface but delaminate into multipolar bIP without an additional division (Hevner 2019).

2.1.4 Migration of locally or distally produced cortical neurons: building cortical complexity

When undergoing a consumptive division, bIP lose TBR2 expression and the newborn neurons start expressing TBR1 instead (Englund et al. 2005). Newly generated projection neurons that are born in the VZ or SVZ migrate through the intermediate zone (IZ) towards the cortical plate (CP), using the basal processes of the aRGC as a migration scaffold (Llorca and Marín 2021).

Although neurons of all layers can be generated by bIP, the production of neuronal subtypes is region-specific and follows a temporal pattern in a stochastic and somewhat heterogeneous manner, regulated by external (CSF) and internal signaling (Hevner 2019; Llorca and Marín 2021). Successive waves of neurogenesis create the six functionally specialized cortical layers in an inside-out progression: Deep-layer (DL) neurons are generated first (E11 to E14), and upper layer (UL) neurons are added later (E14 to E17), migrating through established layers of earlier-born neurons (Agirman et al. 2017; Uzquiano et al. 2018; Llorca and Marín 2021). Cells derived directly from apical or basal RGC maintain their polarity, while neurons generated from bIP have to establish it *de*

novo (Namba and Huttner 2017). Thus, late-born neurons first have to reacquire a bipolar shape and attach to the basal process of aRGC to commence migration to the UL (Agirman et al. 2017).

Cortical interneurons are contributed by the ventral telencephalon-derived ganglionic eminences (GE) (Figure 2A). The medial GE (MGE) and caudal GE (CGE) produce cortical GABAergic interneurons, which migrate first tangentially towards the cortex, and then radially infiltrate the cortical layers, where they integrate, with clonally related cells from the MGE forming spatially organized clusters (Agirman et al. 2017; Sultan et al. 2013). The lateral GE (LGE) contributes olfactory bulb (OB) neurons of several subtypes resulting from distinct progenitor populations, which migrate along the rostral migratory stream (RMS) towards the OB (Stenman et al. 2003). They are generated by aRGC via subapical progenitors (SAP), which resemble SNP, but are capable of rapid self-renewal and generating different types of progenitors (Pilz et al. 2013).

2.1.5 Gliogenesis: adding a scaffold to the brain

The neurogenic period in murine cortex lasts from about E10 to E18 and is then superseded by gliogenesis, the production of macroglia and their progenitors, which continues to postnatal stages, when the cortical SVZ contains mostly glial progenitors (Agirman et al. 2017; Götz et al. 2015). Interestingly, an inside-out temporal layering similar to that of neurons has also been suggested for macroglia genesis (Kriegstein and Alvarez-Buylla 2009).

As were the neurons, the glial lineage is also generated by the RGC. However, the RGC population is, in contrast to NEC, already restricted in their fate: of the RGC pool at the onset of neurogenesis, most cells will produce only one lineage overall, or a combination of neuronal and one other macroglial lineage, i.e. neurons and astrocytes or neurons and oligodendrocytes. Indeed, most glial cells stem from specialized RGC that were not involved in neurogenesis, and only about one in six cells of the RGC pool goes on to generate glial cells and progenitors (Gao et al. 2014). It has been suggested that the remaining RGCs either undergo a terminal consumptive neurogenic division (Gao et al. 2014) or lose their apical attachment and differentiate into astrocytes (Kriegstein and Alvarez-Buylla 2009).

The first macroglial cells to appear are oligodendrocytes derived from the ventral telencephalon, which migrate towards the cortex and arrive there around E16, although whether these survive until adulthood is unclear. Around E18, oligodendrocytes are produced from empty spiracles homeobox 1 (EMX1)-expressing cells, indicating their genesis from the dorsal telencephalon (Kriegstein and Alvarez-Buylla 2009). The production of oligodendrocyte progenitor cells (OPC), oligodendrocytes and NG2 glia continues and the cells are dispersed throughout the cortex. NG2 glia remain as a, possibly initially quiescent, resident glial population that can self-renew and generate OPC and myelinating oligodendrocytes, and at postnatal stages also astrocytes (Nishiyama et al. 2009; Dimou and Gallo 2015; Kriegstein and Alvarez-Buylla 2009).

The astrocytes generated from gliogenic RGC disperse throughout the cortex in an evenly spaced manner, with local proliferation by symmetrical division in the postnatal cortex (Ge et al. 2012; García-Marqués and López-Mascaraque 2013; Götz et al. 2015; Kriegstein and Alvarez-Buylla 2009).

Another cell type that appears around birth are the multiciliated ependymal cells. While most are born from RGC at embryonic stages, ciliation only begins around birth. These cells are postmitotic and do not possess any remaining stem cell potential (Spassky et al. 2005).

2.2 ADULT NEUROGENESIS (AND GLIOGENESIS) IN MICE AND HUMANS

While most of neurogenesis comes to an end shortly before birth in mice, there are some niches in the adult mouse brain that retain neurogenic potential (Figure 2). These include the subependymal zone of the lateral ventricle (SEZ), which derives from the LGE, and the secondary niches of the hippocampal dentate gyrus (DG) and the hypothalamus (Ninkovic and Götz 2013; Falk and Götz 2017; Obernier and Alvarez-Buylla 2019; Jurkowski et al. 2020).

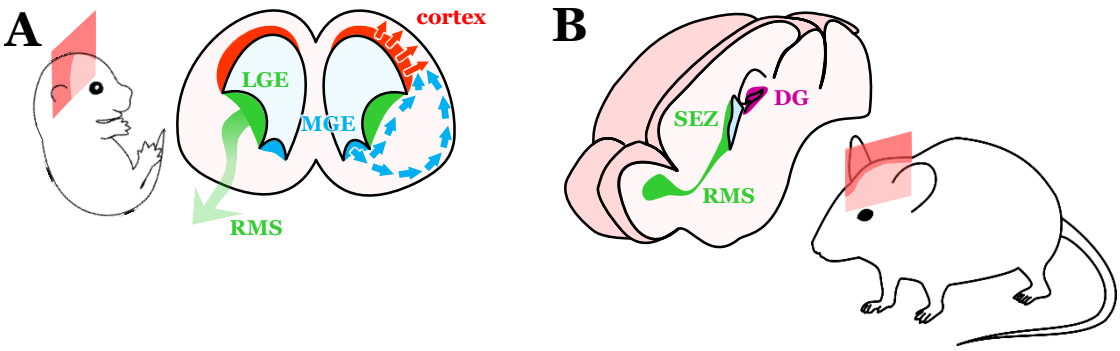

Figure 2: Comparison of neurogenic niches in embryonic and adult mouse brain

A. *In embryonic development, projection neurons are generated in the cortex and migrate radially, while interneurons are generated in the MGE/LGE and migrate tangentially to the cortex or along the RMS to the OB, respectively.* ***B.*** *The best-characterized adult neurogenic niches in the adult mouse brain are the hippocampal DG, a secondary niche, and the SEZ, which is derived from the embryonic LGE. (MGE/LGE: medial/lateral ganglionic eminence, RMS: rostral migratory stream, OB: olfactory bulb, SEZ: subependymal zone, DG: dentate gyrus.)*

As with all other cells, the adult neural stem cells (aNSC) in the SEZ are generated by the RGC (Merkle et al. 2004), and aNSC retain radial glia-like characteristics with long-term self-renewal capacity and the generation of transit-amplifying progenitors (TAP) before neuronal differentiation (Ninkovic and Götz 2013). The cells that are to become the aNSC of the SEZ are set aside from the LGE RGC pool during embryonic neurogenesis, between E13 and E15 (Furutachi et al. 2015; Fuentealba et al. 2015; Falk et al. 2017). A temporally strictly regulated alteration of the cleavage plane, regulated by inscuteable homolog (INSC) and LGN, defines the number of emerging aNSC by influencing the expression of p57 (Falk et al. 2017), which slow down the cell cycle to become resting aNSC (Furutachi et al. 2015). These cells retain their RGC morphology and apical endfoot with prominin$^+$ primary cilium, with the basal process often connected to a blood vessel (Mirzadeh et al.

2008; Beckervordersandforth et al. 2010; Obernier and Alvarez-Buylla 2019). The apical endfoot is surrounded by ependymal cells in a pinwheel-like structure, which displace the cell body away from the VZ into the SVZ, or SEZ (Mirzadeh et al. 2008).

Interestingly, while the correct orientation of the ependymal cells is not required for the generation of aNSC – which seems to be regulated by cell-intrinsic mechanisms – it is crucial for the proper neurogenesis and neuroblast migration (Paez-Gonzalez et al. 2011). Generally, there is a notable influence of the (glial) niche population on the aNSC: niche astrocytes regulate SEZ neurogenesis via Wnt and BMP signaling, and neurogenesis is niche-dependent (Falk and Götz 2017). This discrepancy of glial influence may arise because at the developmental stage when aNSC are set aside, the RGC are the dominating glial cell population, whereas in the niche of the adult brain, they are surrounded by other glial cell types such as astrocytes, ependymal cells, oligodendrocytes/OPC and microglia (Falk and Götz 2017).

Upon signaling by niche astrocytes or factors such as NOGGIN/BMP in the CSF, the aNSC produce first TAP, which divide two or three times to produce neuroblasts, which again divide one or twice and then migrate along the same RMS as their embryonic LGE counterparts (Falk and Götz 2017; Ninkovic and Götz 2013; Carleton et al. 2003; Jurkowski et al. 2020). The newborn neurons differentiate along the RMS and, once arrived in the OB, mature into granule cells (GC) and integrate into the existing neuronal network (Carleton et al. 2003; Obernier and Alvarez-Buylla 2019). Notably, different subtypes of OB neurons (such as GC or periglomerular cells) are generated by different subsets of aNSC, whose lineages already separate in embryonic stages (Merkle et al. 2007; Fuentealba et al. 2015). In addition, neuronal output subtypes change with age from embryonic over postnatal to adult stages (Weinandy et al. 2011).

A secondary neuronal niche is the dentate gyrus of the hippocampus. Receiving cortical sensory input from the entorhinal cortex, but almost no output, it is the first step in the formation of episodic memory. It consists of three layers, a molecular layer containing mainly dendrites of GC, the densely-packed granule cell layer and a polymorphic layer with mossy cells (Amaral et al. 2007).

During embryonic neurogenesis, the DG is populated by a single precursor population expressing HOP homeobox (HOPX) in the dentate neuroepithelium, which travel to the primitive embryonic DG. During the early postnatal period, they adopt aRGC-like

(aRGL) properties and reside in the subgranular zone (SGZ) between the hilus and the granule cell layer (Berg et al. 2019). The aRGL exist in two quiescent states, regulated by achaete-scute family bHLH transcription factor 1 (Ascl1) – dormant, which have never divided, and resting, which have undergone neurogenic division but returned to quiescence, and will preferentially re-activate – to ensure the maintenance of an adequate pool until adulthood (Harris et al. 2021).

When the aRGL cells start to divide, they make a commitment to either neuronal fate or self-renewal, and then undergo the same differentiation program as in embryonic development: from a RGL to nbIP, to neuroblasts, and then immature GC neurons that settle in the GC layer and mature (Hochgerner et al. 2018; Jurkowski et al. 2020). This program can be viewed as a continuous process from embryonic development (Berg et al. 2019; Hochgerner et al. 2018). As in the SEZ, the residing niche astrocytes can regulate neurogenesis in the SGZ via specific signaling molecules (Barkho et al. 2006). Interestingly, these niche astrocytes can also be the progeny of aRGL cell, as they can divide symmetrically or asymmetrically and, next to self-renewal, generate astrocytes and neurons, potentially in the same clone (Bonaguidi et al. 2011).

While these adult neurogenic niches are still active in the postnatal, fully developed brain, in fact, the most abundant cycling cell type there are a pool of proliferating NG2 glia dispersed throughout the parenchyma. These continue to produce cells of the oligodendrocyte lineage, such as myelinating oligodendrocytes in the white matter and NG2 glia in the grey matter (Ninkovic and Götz 2013; Geha et al. 2010).

Adult hippocampal neurogenesis has been claimed in humans, with an annual turnover rate of 1.75 % and comparable between middle-aged human and mice (Spalding et al. 2013). It has been suggested that, in healthy humans, this is present throughout life even in very old age (Eriksson et al. 1998; Moreno-Jiménez et al. 2019). However, these claims have recently been disputed, with newer studies claiming DG neurogenesis to be present only in children and rapidly declining with age, and pointing out the different developmental timing between peri- and postnatal DG formation in mouse compared to embryonic completion of DG formation in human (Snyder 2019; Sorrells et al. 2018). Whether these varying findings are due to technical limitations, such as poor choice of cell type markers, or are difficult to interpret due to species differences – a “postmitotic latency phase” has been suggested for human neuroblasts – remains to be elucidated (Kempermann et al. 2018).

Additionally, another region of neurogenesis in adult humans has been reported, with newborn interneurons integrating in the striatum (Ernst et al. 2014). Whether these cells originate from the neighboring SEZ is not clearly established (Jurkowski et al. 2020; Falk and Götz 2017). SEZ neurogenesis is also active for some time in the primate postnatal brain, but strikingly, the nature and target region of migrating neuroblasts is modified compared to mice. A chain migration along the RMS is not observed, as neuroblasts are too sparse, and subtype composition of OB neurons is altered. However, for a few weeks after birth, newborn neurons of SEZ origin are found in the frontal lobe and prefrontal cortex – a feature that is relatively frequent in humans, moderately observed in non-human primates, and very limited in rodents (Akter et al. 2020). This emphasizes the evolutionary specialization of adult neurogenesis, which has to be taken into account for regenerative therapeutic strategies.

2.3 DETERMINANTS OF NEUROGENIC FATE SWITCHES

Over the progression of neurogenesis, several fate switches occur on the population level: First the switch from proliferation and expansion of NEC to the start of neurogenesis by RGC, followed by the temporal progression through the generation of different neuronal and progenitor subtypes. Subsequently, the RGC must progress to a gliogenic fate, and finally lose their stem cell identity. In addition, the fate of individual cells, such as the choice to differentiate, or the entrance into quiescence for aNSC, have to be regulated. Some of the most important known factors regulating these switches are described in the following chapters.

2.3.1 Soluble morphogens in CSF regulate populations

Several morphogens are present in the CSF of the developing brain and change along with the temporal progression of corticogenesis, eliciting different signaling cascades and pathways (Agirman et al. 2017). An interesting example is Wnt signaling, which has different functions during different stages. Acting by a cascade that stabilizes β-catenin to activate target genes, it is involved in patterning of the telencephalon during neurogenesis. However, it also regulates the balance between proliferation and differentiation, in early stages promoting proliferation of NEC and RGC by decreasing cell-cycle exit, later favoring neurogenic differentiation (by inhibiting *Notch* via upregulation of *N-Myc*, see also Chapter 2.3.3), and finally promoting the generation of OPC and oligodendrocytes from gliogenic RGC (Agirman et al. 2017; Mukhtar and Taylor 2018; Uzquiano et al. 2018).

An example of region-specific functionality is *Shh*, which in dorsal telencephalon promotes self-renewal of RGC, but contributes to the generation of interneurons and oligodendrocytes in the ventral telencephalon (Agirman et al. 2017). FGF signaling mainly regulates patterning, but by activating *Hes1* in a synergy with *Notch* (see also Chapter 2.3.3) can also promote self-renewal and stemness of RGC (Agirman et al. 2017; Mukhtar and Taylor 2018).

Finally, BMP signaling during the neurogenic phase favors neuronal differentiation of RGC, and regulates postmitotic processes such as the transition from multipolar bIP

morphology to bipolar morphology of migrating neurons. In gliogenesis, it inhibits neuronal differentiation and promotes glial fate, specifically favoring the astroglial fate over the generation of OPC (Agirman et al. 2017; Mukhtar and Taylor 2018).

2.3.2 Cell cycle duration determines proliferative potential

Cell cycle length is crucial for the progression of neurogenesis. Reduction of G1 duration by cyclin D promotes the expansion of neural stem cells, whereas NEC lengthen their G1 phase upon the onset of neurogenesis, which has been suggested to be causal for differentiation capacity by allowing differentiation factors enough time to exert their function (Ohtsuka and Kageyama 2019). Indeed, as the stem cells switch from proliferative, to asymmetrical, to consumptive divisions over the course of development, the cell cycle is progressively slowed (Uzquiano et al. 2018; Taverna et al. 2014).

In contrast, committed progenitors shorten their S phase and reduce their time spent on DNA damage examination and repair, which may be an explanation for the high rate of somatic mutations observed in neurons (Arai et al. 2011).

2.3.3 Notch signaling/bHLH transcription factors decide differentiation fate on a cellular level

To regulate the fate decision between proliferation and differentiation in individual cells, the *Notch* pathway acts via cell contacts on a local level. *Notch* receptors are expressed on the surface of aRGC, and binding of delta-like canonical Notch ligand 1 (*Dll1*) elicits a signaling cascade that activates the transcription of several genes, among them the basic helix-loop-helix (bHLH) transcription factor (TF) family hairy and enhancer of Split (*Hes*). In turn, *Hes1* and *Hes5* genes repress the transcription of proneural factors, thereby maintaining proliferation and stemness (Agirman et al. 2017; Mukhtar and Taylor 2018).

Regulation of differentiation is achieved by an oscillating expression of *Hes1*, which upon expression represses its own promoter, creating a negative feedback loop of about 2 hours duration. Differentiation factors repressed by *Hes1* include proneural *Ascl1* and

neurogenin (*Neurog*) 2, as well as proglial oligodendrocyte transcription factor 2 (*Olig2*), all bHLH TF as well, which are also oscillating due to the periodical repression. Upon differentiation to neurons, *Hes1* expression is lost, and sustained expression and activity of proneural factors allows the transcription of neuronal genes. In turn, *Dll1* expression is also upregulated, thus signaling the neighboring cell to maintain proliferation, avoiding precocious differentiation of all progeny. This lateral inhibition is also present before the onset of neurogenesis, when an oscillation of *Dll1* expression in aRGC promotes proliferation of the stem cell pool. During glial differentiation, however, both *Hes1* and *Olig2* expression are sustained, thus leading to an association of oscillating gene expression with stemness maintenance, and sustained expression with differentiation (Kageyama et al. 2019).

While both *Neurog1* and *Neurog2* have long been viewed as partly redundant proneural bHLH factors, a function of *Neurog1* as negative regulator of neuronal differentiation has been proposed. In this model, *Neurog1* activates *Hes5* and *Dll1* expression, and *Neurog1* and *Neurog2* exert cross-repressive effects by heterodimerization, preventing the activation of neuronal genes and promoting proliferation. Reduction of *Neurog1* expression over the progression of development would then allow more and more efficient differentiation initiation by *Neurog2* (Han et al. 2018). Thus, the canonical role of *Neurog1* as strictly proneural is challenged, revealing another layer of complexity to bHLH-mediated regulation of differentiation.

2.3.4 Epigenetic determinants of the neurogenic-to-gliogenic switch

Few mechanisms have been elucidated so far that regulate the fate switch from neurogenic to gliogenic aRGC, but chromatin remodeling seems to be essential for this restriction of fate potential.

It has been reported that the Polycomb repressor complex (PrC) represses *Neurog1* in late-stage embryonic radial glia, putatively leading to loss of neurogenic potential. Correspondingly, deletion of PrC subunit RING finger protein 1B (*Ring1b*) during neurogenesis extended the neurogenic period of RGC and suppressed the switch to astrogenic fate. However, neurons generated by this prolonged neurogenesis failed to integrate and un-

derwent apoptosis. The same mechanism was suggested for Polycomb repressor complex 2 (PRC2), in which deletion of subunits enhancer of zeste 2 (*Ezh2*) or embryonic ectoderm development protein (*Eed*) had the same effect (Hirabayashi et al. 2009). However, another study found the opposite phenotype, in which deletion of *Ezh2* before the onset of neurogenesis led to its acceleration and an early onset of gliogenesis by upregulation of gene expression due to the removal of histone methylation marks. The suggested explanation would be that impairment of PrC/PRC2 generally leads to dysregulation of the balance between self-renewal and differentiation, with the downstream effects being secondary and dependent on timing of deletion (Pereira et al. 2010).

The genome-wide regulation of the chromatin state has also been suggested to be related to the fate plasticity of RGC, with the chromatin accessibility gradually decreasing around the loci of neurogenic and neuronal genes concurrently with the progression of development. This seemed to be directly regulated by the high mobility group A (HMGA) chromatin remodelers HMGA1/HMGA2, and their deletion again led to a prolongation of neurogenic fate potential (Kishi et al. 2012). A link between this chromatin modification and *Notch* signaling (see Chapter 2.3.3) has been revealed to be the repression of *Hmga1*/*Hmga2* expression by *Hes5*, which is expressed in an oscillating manner in RGC, increasing in levels from the onset of neurogenesis to its end. Accordingly, the levels of *Hmga1*/*Hmga2* decrease over time, progressively restricting the fate and plasticity of the RGC. This interaction, and the resulting chromatin state, seem to be important for the proper execution of the sequential switches from proliferation to neurogenesis, and then gliogenesis (Bansod et al. 2017).

A transcription factor that has been reported to play a role in the neurogenic-to-gliogenic switch is Nuclear Factor Kappa B (NF-κB), which first suppresses the commitment of neurogenic RGC to a gliogenic fate, and then that of gliogenic RGC to oligodendrocyte/OPC generation, but seems to support astrocyte generation and differentiation. However, neither the upstream nor the downstream mechanisms of this regulation are clear (Methot et al. 2018).

Generally, the mechanisms which regulate the concerted effects of different chromatin remodelers and epigenetic factors (PrC/PRC2/HMGA) have not been entirely elucidated yet, and the upstream regulation of the intrinsic governors of the neurogenic-to-gliogenic switch remains unclear (Ohtsuka and Kageyama 2019). However, external factors likely play a role as well, as maternal influence on the duration of gestation has been shown to

extend or reduce the duration of neurogenesis, specifically UL neurogenesis, by linking its end to the timing of birth (Stepien et al. 2020).

2.3.5 NuRD complex is a modulator of gene expression at fate switches

As chromatin remodeling has now been shown to play a role in the neurogenic-to-gliogenic switch, and thus the duration or prolongation of neurogenesis, it was of note that the expression of two subunits of the nucleosome remodeling and deacetylase (NuRD) complex were found to be regulated between neurogenic and gliogenic cortical RGC, namely metastasis-associated protein 3 (*Mta3*) and *Gatad2b* (Pinto et al. 2008).

NuRD is an unusual chromatin remodeler that fulfills two enzymatic functions within the same complex: epigenetic histone modification by histone deacetylase (HDAC) proteins and ATP-dependent nucleosome remodeling by chromodomain helicase DNA binding protein (CHD) family members (Allen et al. 2013). While NuRD is generally viewed as a repressor complex, similar to Polycomb, its function is much more diverse.

Much of the study of general NuRD function has been performed in embryonic stem cells (ESC). Here, NuRD binds to the transcription start site (TSS) and enhancers of actively transcribed genes, silencing them or modulating their transcription level, thus suppressing transcriptional "noise". It controls the dynamic range of transcription and the transcriptional population heterogeneity (Reynolds, Latos, et al. 2012; Reynolds, Salmon-Divon, et al. 2012; Burgold et al. 2019). This is especially notable on bivalent genes, where it regulates the dynamic between acetylation and methylation of H2K27. These bivalent genes are often defining for cell fate decisions, and as such, it represents a balancing switch between cell states. NuRD controls the transition out of the self-renewing state in ESC, and the NuRD-mediated transcriptional heterogeneity correlates with the ability of the cells to commit to differentiation (Reynolds, Latos, et al. 2012; Reynolds, Salmon-Divon, et al. 2012). Accordingly, knockdown of a specific NuRD assembly (MBD3-GATAD2A-CHD4) facilitates deterministic reprogramming of fibroblasts into pluripotency (Mor et al. 2018).

The canonical subunits of the NuRD complex (Figure 3) include the two enzymatically active protein families HDAC with family members HDAC1/2 and CHD with CHD3/4/5.

Further canonical subunits include the core protein families retinoblastoma binding protein (RBBP) with RBBP4/7; MTA with MTA1/2/3; methyl-CpG-binding domain protein (MBD) with MBD2/3; and GATA zinc finger domain containing 2 (GATAD2) with GATAD2A/B (Smits et al. 2013).

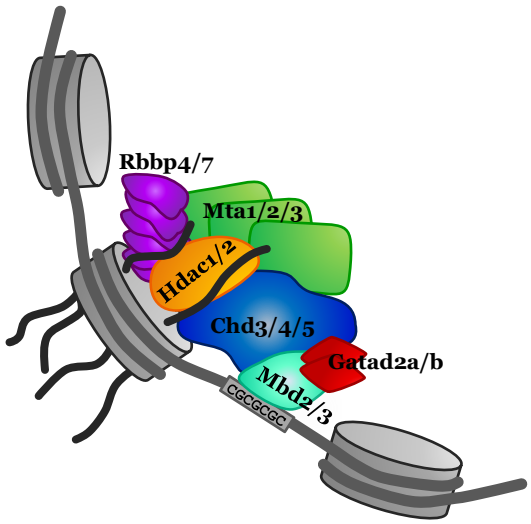

Figure 3: Schematic representation of canonical NuRD assembly

The visualization was based on several, partly conflicting, reports of NuRD stoichiometry and assembly and represents the author's notion of a putative canonical NuRD complex (Reynolds, Latos, et al. 2012; Reynolds, Salmon-Divon, et al. 2012; Bode et al. 2016; Allen et al. 2013; Kloet et al. 2015; Guezennec, Le et al. 2006; Alqarni et al. 2014; Smits et al. 2013; Brackertz et al. 2006; Burgold et al. 2019; Millard et al. 2016; Torchy et al. 2015).

HDAC1 and HDAC2 catalyze the deacetylation of histone tails, while CHD3/4/5 perform ATP-dependent nucleosome remodeling, "sliding" the histone octamers along the DNA to regulate the accessibility of DNA loci (Allen et al. 2013). MBD2 and MBD3 are generally viewed as the subunits crucial to core assembly and recruiting the NuRD complex (Reynolds, Latos, et al. 2012; Allen et al. 2013), and can target the complex to a set of genes via binding to CpG islands (Allen et al. 2013). RBBP4 and RBBP7 are the most dynamic core subunits and are shared with the PRC2 (Kloet et al. 2015; Kuzmichev et al. 2002).

Conflicting statements have been reported about subunit dimerization, redundancy and exclusivity, such as a dispute if the MBD2/MBD3 subunits are mutually exclusive, or, on the contrary, even form heterodimers (Allen et al. 2013; Guezennec, Le et al. 2006), and this may be based in the fact that NuRD complex assembly varies greatly between cell

types. This subunit heterogeneity likely facilitates a functional specialization of a complex that is otherwise ubiquitously present, even allowing different functions and interactors of mutually exclusive assemblies in the same cells (Bowen et al. 2004; Guezennec, Le et al. 2006; Bode et al. 2016).

MTA protein family members have first been implicated in cancer development, but are ubiquitously expressed and perform diverse functions, such as MTA3 regulating proliferation in ovaries and in hematopoiesis (Kumar and Wang 2016; Sen et al. 2014). MTA proteins have a GATA-zinc finger (Znf) domain that recognizes a specific DNA sequence and can also recruit proteins (Allen et al. 2013). MTA1 and MTA2 both have two RBBP binding domains that improve recruitment to the complex, however, MTA3 lacks the second motif and is thus only completely stabilized when bound to MBD3, and prefers and intact NuRD complex (Burgold et al. 2019). In ESC, the MTA family members can form all possible combinations of homo- and heterodimers and seem to be functionally redundant (Burgold et al. 2019).

GATAD2A and GATAD2B contain a complement receptor (CR) 1 region that enables them to bind all NuRD subunit families, specifically MBD3, MTA2, HDAC1/2 and RBBP4/7, dependent on SUMOylation (Allen et al. 2013; Gong et al. 2006). The family members have been reported to be mutually exclusive (Spruijt et al. 2016). They are able to bind to the tails of all octameric histones, but binding ability is reduced in the acetylated state, and thus binding is more stable after NuRD has exerted its function of histone deacetylation, representing a "two-interaction forward feedback binding mode" (Brackertz et al. 2006; Spruijt et al. 2016). Of note, several cases of intellectual disability have been clinically described for mutations of GATAD2B in different modalities, implicating an as of yet unknown role in neurogenesis (Willemsen et al. 2013; Ueda et al. 2019; Luo et al. 2017; Rabin et al. 2018; Trubnykova et al. 2019; Vera et al. 2020).

NuRD function in different aspects of neurogenesis and cortical development has been previously examined in mice. The deletion of core assembly subunit MBD3, for example, leads to reduced cortical thickness, aberrant progenitor production and differentiation. Cortical projection neurons are improperly specified, some expressing markers for both DL and UL within the same cell, and eventually the deficit leads to neonatal death (Knock et al. 2015).

For HDAC1 and HDAC2, functional redundancy in neuronal development has been suggested, with the loss of both proteins being necessary for the phenotype of gross abnormalities in cortical and hippocampal architecture, and increased cell death. Here, the role in precursors differentiating into neurons may be mainly dosage-sensitive (Montgomery et al. 2009). In contrast, no functional redundancy has been found for the subunits CHD3/4/5 in neurogenesis (Nitarska et al. 2016). Although all are expressed in postmitotic neurons, they are not necessarily associated with the complex, whose composition varies over the course of development. Deletion of CHD4 led to premature cell cycle exit, depletion of bIP, and reduced UL thickness (Nitarska et al. 2016); a phenotype strikingly similar to that of MBD3 depletion (Knock et al. 2015). CHD4 thus seems to be necessary for proper progenitor proliferation. On the other hand, CHD5 regulated the early stages of young neuron migration, while CHD3 is implicated in the late stages of radial migration and laminar specification (Nitarska et al. 2016).

NuRD works in cooperation with PRC2 by regulating its substrate availability, binding to a specific set of PRC2 target genes and deacetylating local H3K27, which makes them available for binding by PRC2 (Reynolds, Salmon-Divon, et al. 2012). A mechanism for the function of CHD5 in the terminal fate switch of neuronal progenitors has been revealed to be the recruitment to Polycomb targets, where NuRD is necessary to aid in repression of non-neuronal genes (Egan et al. 2013).

With some functions of different NuRD assemblies in neurogenesis already known, and a link to PRC2 as a known regulator of the neurogenic-to-gliogenic switch, the function of the relatively unknown subunits MTA3 and GATAD2B in neurogenesis thus presents an intriguing target for study.

2.3.6 Genome-wide approach to identify neurogenic fate determinants

As has been delineated above, several different aspects play a role in determining the fate of a cell and its identity, and many of the involved pathways either converge or compete in a complex manner. To understand crucial connections and correlations, it is therefore necessary to look at the development of the embryonic brain not only in terms of passing time, but also other aspects. Namely, what makes the stem cells switch their fate towards a narrower potential and ultimately loss of stemness? Why do some stem cell niches, like

the LGE that develops into the SEZ, stay active even in the adult while others, like the cortex, deplete early on and lose any regenerative potential? And what are the changes in the cells themselves when they go on to differentiate?

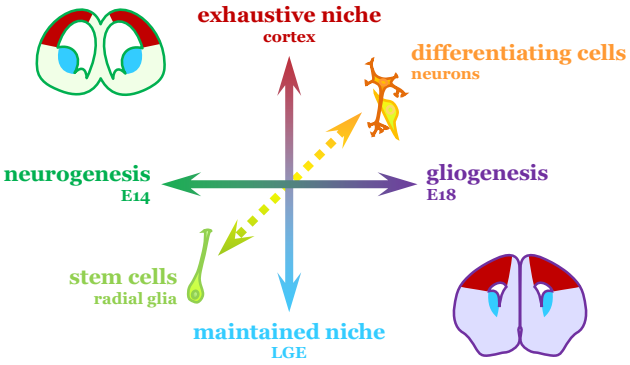

Figure 4: A multi-dimensional, genome-wide approach to understand the transcriptomic framework of fate switches

This multidimensional approach will allow a more comprehensive look at the different fate decisions and cell states, aiding in the identification of novel neurogenic factors, and in pinpointing which of these are upstream of converging or diverging pathways. These candidates will then represent promising targets to try and manipulate the progression of the fate decisions, and to prolong neurogenesis in the cerebral cortex.

2.4 GENOME EDITING IN NEURAL STEM CELLS

As has been established in Chapter 2.1, the developing cortex mainly comprises of rapidly dividing stem and progenitor cells. To study the function of genes or factors in the cortical neural stem cell system poses the challenge of a suitable method of delivery for modulating factors.

Application is generally very favorable in the embryonic cortical aRGC. As these line the lateral ventricles at neurogenic stages, injection in these cavities will exclusively target the desired cell type. However, effectors need to be applied in a system that allows genomic integration of the effector cassette, since it will otherwise rapidly be diluted and thus lose its effectiveness, possibly masking an elicited phenotype.

2.4.1 Integrating systems for effector delivery: the piggyBac transposon

Popular integrating systems include viral transduction with retro- or lentivirus (Artegiani and Calegari 2013). While the immune reaction upon transduction has been reduced by optimizing the retroviral system, using HIV-1 derived Lentivirus (LV) (Piras et al. 2017), infection typically is sparse and untargeted upon injection in the embryonic lateral ventricle. The typical advantage of LV, namely the possibility to genomically integrate into postmitotic and non-cycling cells (Naldini et al. 1996), is not a deciding factor in the very proliferative embryonic cortex.

An alternative are transposable elements, such as Sleeping Beauty (SB) or the piggyBac transposon system, both having been discovered decades ago (Cary et al. 1989; Ivics et al. 1997). The piggyBac system was first discovered in a cell line from the moth *Trichoplusia ni*, which was used for passaging *Baculovirus*. Virus passaged in these cells showed a *de novo* integration of foreign DNA, namely transposon elements from *T. ni* (Cary et al. 1989). The integration was specifically found at genomic TTAA sites, which were duplicated by the integration (Cary et al. 1989), and the transposon was found to contain certain repetitive elements – later identified and named as terminal repeats (TR) – that were necessary for transposition (Li, X. et al. 2005).

For a long time, this system was only used in insect cells, until it was discovered that efficient integration is also possible in vertebrate and mammalian systems, such as mouse and human, as demonstrated by the generation of transgenic animals with stable inheritance (Ding et al. 2005). When the piggyBac transposon is delivered together with its specific transposase, even at low enzymatic levels, it is very efficiently transposed, while showing very little unspecific integration on its own; and even high expression of the transposase enzyme does not inhibit transposition (Wang, W. et al. 2008; Cadiñanos and Bradley 2007; Ding et al. 2005).

The piggyBac transposon is integrated in a completely seamless manner and can be re-excised without leaving a footprint (Figure 5). This is possible by the specific integration mechanism in which the transposase nicks the DNA at TTAA sites and induces transient double strand breaks. The repair using the transposon as template is not achieved by DNA synthesis, as in homologous recombination, but by DNA ligation (Mitra et al. 2008).

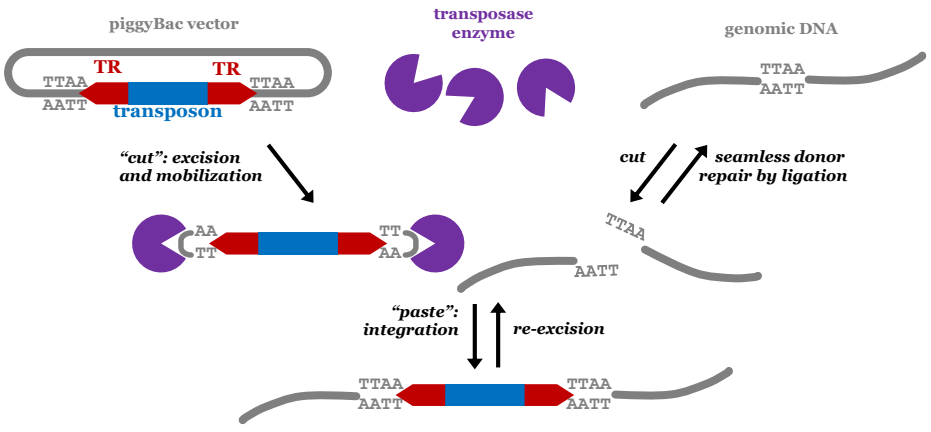

Figure 5: Mechanism of piggyBac transposon integration

The piggyBac transposon is seamlessly integrated and re-excised at TTAA sites of the genomic DNA by its corresponding specific transposase.

PiggyBac transposon exhibits a strong preference to integrate into transcription units, i.e. highly transcriptionally active sites and accessible chromatin, but no bias for chromosomal location (Ding et al. 2005; Wang, W. et al. 2008; Elick 1996; Li, M. A. et al. 2013; Yoshida et al. 2017). Whether the transcription of the integrated transposon may

be silenced, or transposition hindered, by epigenetic modifications of the piggyBac plasmid or transposon is not clear (Ding et al. 2005; Wang, W. et al. 2008).

Efficient cloning strategies facilitate the use of the piggyBac transposon for *in vivo* screening (Xu et al. 2017). In addition, piggyBac transposon allows an exceptionally large cargo, with transposons reaching 100 kilo-base pairs (kbp) reportedly integrating in the genome – albeit at lower efficiency –, and fully efficient integration up to a size of approx. 9 kbp (Ding et al. 2005; Li, M. A. et al. 2011). Another great advantage especially for translational studies, is the possibility of re-excising the transposon without leaving a footprint in the genomic DNA, thus allowing temporally controlled effector delivery (Woltjen et al. 2009; Behringer et al. 2017).

For the use in systems other than insect cells, e.g. mammalian cells or organisms, modified transposase enzymes based on the original PBase have been created. In ES cells, mPB, a mouse-codon optimized version of PBase with the same amino acid, but modified nucleotide sequence has a 20-fold higher transposition activity, possibly due to higher expression after facilitation the translational efficiency (Cadiñanos and Bradley 2007). An even further optimized enzyme, the hyperactive piggyBac transposase hyPBase, was created by the introduction of seven point mutations in the mPB sequence (Yusa et al. 2011) for application in mammalian systems.

Despite the stated advantages of the piggyBac transposon system, there is the drawback of its integration at (semi-) random genomic sites, and a propensity for "locus hopping", in which the transposon is repeatedly re-excised and re-integrated, usually within the vicinity of the previous site (Ding et al. 2005; Li, M. A. et al. 2013). Together with the bias of integration into transcriptionally active loci, which likely represent genes necessary for normal cellular function, this could cause unwanted off-target effects, which may be difficult to determine and combat for *in vivo* systems.

2.4.2 Targeted genome, transcriptional and epigenetic editing with the CRISPR/(d)Cas9 system

After having been limited for a long time to the overexpression, knockdown or knockout of single factors, also for introducing epigenetic modifications which were then global, the discovery of the Clustered Regularly Interspaced Short Palindromic Repeats/

CRISPR associated protein 9 (CRISPR/Cas9) systems opened a plethora of new possibilities in genome editing.

The Cas9 endonuclease is originally a defense mechanism of bacteria and archaea against phages. The dCas9 enzyme is guided by short RNA fragments, the guide RNAs (gRNAs), to bind on the complementary sequence on the (phage) DNA. With the enzymatic activity of Cas9 directed to this specific locus, it introduces a double-strand break in the DNA, with different options for repair (Figure 6A): non-homologous end joining (NHEJ), and homology directed repair (HDR), allowing for very specific deletion, integration or (single-base) editing of specifically targeted loci (Jinek et al. 2013; Doudna and Charpentier 2014).

The following development of an enzymatically dead version of Cas9 (dCas9), allowed further applications other than genomic editing itself (Figure 6B). When the CRISPR/dCas9-gRNA complex, called CRISPRi, is bound to its target sites, it sterically interferes with transcription (Qi et al. 2013). It may also be used as a shuttle to deliver effector proteins to a target site by way of fusion proteins, for example enzymes that allow base editing without introducing the double-strand breaks that are prone to side effects (Komor et al. 2016), or non-enzymatic effectors such as the strong artificial transcription activator VP64-p65-Rta tripartite activator (VPR) (Chavez et al. 2015).

These possibilities open a toolbox of epigenetic or transcriptional editing in addition to classical genome editing, which dramatically increases the accuracy and possibilities of interventions at specifically targeted sites, and by combination of several gRNAs, multiple sites at once (Breunig et al. 2018). The feasibility of CRISPR/Cas9-mediated knock-in and knock-out has already been demonstrated *in vivo*, with the constructs delivered by *in utero* electroporation (IUE) into the developing brains of different species such as mouse or ferret (Suzuki et al. 2016; Shinmyo and Kawasaki 2017).

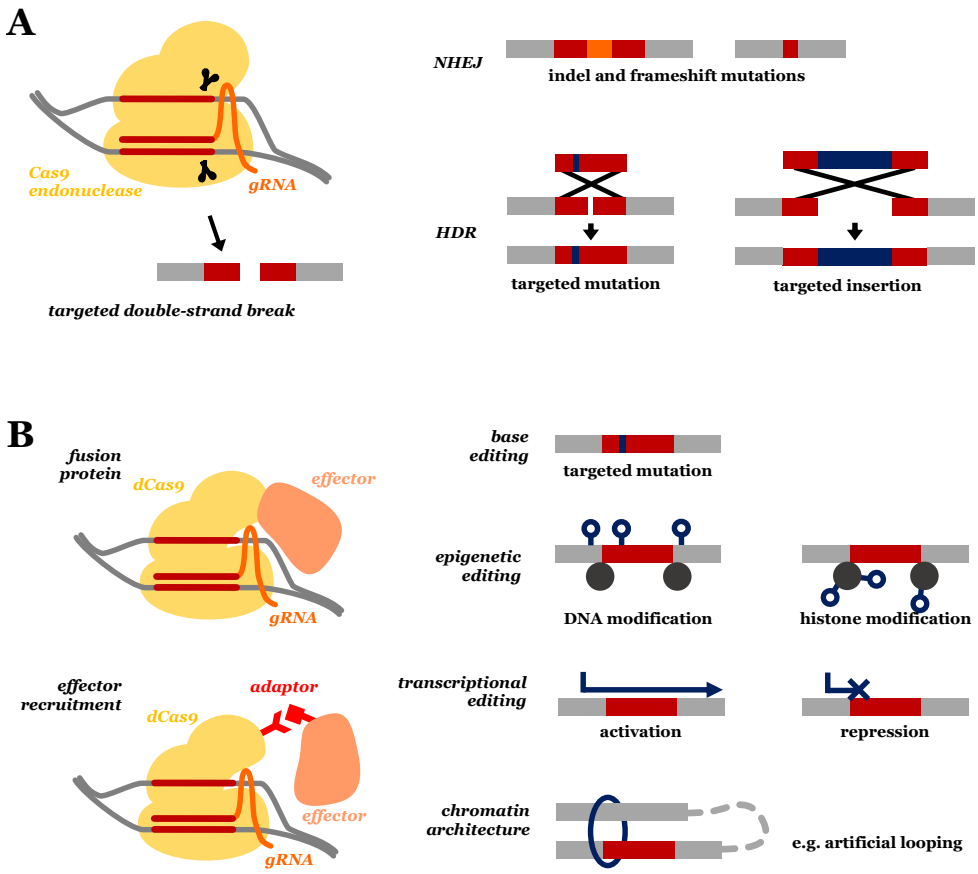

Figure 6: Genomic, epigenetic and transcriptional editing possibilities with the CRISPR/(d)Cas9 system

A. Genomic editing with CRISPR/dCas9 works by introducing a double strand break that can be repaired by NHEJ or HDR. B. By using dCas9, delivery of effector proteins to specifically targeted sites opens new editing possibilities.

A drawback of the system is the possibility of off-target effects, as well as the variable efficiency of gRNAs, which make application unpredictable especially in the long term. The recently developed ribonucleoprotein complexes (RNP), in which the gRNAs are bound to nanoparticles or delivered in lipid droplets, have the advantage of providing a short window of editing activity before the RNPs are degraded, which reduces off-target effects and avoids Cas9-elicited immune response and cellular stress due to high-level expression of foreign transgenes (Staahl et al. 2017; Lee et al. 2017; Chew 2018). In addition, the delivery of such a large protein complex – or the encoding DNA – can be difficult, but here, the piggyBac transposon system, with its large cargo capacity (Li, M. A. et al. 2011), is a good option for *in vivo* application.

2.5 AIMS OF THIS THESIS

In the work of this thesis, I wanted to clarify a possible role for NuRD complex subunits MTA3 and GATAD2B in neurogenesis. These candidates were identified as putatively regulated between E14 neurogenic and E18 gliogenic aRGC in a previous study of the lab (Pinto et al. 2008). I wanted to achieve this by analyzing the phenotype of *in vivo* knock-down during neurogenesis.

Furthermore, I aimed to identify more genes that could be implicated in the regulation of neurogenesis. To this end, I performed RNA sequencing (RNA-Seq) of different time points (neurogenic vs. gliogenic), regions (exhaustive vs. maintained niche) and cell types (stem cells vs. differentiating cells) from mouse embryonic telencephalon to gain a broad overview of transcriptomic changes in the developing mouse brain.

Lastly, I aimed to prolong the neurogenic potential of aRGC *in vivo* by concurrently activating the transcription of several of the factors identified in my transcriptomic analysis. To this end, a system needed to be developed that allows the delivery of a dCas9-VPR transcriptional activator fusion protein together with the gRNAs targeting the selected factors. This system needed to be applicable *in vivo* and genomically integrating. With the system established, the aim was to find a putative effect on neurogenesis and its maintenance after application of the system *in vivo*.

3 RESULTS

3.1 THE NURD SUBUNITS MTA3 AND GATAD2B IN EMBRYONIC CORTEX DEVELOPMENT

Declaration of author contributions: *The plasmid containing the miRNA control was kindly provided by Dr. Adam O'Neill. Contributions are detailed in the Declaration of Author Contributions on page XXXIV.*

3.1.1 NuRD subunits MTA3 and GATAD2B have distinct expression patterns in murine embryonic brain development

As has been shown for one of the active enzymatic subunits of the NuRD complex – family members CHD3, CHD4 and CHD5 – the correct expression and activation of chromatin remodelers can be crucial for the correct differentiation and migration in cells of the developing cortex (Nitarska et al. 2016). To find if this applies to the NuRD complex subunits MTA3 and GATAD2B as well, I performed immunohistochemistry on embryonic brain tissue sections at two different time points. At E14, neurogenesis is at its peak, whereas at E18, it has mostly subsided as the radial glia switch their program towards a gliogenic fate (Agirman et al. 2017).

During peak neurogenesis at E14, MTA3 is expressed in the entire forebrain from rostral to caudal (Figure 7A). It is expressed in a salt-and-pepper pattern along the VZ of the cortex and the lateral part of the LGE, and another band of expression can be observed in the cortical plate (Figure 7B). Strikingly, very little expression is visible in the SVZ and IZ, suggesting a temporary reduction of protein expression during the migration of differentiating neurons.

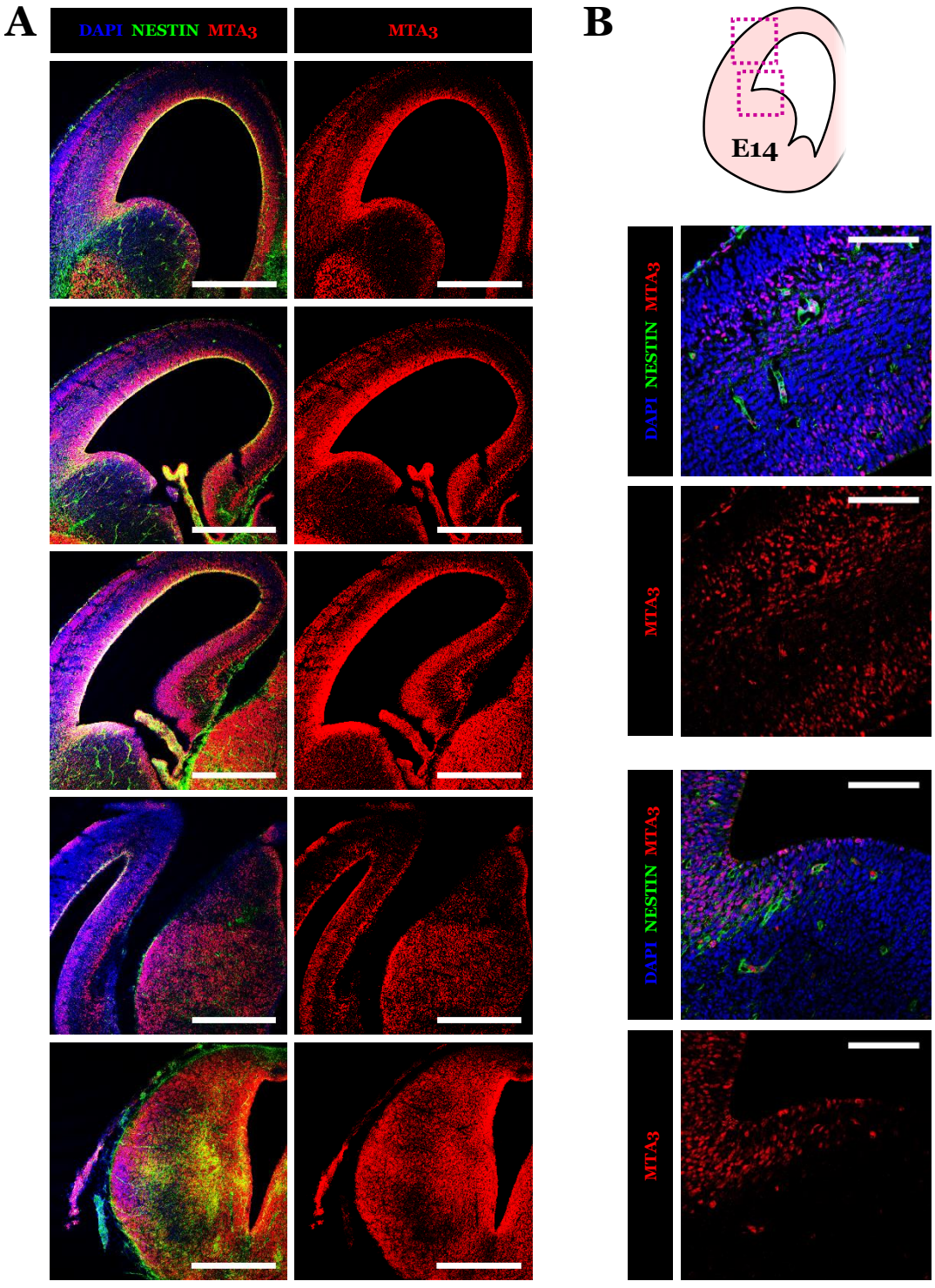

Figure 7: Protein expression and localization of MTA3 in E14 embryonic forebrain.

Fluorescence confocal images of E14 mouse brain after IHC for MTA3 and NESTIN. ***A.*** *At E14, MTA3 is expressed throughout the brain from rostral to caudal, including the midbrain. (Scale bars: 500 µm)* ***B.*** *The protein is expressed in a salt-and-pepper pattern along the ventricle, both in the cortical VZ and the LGE, and in the cortical plate. (Scale bars: 100 µm)*

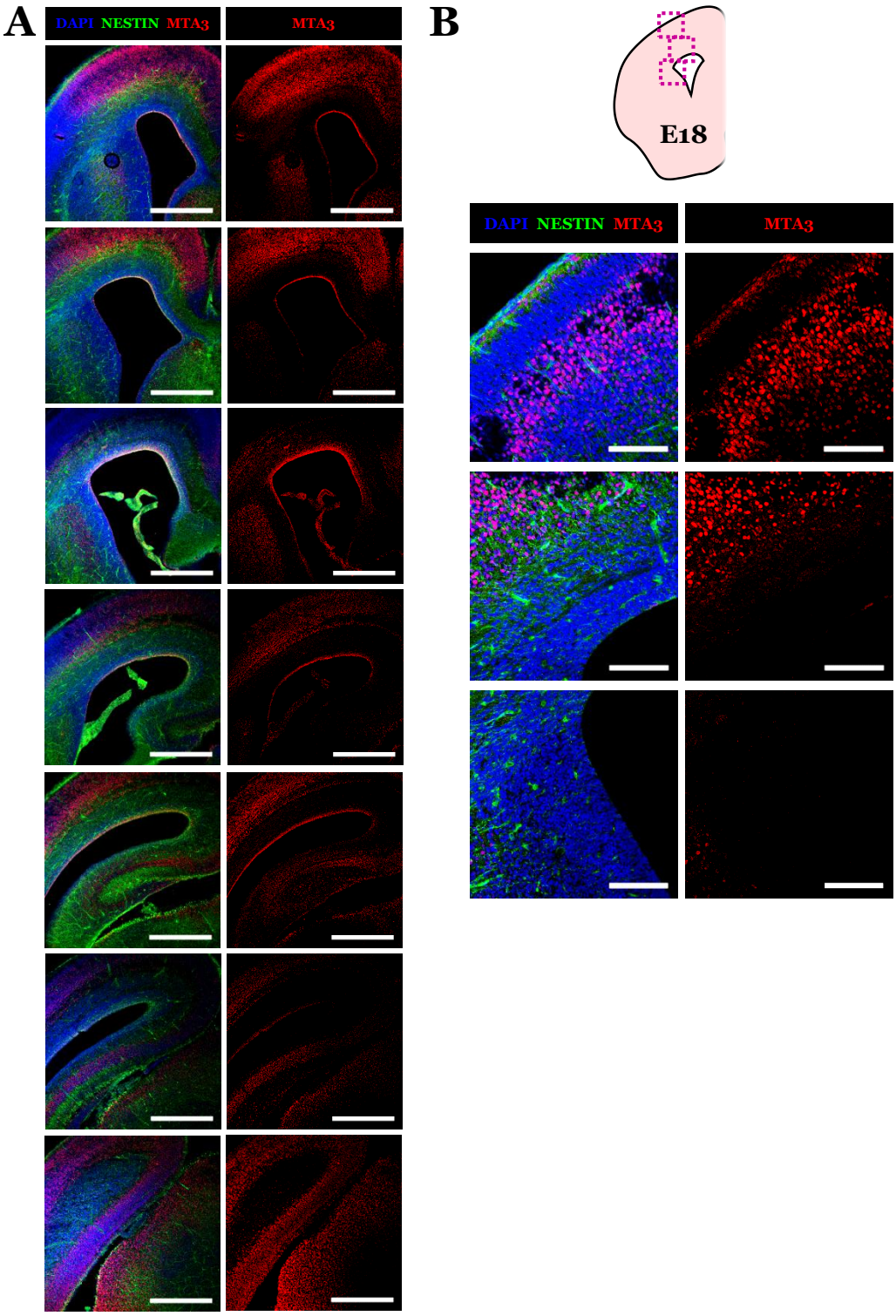

Figure 8: Protein expression and localization of MTA3 in E18 embryonic forebrain.

Fluorescence confocal images of E18 mouse brain after IHC for MTA3 and NESTIN. ***A.*** *At E18, MTA3 continues to be strongly expressed in the forebrain from rostral to caudal, however it is now specialized to the lower cortical plate. (Scale bars: 500 µm)* ***B.*** *Expression in the ventricular zone is completely abolished both in the cortex and LGE at E18 post-neurogenic stage, while the deep layer cortical plate continues to exhibit a salt-and-pepper expression. (Scale bars: 100 µm)*

After neurogenesis has largely subsided, MTA3 is still expressed from rostral to caudal at E18 (Figure 8A), however the expression is now specialized to the lower cortical plate. No protein can be observed at the VZ or in the LGE/SEZ, but the salt-and-pepper pattern continues to be present exclusively in the deep layer of the cortical plate (Figure 8B).

As expected for the subunit of a chromatin remodeling complex, the MTA3 protein localizes in the nucleus, as shown by colocalization with DAPI (Figure 9A) both in the VZ and the CP at E14.

The NuRD complex does not only recruit three different members of the MTA protein family, but the *Mta3* gene is additionally expressed in different transcript variants (tv). Four different protein coding transcripts are currently listed in ENSEMBL with a transcript support level of 1 (TSL:1), indicating high confidence in the correctness of all splicing sites, and additional putative transcripts are listen in ENSEMBL and NCBI Gene (Figure 9B).

Mta3 is quite ubiquitously expressed (Kumar and Wang 2016), and a preference for different transcript variants in different tissues may help to achieve functional specificity. As determined by quantitative real-time polymerase chain reaction (qRT-PCR) on E14 wild type (C57BL/6) mouse embryo, with primers specific for tv1, tv2, or tv3+4 – the latter only differ in one amino acid – there is a strong preference for tv2 in all observed tissues (Figure 9C). In both telencephalic regions examined, the cortex and GE, as well as the prepontine hindbrain, and dorsal skin and muscle, tv2 is by far the strongest expressed, while tv3+4 together make up the smallest proportion of the *Mta3* transcripts. In addition, expression levels vary only slightly between these different tissues, with a slight downward trend in the brain from rostral to caudal.

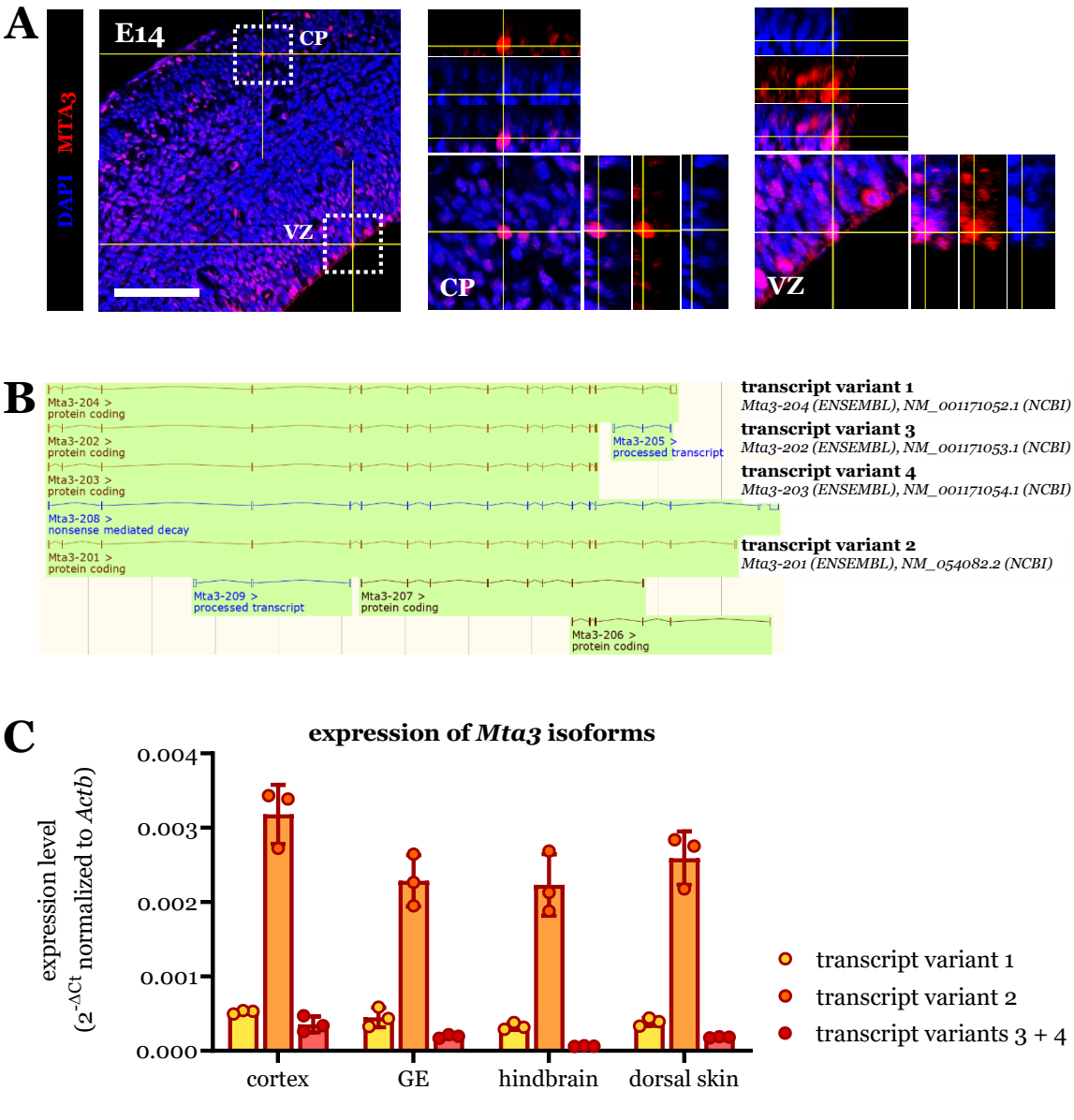

Figure 9: Subcellular localization of MTA3 and transcript variant expression of *Mta3* mRNA.

A. *Fluorescence confocal image of E14 mouse brain after IHC for MTA3. The protein localizes to the nucleus as shown by the colocalization with DNA marker DAPI in the orthogonal slice of a z-stack, both when it is present in the ventricular zone and the cortical plate at E14. (Scale bar: 100 µm)* ***B.*** *Four different transcript variants have been confirmed for Mta3 and are listed in ENSEMBL (*ENSEMBL release 103, www.ensembl.org/id/ENSMUSG00000055817, *retrieved 07.03.2021) and NCBI Gene (*www.ncbi.nlm.nih.gov/gene/116871, *retrieved 07.03.2021).* ***C.*** *As observed by qRT-PCR with transcript variant-specific primers, a preference for tv2 is strongly present in all examined tissues at E14, with tv3+4 being the least expressed. (Mean ± S.D., n=3 biological replicates.)*

The protein expression of GATAD2B differs strongly from that of MTA3. During neurogenesis, it is similarly expressed throughout the brain (Figure 10A), however the salt-and-pepper expression pattern is limited to the cortical plate (Figure 10B) and no protein expression is observed with this antibody in the VZ, SVZ or IZ.

At E18, the GATAD2B protein continues to be present in the cortex from rostral to caudal and is strongly expressed in the hippocampus (Figure 11A). The cortical expression is now considerably stronger and, especially compared to the distinct salt-and-pepper pattern present at E14, quite uniform throughout all cortical layers (Figure 11B).

As a chromatin remodeling factor, like MTA3, it is distinctly localized to the nucleus as shown by colocalization with DAPI (Figure 12A). The *Gatad2b* mRNA is expressed in several embryonic tissues at E14 (Figure 12B), with a preference towards the telencephalon and especially the cortex, in accordance with the protein localization.

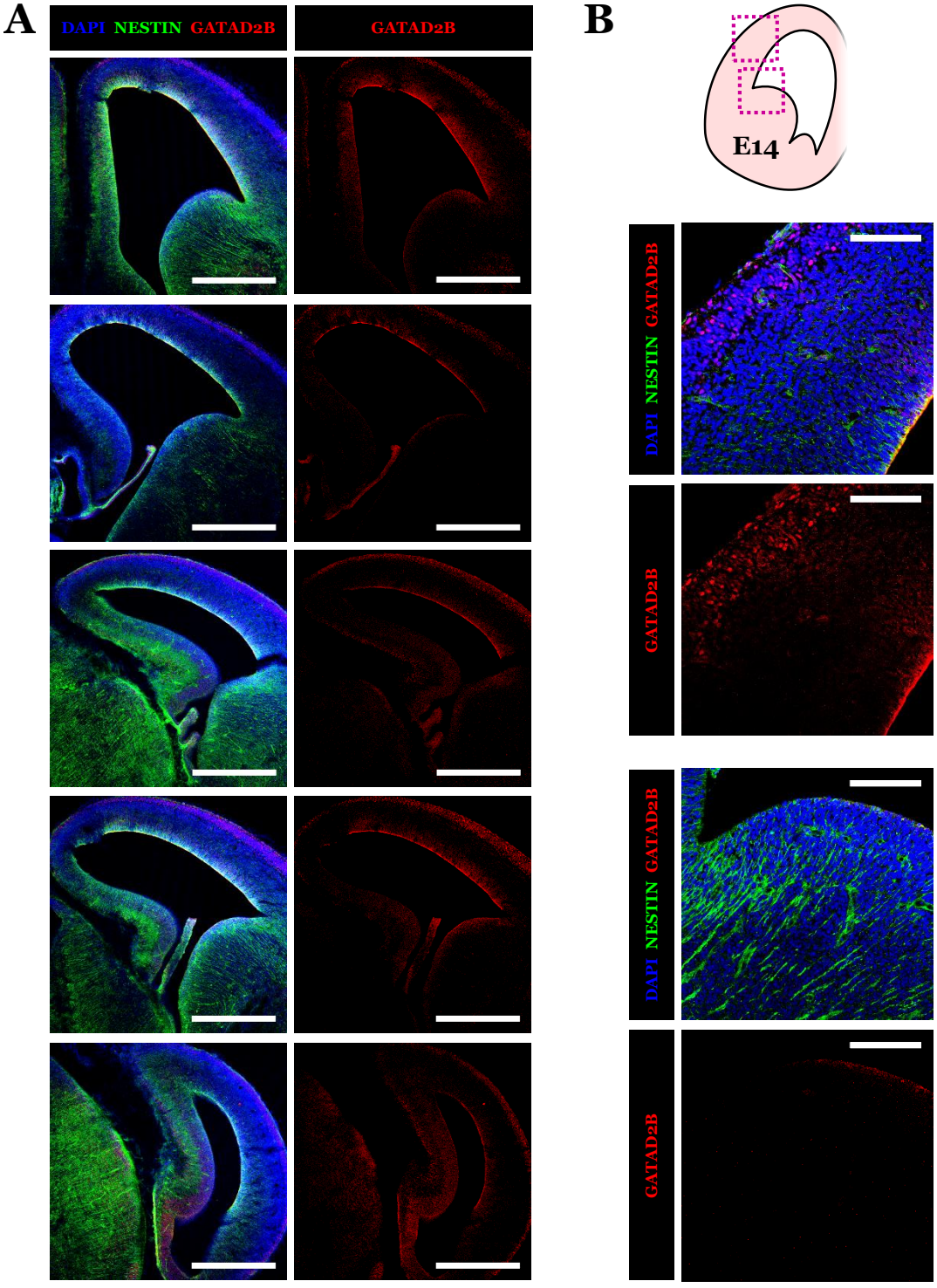

Figure 10: Protein expression and localization of GATAD2B in E14 embryonic forebrain.

Fluorescence confocal images of E14 mouse brain after IHC for GATAD2B and NESTIN. ***A.*** *At E14, GATAD2B is expressed throughout the brain from rostral to caudal regions. (Scale bars: 500 µm)* ***B.*** *The salt-and-pepper expression is limited to the cortical plate, with no nuclear protein observed near the VZ. (Scale bars: 100 µm)*

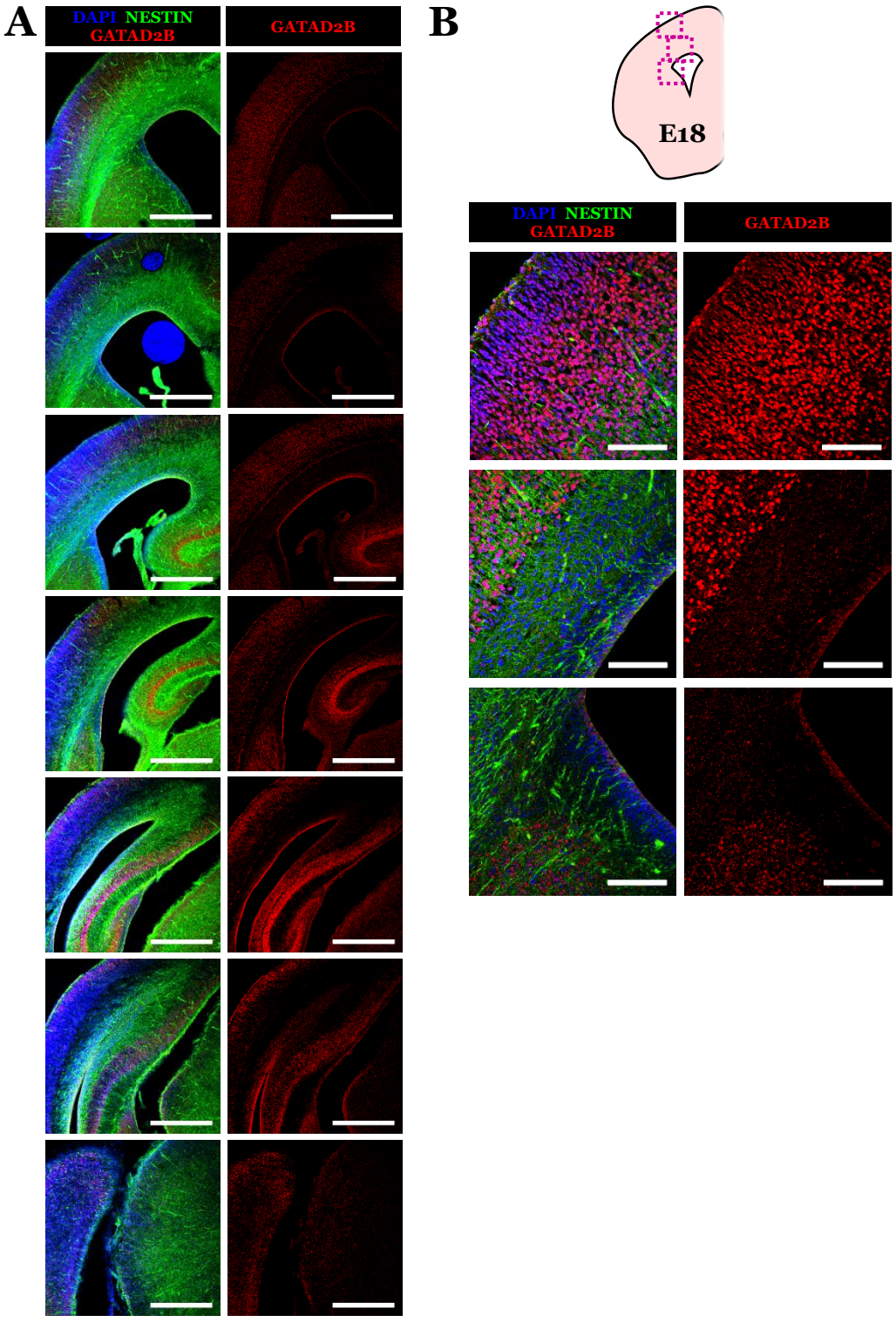

Figure 11: Protein expression and localization of GATAD2B in E18 embryonic forebrain.

Fluorescence confocal images of E18 mouse brain after IHC for GATAD2B and NESTIN. ***A.*** *At E18, GATAD2B remains expressed throughout the telencephalon. (Scale bars: 500 µm)* ***B.*** *Compared to the salt-and-pepper pattern at E14, a more uniform expression can now be observed in the entire cortical plate. (Scale bars: 100 µm)*

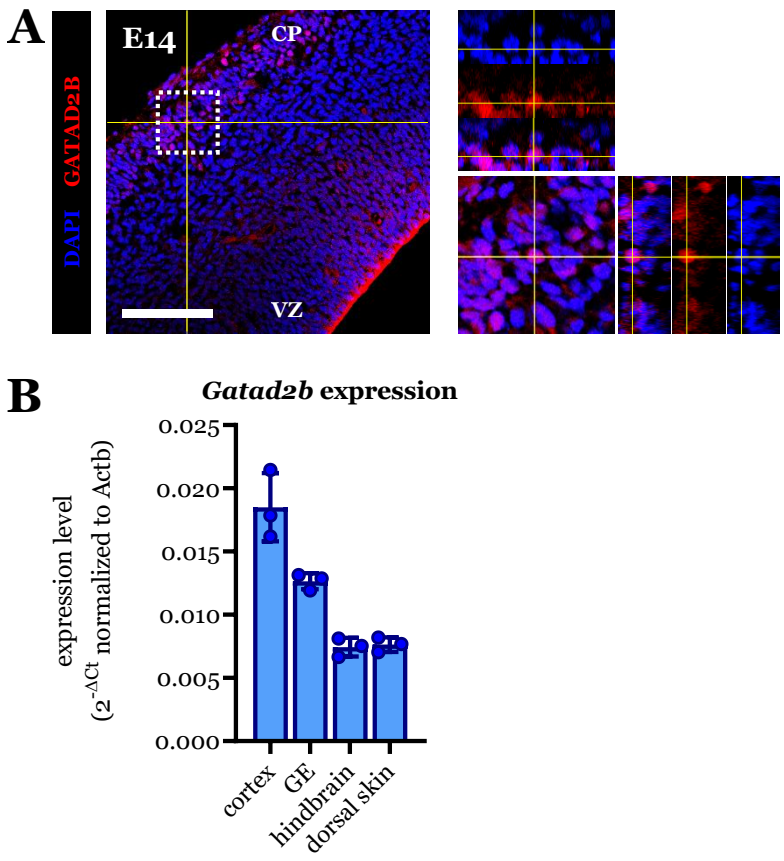

Figure 12: Subcellular localization of GATAD2B and mRNA expression of *Gatad2b* at E14.

A. *Fluorescence confocal image of E14 mouse brain after IHC for GATAD2B. GATAD2B localizes to the nucleus, as shown by colocalization with DAPI in the orthogonal slice of a z-stack. (Scale bar: 100 µm)* ***B.*** *As detected by qRT-PCR, Gatad2b mRNA is highly expressed in several embryonic tissues at E14, with a preference for telencephalic tissues and especially in the cortex. (Mean ± S.D., n=3 biological replicates.)*

3.1.2 *Mta3* and *Gatad2b* knockdown leads to a retention of cells in the ventricular zone in the developing cortex

Knocking down the mRNA expression of the NuRD complex components *Gatad2b* and *Mta3* via micro-RNA (miRNA) may elucidate their putative mechanism in neurogenesis. The miRNAs were cloned into a construct with emGFP as a fluorescent marker (Figure 13B). For each gene, several different miRNAs were cloned to select for high knockdown efficiency. For *Mta3*, however, there was no miRNA found with a predicted effect on all transcript variants, leading to putative isoform-specific constructs.

To evaluate the knockdown potential of different miRNAs, the ESC-like mouse teratoma line P19 lends itself as a model (McBurney 1993). The P19 cells were isolated by fluorescence-activated cell sorting (FACS) by emGFP fluorescence 48 hours after transfection with miRNA or the untargeted miRNA control and knockdown efficiency was evaluated by qRT-PCR (not shown). As both genes belong to protein families with possibly functionally redundant family members, indeed the knockdown by some of the miRNAs led to compensatory upregulation of the expression of those genes, and miRNAs with the smallest effect on other NuRD subunits, as well as good knockdown efficiency, were chosen. The remaining mRNA expression of these varied between ~50 % for *Gatad2b-miRNA2*, ~37 % for *Mta3-tv3+4-miRNA1* and ~12 % for *Mta3-tv2-miRNA1*. For the latter, the drastic reduction in mRNA levels was also visible in a staining of transfected P19 cells (Figure 13A), where miRNA control transfected cells showed a uniform MTA3 expression, which was drastically reduced in GFP^+ transfected cells with *Mta3-tv3+4-miRNA1*.

To examine the effect of NuRD knockdown on neurogenesis in the embryonic cortex, the miRNA constructs were delivered by *in utero* electroporation at E13, during a highly neurogenic period, and the effect examined three days later at E16 (Figure 13B). The effect was quantified by dividing the cortex into five equidistant bins, as is standard in the field (see e.g. Buchsbaum et al. 2020; Esgleas et al. 2020; Camargo Ortega et al. 2019), and determining the number of $reporter^+$ cells and their colocalization with cell type markers (Figure 13C).

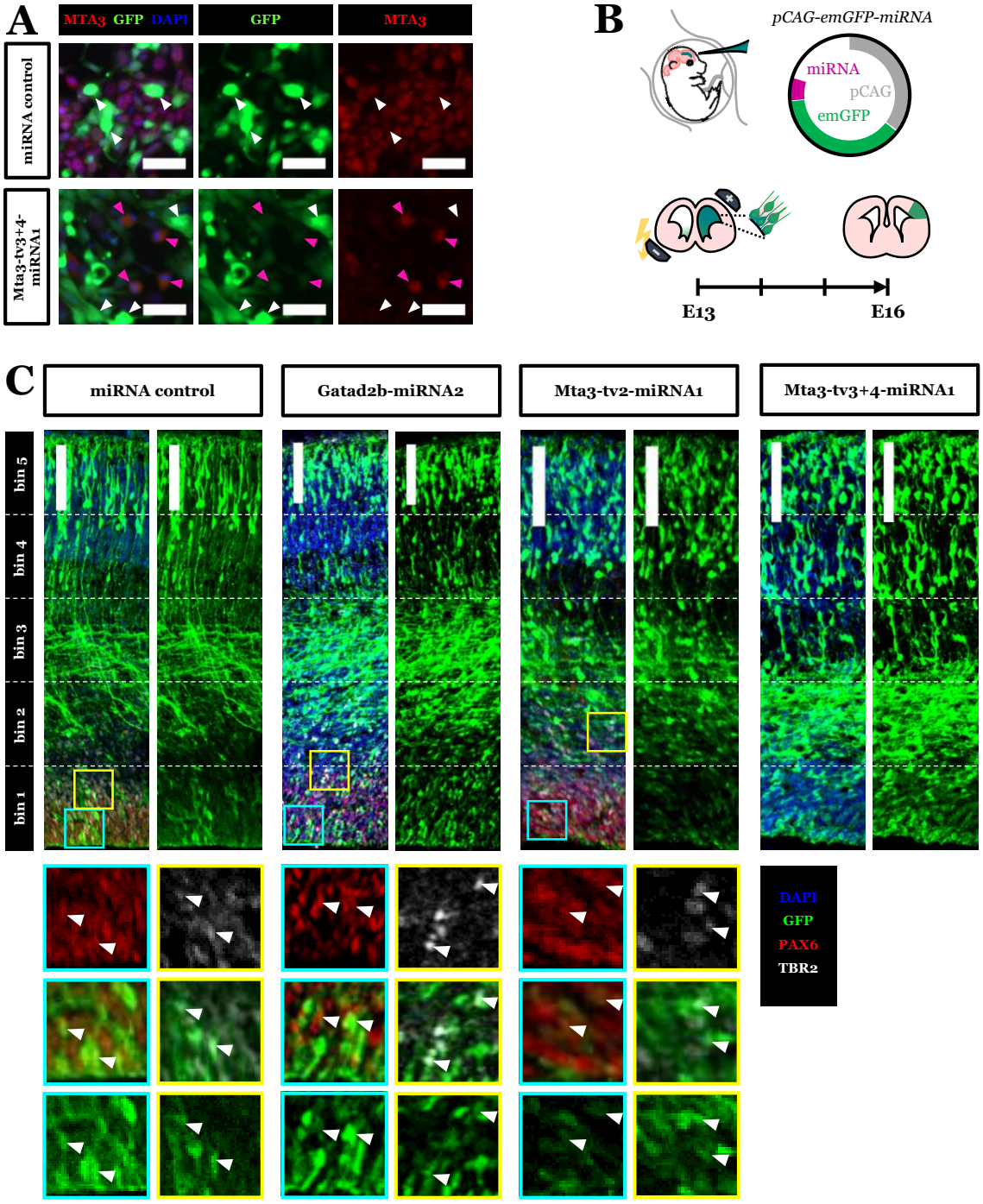

Figure 13: Knockdown of NuRD subunits by *in utero* electroporation of miRNAs.

A. *Fluorescence images of IHC for GFP and MTA3 in P19 cells, 48 hours post-transfection with* pCAG-emGFP-miRNA. *MTA3 is expressed in cells transfected with miRNA control, but drastically reduced in cells by* Mta3-tv3+4-miRNA1 *(white arrows). Untransfected cells in the same culture retain MTA3 expression (magenta arrows). (Scale bars: 50 µm)* ***B.*** *Schematic of the treatment paradigm. Wild type embryos were electroporated with* pCAG-emGFP-miRNA *at E13 and analyzed three days later at E16.* ***C.*** *Representative fluorescence confocal images of electroporated cortices at E16 with IHC for GFP, PAX6 and TBR2. Quantification was performed by dividing the cortex into five equidistant bins and analyzing reporter colocalization with nuclear stain (DAPI) and markers PAX6 and TBR2. (Scale bars: 100 µm)*

Indeed, knockdown of *Mta3* with *Mta3-tv3+4-miRNA1* leads to a significant accumulation of cells in the ventricular zone, while they are significantly depleted in the upper cortical plate (Figure 14A). The same trend, although not significant, can be observed for *Mta3-tv2-miRNA1*, and *Gatad2b-miRNA2*, where there is a significant increase in cells in the SVZ.

The identity of these cells, however, is not clear. Co-staining for PAX6, a stem cell marker, and TBR2, a marker for intermediate progenitors (Englund et al. 2005), does not show an increase in retained stem or progenitor cells (Figure 14B) that would usually be found in these niches.

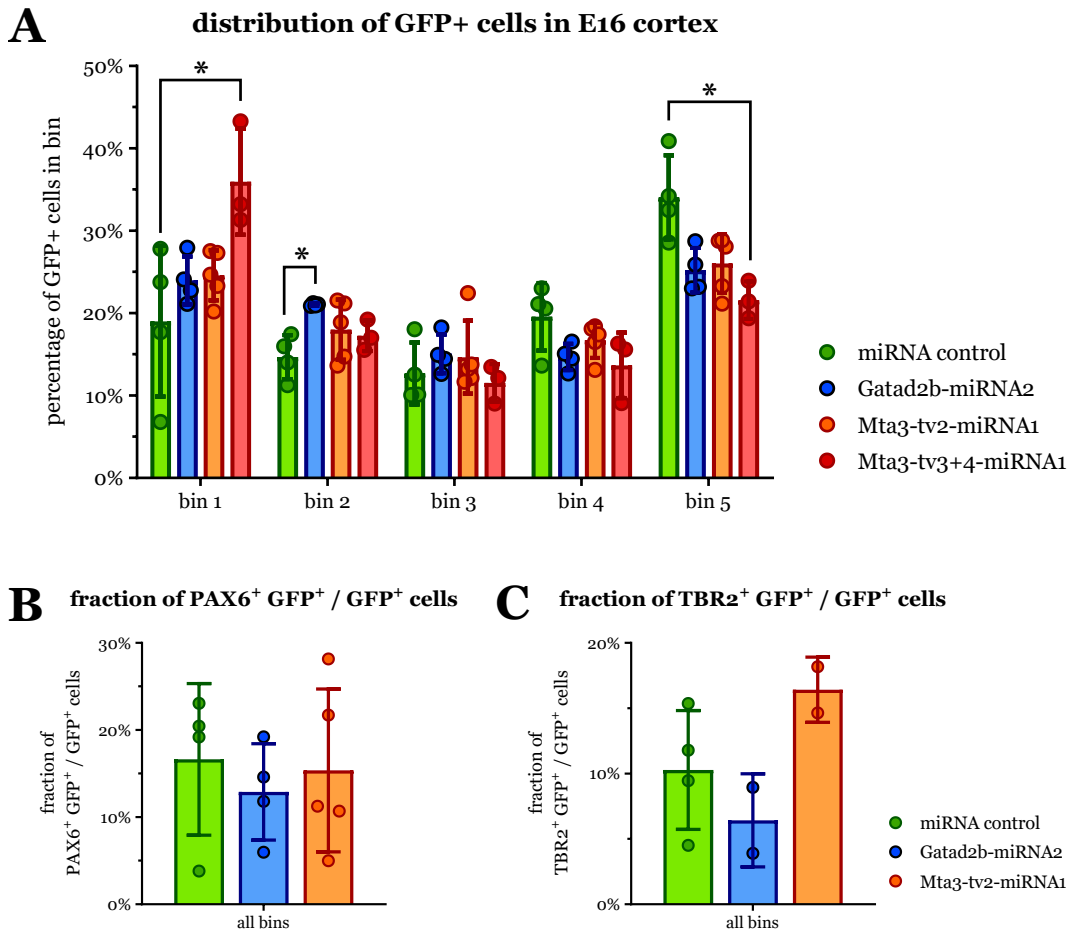

Figure 14: Distribution and marker colocalization of cells electroporated with NuRD knockdown miRNAs.

A. *The distribution of electroporated cells was altered significantly by the NuRD subunit knockdown, with more cells remaining near the apical side.* ***B.*** *The fraction of PAX6⁺ or* ***C.*** *TBR2⁺ cells was not changed significantly. (Mean ± S.D., biological replicates are shown as dot plot; Kruskal-Wallis ANOVA with Dunn's multiple comparisons test, * p<0.05)*

3.2 A GENOME-WIDE APPROACH TO UNDERSTAND THE TRANSCRIPTOMIC FRAMEWORK OF FATE SWITCHES IN BRAIN DEVELOPMENT

Declaration of author contributions: *Raw data of RNA-Sequencing was processed and partly analyzed by Dr. Pawel Smialowski. His contributions are declared as such in the text and are detailed in the Declaration of Author Contributions on page XXXIV.*

3.2.1 Obtaining the different cell populations of the developing embryonic mouse brain

As shown by the knockdown of NuRD subunits, manipulating a single factor of a complex network may not be sufficient to change the cell fate towards prolonging the phase of high neurogenic potential. A multi-dimensional approach, analyzing different time points, brain regions and cell types, allows to gain some insight into transcriptomic changes to identify candidates that govern these fate switches (see Chapter 2.3.6). To elucidate the transcriptome of the different aspects of neurogenesis, cells dissociated from the developing mouse brain were isolated by FACS to obtain the different populations and perform a transcriptome analysis.

To this end, embryonic brains from neurogenic (E14) and gliogenic (E18) time points were dissected from the cortex and LGE and the dissociated live cells stained for CD133 (prominin-1), a protein that is located at the primary cilium and apical membrane in radial glia lining the ventricle (Beckervordersandforth et al. 2010; Pinto et al. 2008; Götz and Huttner 2005), or polysialylated neural cell adhesion molecule (PSA-NCAM), an adhesion molecule that appears in immature neurons upon the start of migration (Brusés and Rutishauser 2001). The cells were isolated by FACS (Figure 15) and the purity of the obtained populations was verified by qRT-PCR and immunostaining (not shown) before the samples were analyzed by 100-bp paired-end deep sequencing.

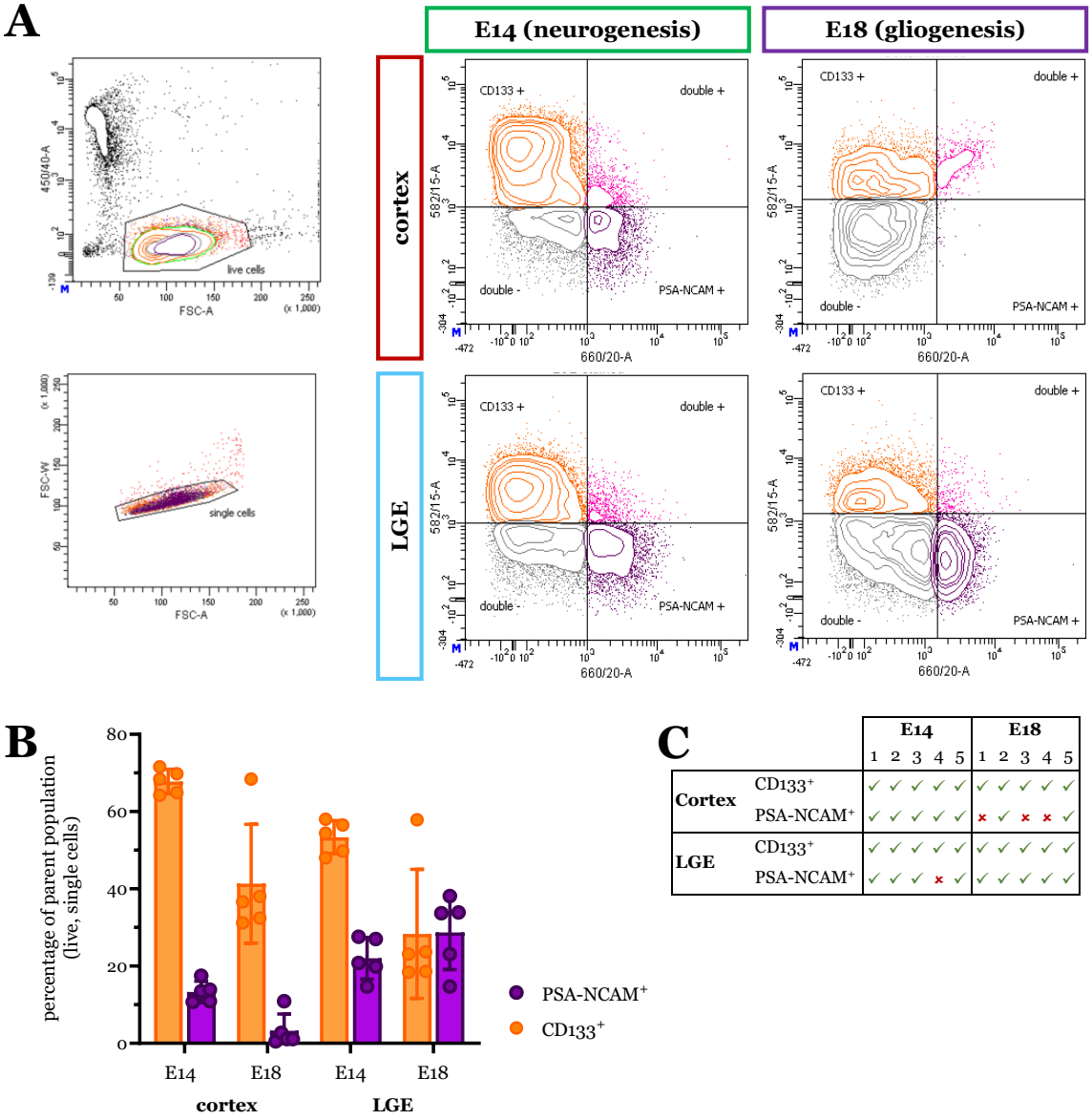

Figure 15: FACS gating strategy and obtained cell populations of the developing mouse brain for RNA-sequencing

A. *After dissection and staining, the cells were isolated by FACS, with the first two gates eliminating debris and doublets and the third gate sorting the cells into the cell type populations. Shown are representative plots for the different regions and time points.* ***B.*** *Population fractions over all collected samples. (Mean ± S.D., n=5)* ***C.*** *Sample libraries for RNA-seq. Five replicates were obtained for most conditions, with late-stage cortical neurons being the exception due to their intolerance to the preparation process.*

Raw data from RNA sequencing was processed by Dr. Pawel Smialowski, who performed quality control and created lists of regulated genes which were then further analyzed. Approx. 50 million reads per sample were obtained from next generation sequencing, of which about 28 million could be uniquely mapped to the mouse genome. When comparing the different conditions, i.e. brain regions, time points and cell types, typically around 16000 genes were detected and 40 % - 50 % of detected genes were significantly regulated (Figure 16).

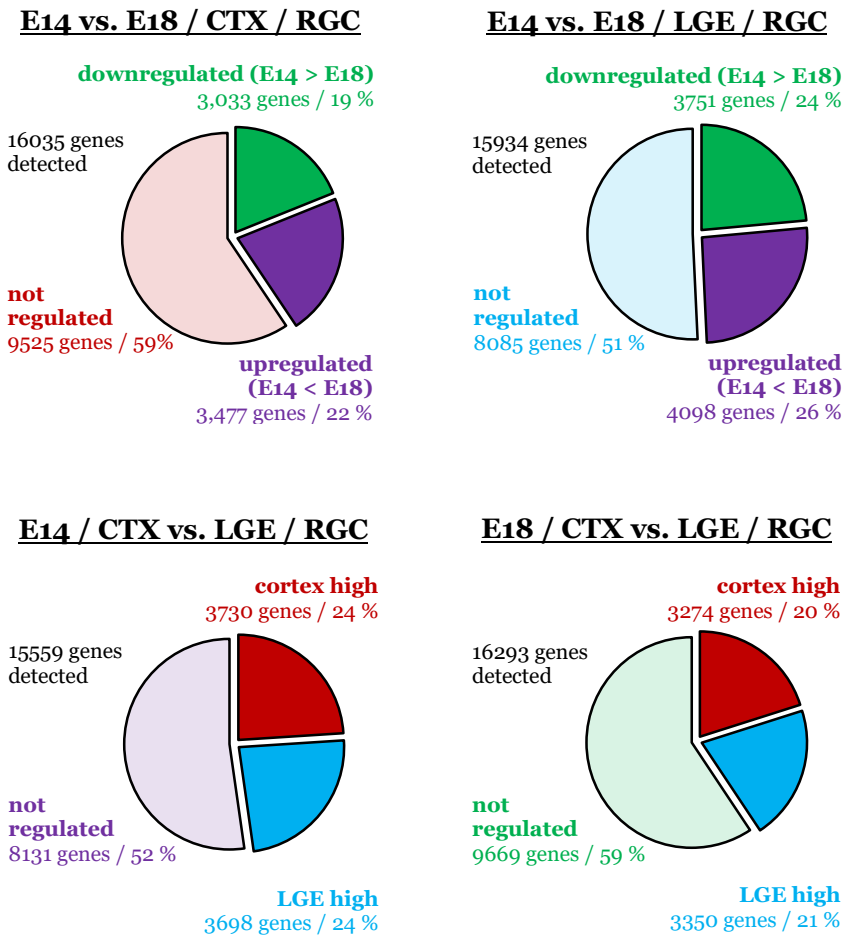

Figure 16: Number of detected and significantly (p_{adj} < 0.01) regulated genes in selected condition comparisons

Comparisons are drawn between two populations, in the presented examples either comparing different regions, i.e. cortex (CTX) or LGE, at the same time point, or different time points in the same region. All depicted analyses were done on the stem cell (RGC, radial glia cells/CD133⁺) populations.

3.2.2 Regulated expression of transcription and chromatin remodeling factors correlates to loss of stemness

To potentially prolong neurogenesis in the cortical niche, it is of great importance to understand the defining factors that separate neurogenic from gliogenic stem cells. To find factors that are very characteristic for their respective cell state, not only the scope of regulation (i.e. fold change) must be taken into account, but also the absolute transcription levels. An analysis of the most characteristic genes (performed by Dr. Pawel Smialowski; Figure 17), i.e. strongly regulated genes whose expression levels indicate biological relevance of this regulation, finds several known genes downregulated from neurogenesis to gliogenesis, such as *Neurog1*, a very well-known proneural factor (Oproescu et al. 2021). Also included are general stemness factors such as spalt-like transcription factor 4 (*Sall4*) (Sakaki-Yumoto et al. 2006) or *Hmga2* (Parisi et al. 2020). Conversely, known gliogenic or glial genes are found to be upregulated, such as *Olig1/Olig2* (Zhou and Anderson 2002) and *Gfap* (Götz et al. 2015).

Transcription factors (TF) are commonly assumed to be the governing factors of determining cell fate, not least because of their successful application in cellular reprogramming. When analyzing the function of the genes that were found to be regulated between different cell fates, it is thus no surprise that a big proportion of them are transcription factors (Figure 18A).

In addition, many of the genes that were downregulated from the more plastic state of neurogenic stem cells toward the more restricted fate of gliogenic radial glia are classified as chromatin remodelers (ChR). However, while many of the TF that are downregulated during this switch of cell identity are compensated by the upregulation of different TF, notably few chromatin remodelers seem to do the same thing (Figure 18A). This points towards a function in keeping the cells plastic and maintaining their stem cell potential, which is then lost as they, despite remaining as gliogenic stem cells, acquire a more differentiated and less plastic identity. This is especially striking when comparing the radial glia in the cortex or the LGE between peak neurogenic and gliogenic stages; however, the same, albeit smaller, effect is apparent between the radial glia in the cortex and the LGE at the same time point, which may be related to the prolonged stemness of the cells that are later to become adult neural stem cells.

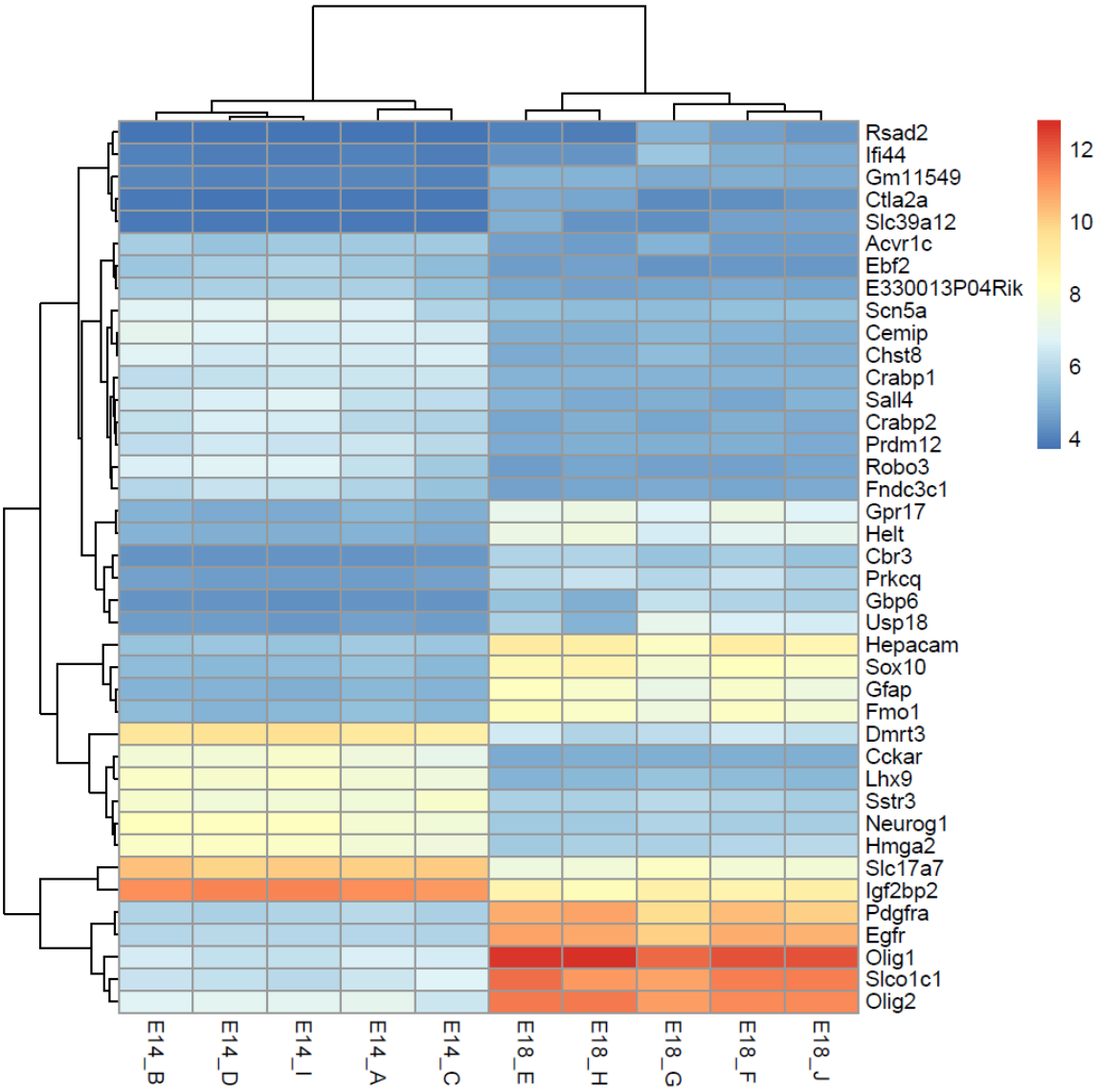

Figure 17: Most characteristic genes regulated between neurogenic and gliogenic cortical radial glia

(Analysis performed by Dr. Pawel Smialowski) Most characteristic genes that are regulated between the two cell states. Log2 fold change must be among the top 20, and the normalized read count must be higher than 45 in the upregulated condition (minimum for biological relevance), but lower than 450 (threshold for clear presence) in the downregulated condition to exclude biological relevance for both cell states.

To influence the fate switch from neurogenic to gliogenic radial glia in the developing cortex, it is important to act at the center of the transcriptomic network defining these cell states. A factor ranking analysis (performed by Dr. Pawel Smialowski; Figure 18B) reveals putative upstream regulators that govern the neurogenic stem cell state of radial glia in the cortical niche, with many other transcription factors and regulatory genes downstream of their effects. In addition to several well-known transcription factors,

such as *Neurog1* and *Neurog2* or *Bcl11b* (also known as *Ctip2*) (Oproescu et al. 2021; Lennon et al. 2017), chromatin remodelers include representatives of the ISWI (*Baz1a*, Goodwin and Picketts 2018), SWI/SNF (*Smarcd2*, Witzel et al. 2017), PRC2 (*Eed* and *Ezh2*, MuhChyi et al. 2013), and, strikingly, several enzymatic subunits of the NuRD complex, namely *Hdac1* and *Hdac2*, and *Chd3* and *Chd4* (Allen et al. 2013), as well as putative NuRD interactors *Sall1* and *Bcl11b* (Lejon et al. 2011). The genes identified by this analysis as upstream regulators are promising candidates to manipulate cell fate switches in the developing cortex.

A

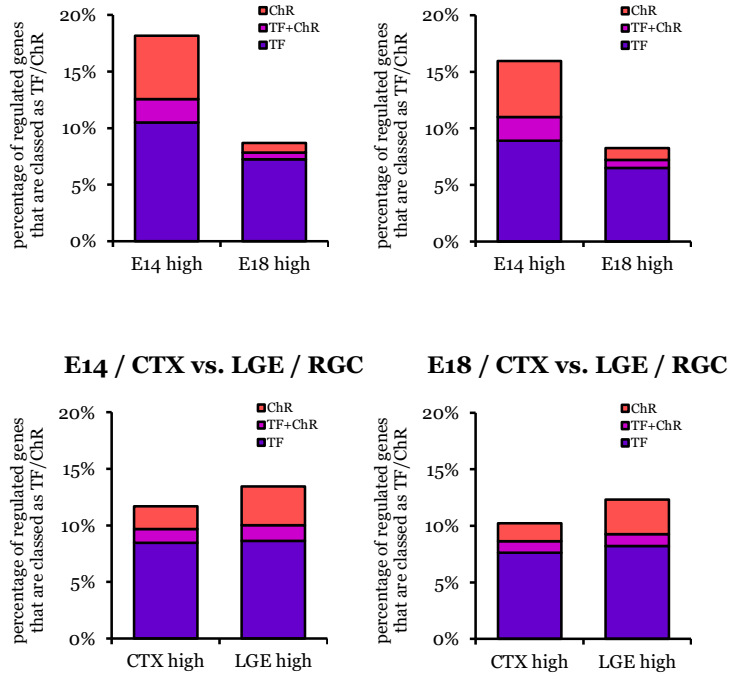

B

	transcription factors	chromatin remodelers
1	*Nfatc2*	*Eed*
2	*Neurog2*	*Hdac5*
3	*Ebf2*	*Baz1a*
4	*Baz2a*	*Smarca4*
5	*Gli3*	*Chd1*
6	*Neurog1*	*Smarca5*
7	*Tcf7l1*	*Smarcd2*
8	*Ebf3*	*Kdm1a*
9	*Emx1*	*Hdac2*
10	*Hes1*	*Ezh2*
11	*Tfap2c*	*Carm1*
12	*Foxn3*	*Cbx2*
13	*Smarcc1*	*Chd3*
14	*Foxp2*	*Chd4*
15	*Foxo6*	*Kat6b*
16	*Lin28b*	*Rnf20*
17	*Sox13*	*Suv39h1*
18	*Bcl11b*	*Hdac1*
19	*E2f3*	*Cecr2*
20	*Nhlh1*	*Ehmt1*
21	*Sall4*	
22	*Tbr1*	
23	*Foxg1*	
24	*Etv6*	
25	*Tfdp2*	
26	*Zfp536*	
27	*Etv3*	
28	*Mybl2*	
29	*Sall1*	
30	*Ssrp1*	

Figure 18: Regulation of transcription factors and chromatin remodelers is correlated to different cell states in radial glia

A. *Proportions of regulates genes that are classed as transcription factors (TF) and/or chromatin remodeling factors (ChR). The expression of chromatin remodeling genes is strongly downregulated in correlation with the loss of neurogenic stem cells.* ***B.*** *Factor ranking to determine the upstream regulators that govern the neurogenic stem cell fate in E14 cortex as compared to E18 gliogenic cortex. This analysis was performed by Dr. Pawel Smialowski.*

3.2.3 Regional differences may uncover factors that are crucial for general maintenance of neurogenesis

To understand the functional differences between the cell states more clearly, it is necessary to identify the physiological implications of a changed transcriptomic network. This was achieved by a pathway overrepresentation test, which considers the occurrence of gene ontology (GO) terms in a given set of genes compared to a reference set to find out which GO terms and pathways are exceptionally prominent in the given condition.

Not surprisingly, when this test is performed on regulated genes that distinguish neurogenic, proliferating radial glia from their gliogenic counterpart in the cortex (CTX) (Figure 19), many terms related to cell cycle, DNA replication and repair, and mRNA processing and transcription define the rapidly proliferating neurogenic radial glia. In contrast, at later gliogenic stages, GO terms related to synaptic communication as well as glial development and myelination are characteristic.

Similarly, when comparing E14 and E18 radial glia in the LGE (Figure 20), many mitotic and transcription-related terms, as well as ribosome activity related to increased translation, represent the younger radial glia. Here, the radial glia at E18 show GO terms that point towards the increasing rate of consumptive divisions in favor of ependymal cells, such as ciliary and cytoskeletal organization, adhesion and metabolic processes.

Interestingly, there is a striking difference between neurogenic radial glia in the cortex and in the LGE (Figure 21). At E14, when both regions are highly neurogenic, the LGE radial glia are again strongly characterized by terms related to proliferation and mitosis. In contrast, the functions of cortical radial glia point towards the extension and guidance of axons and dendrites, as well as synaptic communication. This is reminiscent of the comparison between early and late-stage cortical radial glia and points towards an early specification of the stem cells towards maintained stemness and plasticity in the LGE, and their loss in the cortex.

This notion is emphasized by the fact that, when comparing the regional differences at later stages (Figure 22) when there is a strong difference in terms of neurogenic potential between the cortex and LGE, the overrepresented pathways look very similar to those at E14. This again points towards an early specification to sustain (LGE) or lose neurogenic potential (cortex).

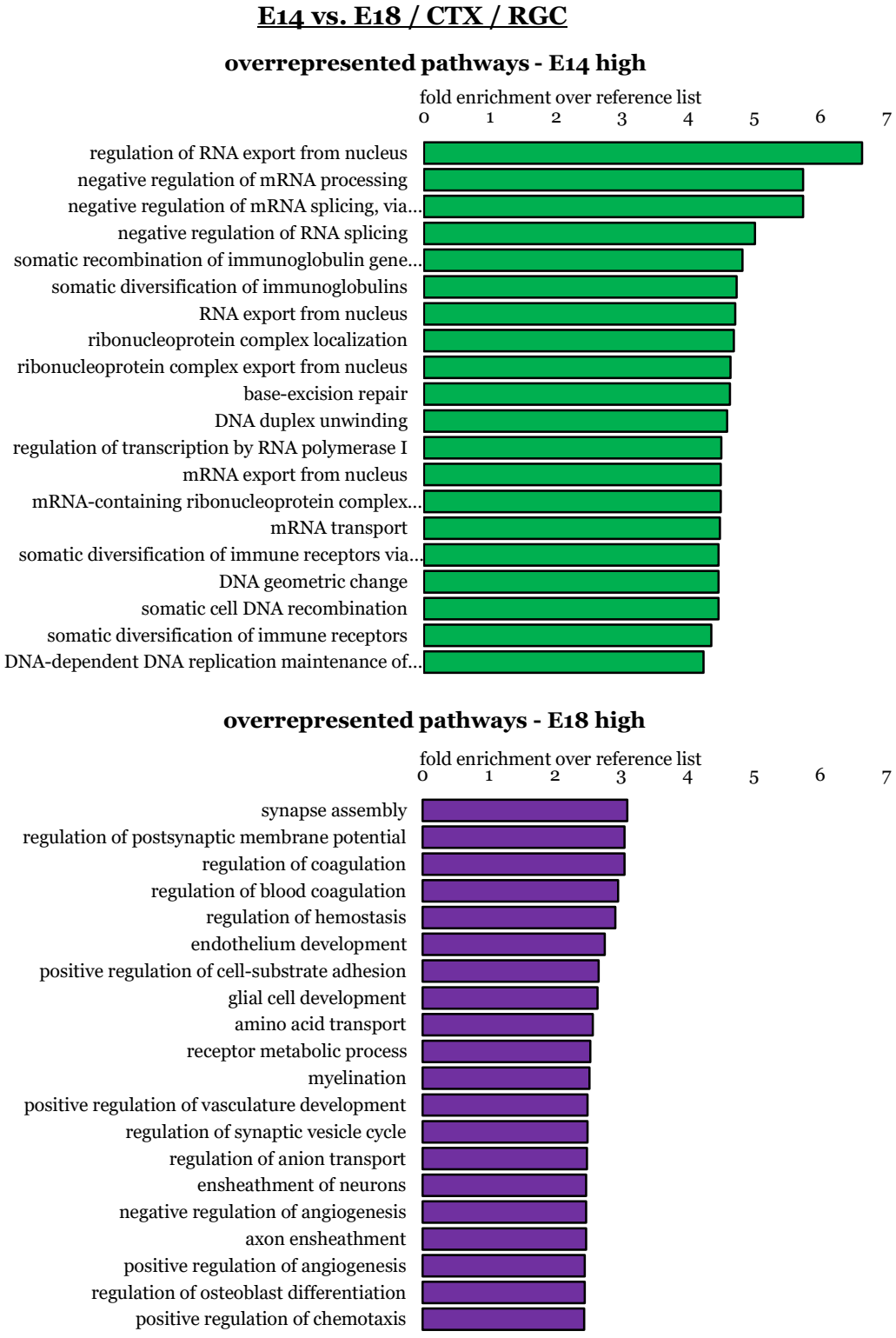

Figure 19: Pathway overrepresentation test for E14 vs E18 / CTX / RGC

Top 20 overrepresented pathways by fold enrichment (Fisher/Bonferroni, significance threshold p<0.05). In the neurogenic, proliferating RGC, most pathways are related to mitosis and transcription, while gliogenic RGC are characterized by many pathways that are related to differentiation, cell-cell contacts and communication.

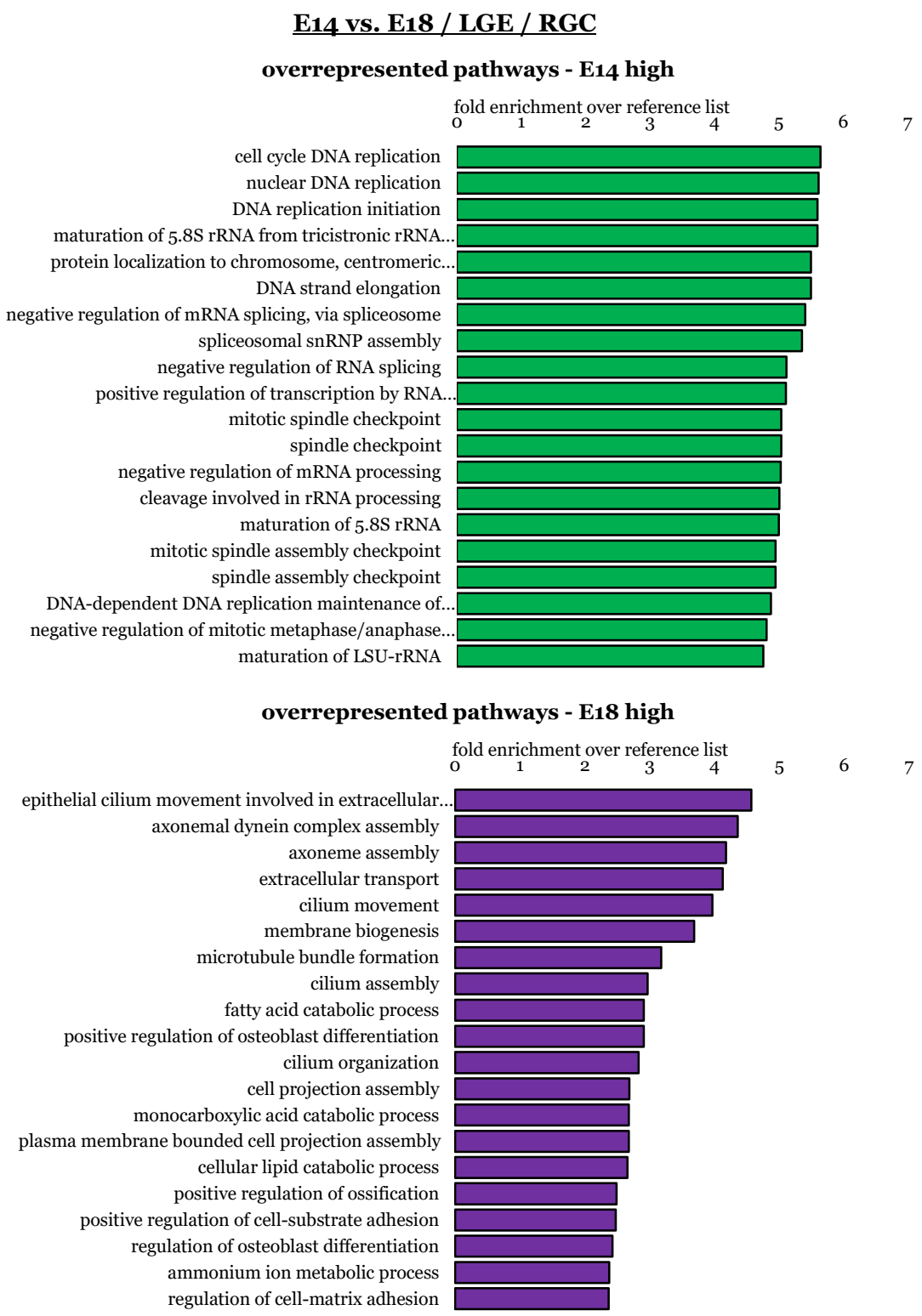

Figure 20: Pathway overrepresentation test for E14 vs. E18 / LGE / RGC

Top 20 overrepresented pathways by fold enrichment (Fisher/Bonferroni, significance threshold p<0.05). In the LGE during peak neurogenesis, the characteristic pathways for RGC are related to proliferation and mitosis. At E18, the abundance of transport- and adhesion-related pathways, as well as ciliar functions, remind of the increasing rate of consumptive divisions towards ependymal cells.

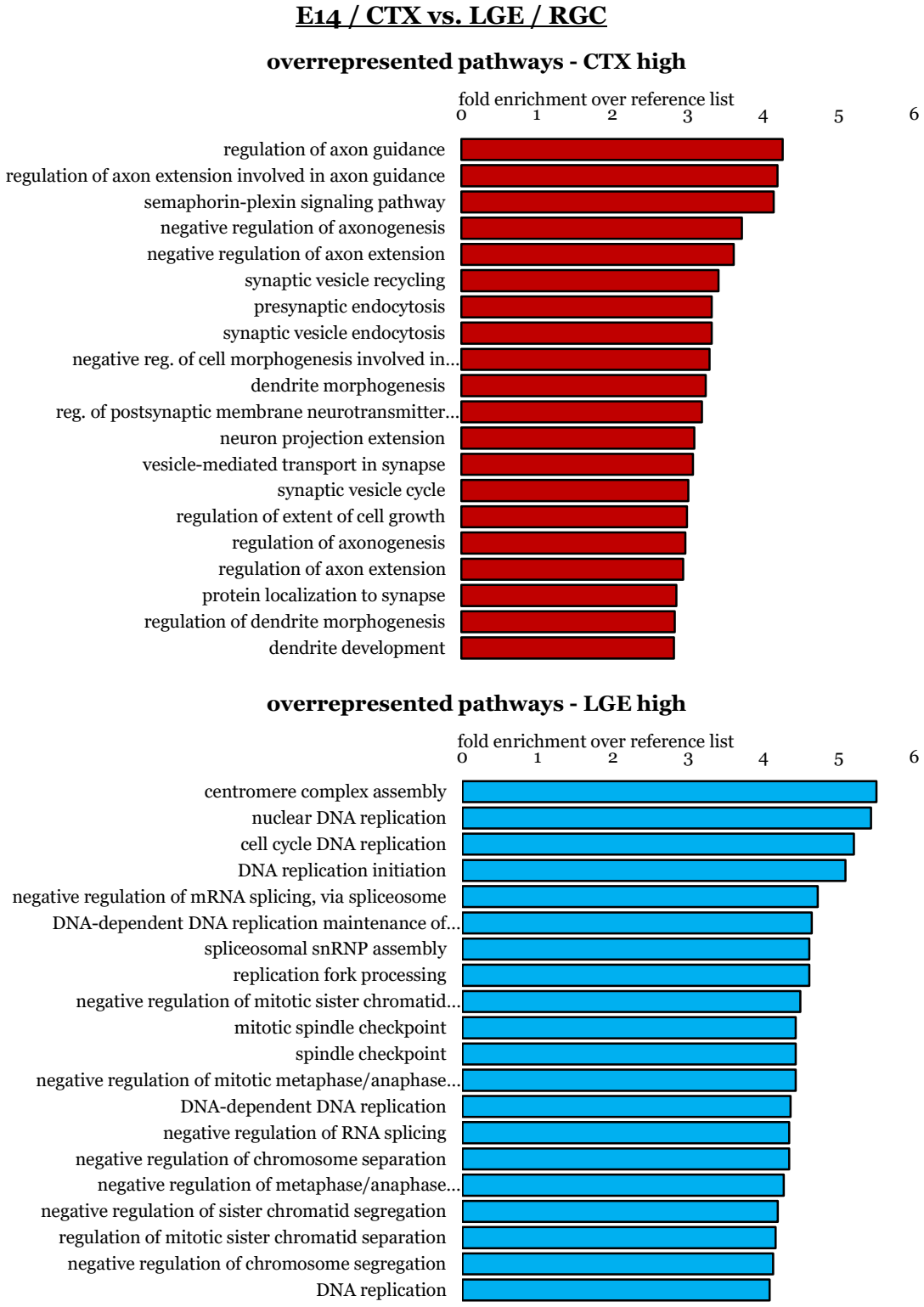

Figure 21: Pathway overrepresentation test for E14 / CTX vs. LGE / RGC

Top 20 overrepresented pathways by fold enrichment (Fisher/Bonferroni, significance threshold $p<0.05$). Even at a stage when both regions are highly neurogenic, the overrepresented pathways between the RGC in different regions suggest a more proliferative fate for the LGE RGC, while the cortical RGC focus on cell-cell communication.

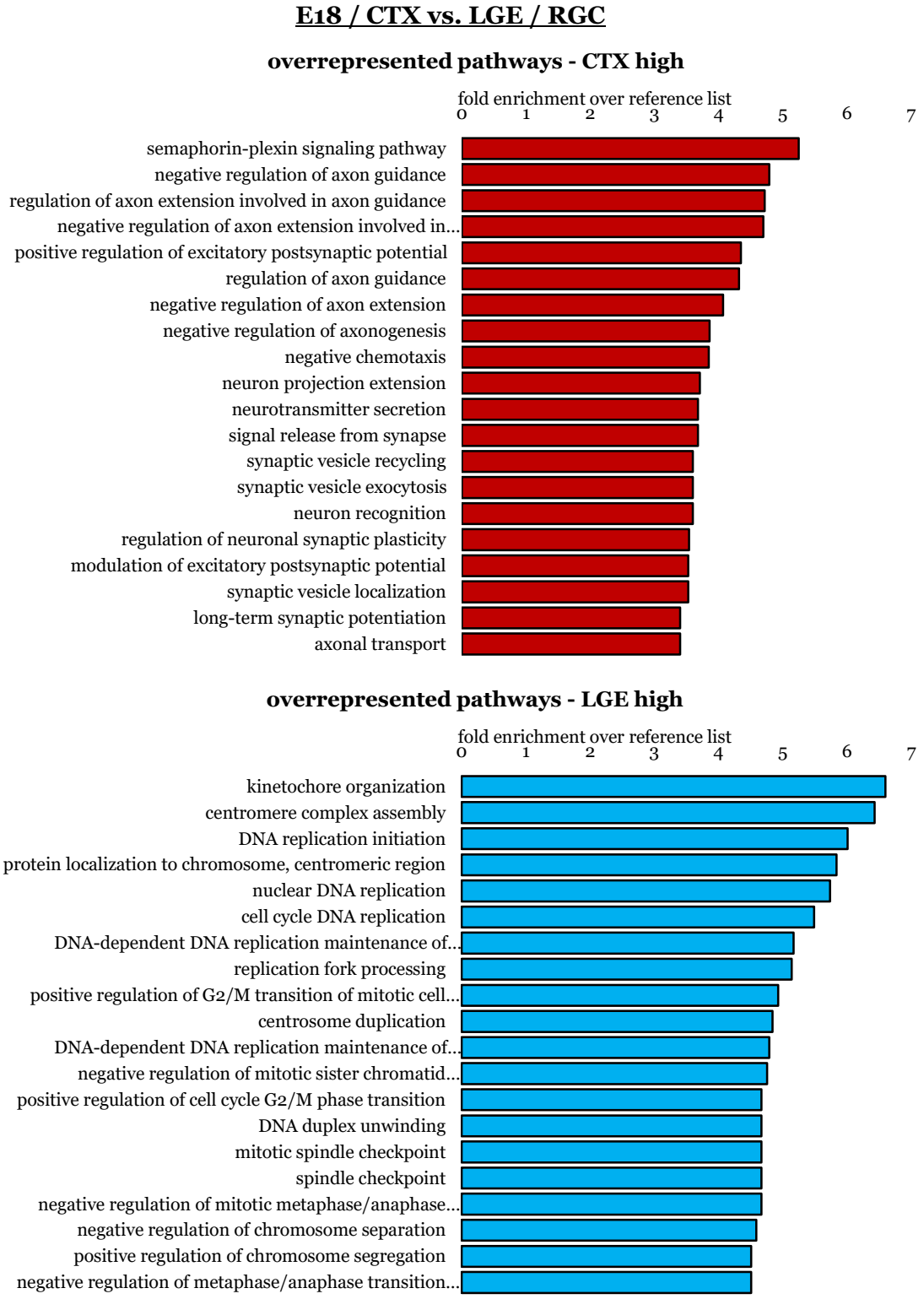

Figure 22: Pathway overrepresentation test for E18 / CTX vs. LGE /RGC

Top 20 overrepresented pathways by fold enrichment (Fisher/Bonferroni, significance threshold p<0.05). At later stages, when neurogenic potential is very different between the two regions, the functional implications suggested by the pathway analysis are strikingly similar to earlier stages.

If these determinants of neurogenic stem cell fate already occur very early in development, it is necessary to not only look at cortical gene expression in neurogenic stages to find the difference to gliogenic radial glia. A comparison with differentially regulated genes between early-stage radial glia in different regions may then uncover factors that define the long-term maintenance of stemness and neurogenic potential very early on and thus represent essential factors for general neurogenesis. As determined before (Figure 18), these fate determinants are likely to come from the pool of transcription factors and chromatin remodelers that are available to the cell during this time.

Lists of regulated transcription factors and chromatin remodelers were overlapped to identify these factors (Figure 23). First, the genes that are regulated between still partly neurogenic LGE and gliogenic cortex at E18 were determined to be important for maintained neurogenic potential. Several of these are however already different at E14 and may include factors that define local patterning and neuronal subtypes, not neurogenic potential, so these were excluded. The remaining genes – i.e. regionally different at E18, but not at E14 – were then overlapped with the factors regulated between neurogenic and gliogenic cortical radial glia, to confirm their putative effect on neurogenic potential in cortical radial glia.

The resulting list of 37 genes, 33 transcription factors and 8 chromatin remodelers, 4 of which fall into both categories according to their GO terms, contains several genes that were already determined to be important for neurogenesis by the upstream factor ranking (Figure 18), namely transcription factors *Etv6*, *Bcl11b* (*Ctip2*), *Tcf7l1*, *Foxp2* and *Zfp536*, and chromatin remodeler *Baz1a*. These genes may be promising to examine in order to find factors that govern the general maintenance of stemness and neurogenic potential.

A

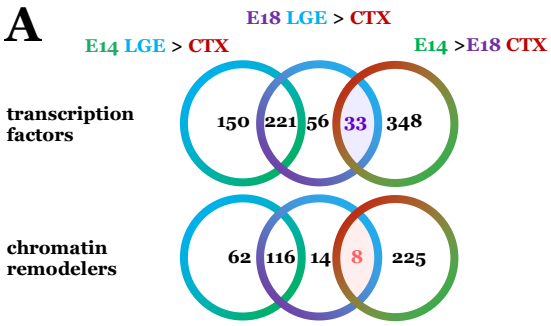

B

	E18 LGE vs. CTX			E14 vs. E18 CTX		
	base mean	fold change	p_{adj}	base mean	fold change	p_{adj}
Bcl11b	3100	3,6	1,5E-44	5945	7,9	1,1E-187
St18	537	7,9	1,0E-46	484	7,1	1,2E-40
Hif3a	214	3,1	2,3E-21	310	4,9	5,4E-31
Tcf7l1	495	1,6	1,4E-05	980	4,1	2,1E-27
Id4	3683	2,1	1,4E-17	5777	3,8	1,2E-28
Tgif1	160	1,8	1,8E-04	255	3,4	5,3E-16
Sox5	1865	1,2	2,0E-04	3657	3,3	2,6E-46
Dach1	470	1,7	8,4E-06	695	3,1	6,8E-15
Sfrp4	42	1,8	2,1E-03	50	2,3	1,3E-07
Nfatc4	625	1,5	7,0E-03	828	2,3	2,0E-08
Atf3	35	3,4	9,4E-07	23	2,0	4,5E-03
Foxp2	651	1,7	1,0E-07	700	1,9	7,9E-20
Yap1	578	1,4	7,1E-04	682	1,9	1,4E-07
Zbtb16	60	1,7	2,3E-03	62	1,8	7,4E-04
Zfp536	1267	1,4	7,3E-08	1461	1,7	3,7E-14
Six5	164	1,6	2,0E-05	172	1,7	3,5E-07
Etv6	697	1,2	2,0E-03	831	1,7	2,1E-11
Fzd2	2368	1,5	5,5E-07	2552	1,7	1,0E-09
Myt1	1830	1,2	1,9E-03	2116	1,5	2,5E-12
Klf13	1669	1,3	2,9E-06	1850	1,5	5,4E-20
Btg2	2894	1,5	1,2E-06	2945	1,5	3,9E-05
Flna	10354	1,3	1,5E-03	11108	1,4	8,8E-06
Tacc1	1437	1,4	3,4E-06	1439	1,4	3,2E-05
Sp1	917	1,2	7,2E-05	952	1,3	7,6E-06
Ncoa2	1360	1,2	1,0E-03	1427	1,3	6,0E-10
Zfp280c	594	1,2	2,0E-04	595	1,3	8,0E-05
Arl2bp	4201	1,2	7,2E-03	4254	1,2	1,6E-03
Med22	2363	1,2	2,3E-05	2351	1,2	1,2E-06
Hipk1	1684	1,4	7,8E-07	1522	1,1	4,2E-03
Prkd1	871	1,4	2,2E-04	912	1,5	9,7E-05
Kdm3a	3205	1,2	2,1E-03	3612	1,5	9,1E-13
Bcor	1189	1,2	2,6E-03	1315	1,5	1,0E-11
Trim37	4752	1,2	8,5E-05	4703	1,1	1,6E-03
Zfp521	674	1,7	1,7E-16	1117	3.5	3,3E-62
Baz1a	534	1,2	3,8E-04	743	2,1	2,7E-23
Arid1a	3171	1,2	1,2E-03	3303	1,3	4,5E-05
Atxn3	595	1,3	1,6E-05	574	1,3	1,3E-03

TF
ChR
classified as both

Figure 23: Identifying factors that may be important for general maintenance of neurogenesis

A. *Overlaps between gene lists reveal factors that may be important for region-independent, general maintenance of neurogenic potential. 33 transcription factors and 8 chromatin remodelers were identified.* ***B.*** *Regulation and expression of the identified factors between gliogenic cortical RGC and their neurogenic counterparts.*

3.3 PITFALLS OF GENOMIC INTEGRATION VIA PIGGYBAC TRANSPOSON IN DEVELOPING MOUSE BRAIN

Declaration of author contributions: *Plasmids were provided by the following contributors: pCAG-PBase, Dr. Germán Camargo Ortega; pCMV-mPB, Rebeca Sánchez González; piggyBac-GFP, Dr. Miriam Esgleas Izquierdo; piggyBac-dCas9-GFP, Dr. Anna Köferle. qRT-PCR primers for UPR genes were provided by Dr. Sonia Najas Sales. mNPC cultures were provided by Andrea Neuner. All contributions are detailed in the Declaration of Author Contributions on page XXXIV.*

3.3.1 Genomic integration of piggyBac transposon by the non-mouse codon optimized PBase leads to a phenotype of ectopia and malformations in the developing mouse brain

Genomic integration of effector sequences is a powerful tool to ensure stable and continuous expression in the target cells. This is especially important in rapidly proliferating cells, such as the neurogenic radial glia, to avoid dilution of constructs by repeated cell divisions. Integration can be achieved by the piggyBac transposon system with its specific transposase, which is available in multiple variants (see also Chapter 2.4.1).

To test the feasibility of the system for experimental application, IUE was performed at E13 with different piggyBac plasmids and either PBase, the original enzyme from *Trichoplusia ni*, or mPB, the same enzyme with a mouse-codon optimized nucleotide sequence (Cadiñanos and Bradley 2007) (Figure 24A, B).

Three days post-IUE, at E16, some brains showed abnormal developmental phenotypes (Figure 24C) of varying severity. These are categorized into different severity levels: no abnormalities; ectopic cells, where $PAX6^+$ and/or $TBR2^+$ cells are located outside their respective niches in the VZ and SVZ; hyperplasia, with an increase of tissue only at the electroporation site; and severe malformations, where an anatomic effect could be observed even outside of the electroporation site.

At E16, IUE of *piggyBac-dCas9-GFP* together with PBase led to the ectopic localization of $PAX6^+$ and $TBR2^+$ cells in the IZ in all examined embryos. This effect seemed to be non-cell autonomous, as the ectopic marker expression did not necessarily colocalize

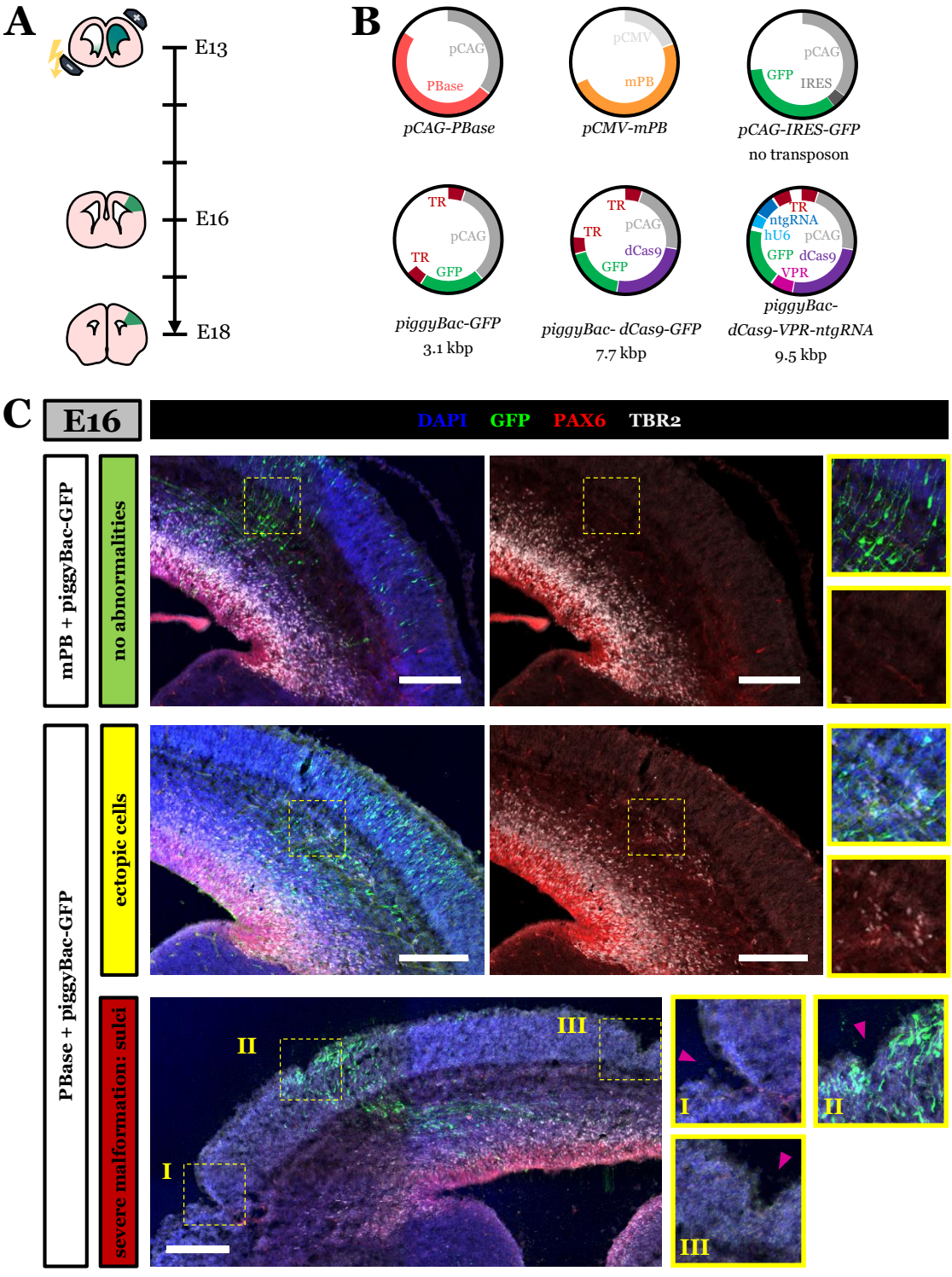

Figure 24: Transposon integration by PBase causes ectopia and malformations in the developing mouse brain after three days

A. *Experimental schematic of piggyBac transposon delivery.* ***B.*** *Plasmid constructs and their transposon size.* ***C.*** *Representative fluorescence confocal images of E16 mouse brain with IHC for GFP, PAX6 and TBR2. Varying phenotypes caused by PBase and mPB three days post-IUE range from normal development to anatomical malformation. (Scale bars = 200 µm)*

with GFP expression. When *piggyBac-GFP* was used together with PBase, the phenotype became much more varied, with some brains developing normally, while others developed ectopia or more severe anatomical malformations, in one case resulting in sulcus-like structures at and farther away from the electroporation site (Figure 24C).

Interestingly, this effect was abolished in the absence of a transposon, as a co-electroporation of PBase and *pCAG-IRES-GFP* did not result in any abnormalities in the examined embryos (Figure 25B).

To observe if these developmental defects would ameliorate over time, the analysis was extended to E18, five days post-IUE (Figure 25A). However, at this stage the phenotypes of PBase with *piggyBac-GFP* were strongly exacerbated, with five of seven animals showing severe malformations and none of them showing a normal phenotype (Figure 25A, B). These abnormalities ranged from ectopia and localized hyperplasia to the most typical malformation, which resembles folding or wrinkling of the brain. In one animal, the septum was underdeveloped, leading to the formation of one large ventricle instead of to separate lateral ventricles.

These phenotypes were ameliorated to a large part when mPB was used instead of PBase (Figure 24B, Figure 25). At E16, co-electroporation of mPB and *piggyBac-GFP* resulted in a normal phenotype in most of the brains, with few showing ectopia, but no hyperplasia or malformations. At E18, the phenotype was again exacerbated compared to the earlier time point, with hyperplasia or malformation present, but a large proportion (four of seven animals) still without visible abnormalities. Interestingly, when co-electroporated with *piggyBac-dCas9-VPR-ntgRNA* (see chapter 3.4.1 and Figure 28B), none of the four analyzed animals showed any abnormalities at E18.

The integration of the piggyBac transposon by the original transposase enzyme PBase can thus lead to detrimental effects and developmental abnormalities, depending on the respective transposon. This phenotype is largely ameliorated by the use of the mouse codon-optimized variant mPB. While still causing some developmental phenotypes, they appear at a much lower rate and decreased severity. mPB thus lends itself better to *in vivo* application in the developing mouse brain, which emphasizes the importance of codon optimization.

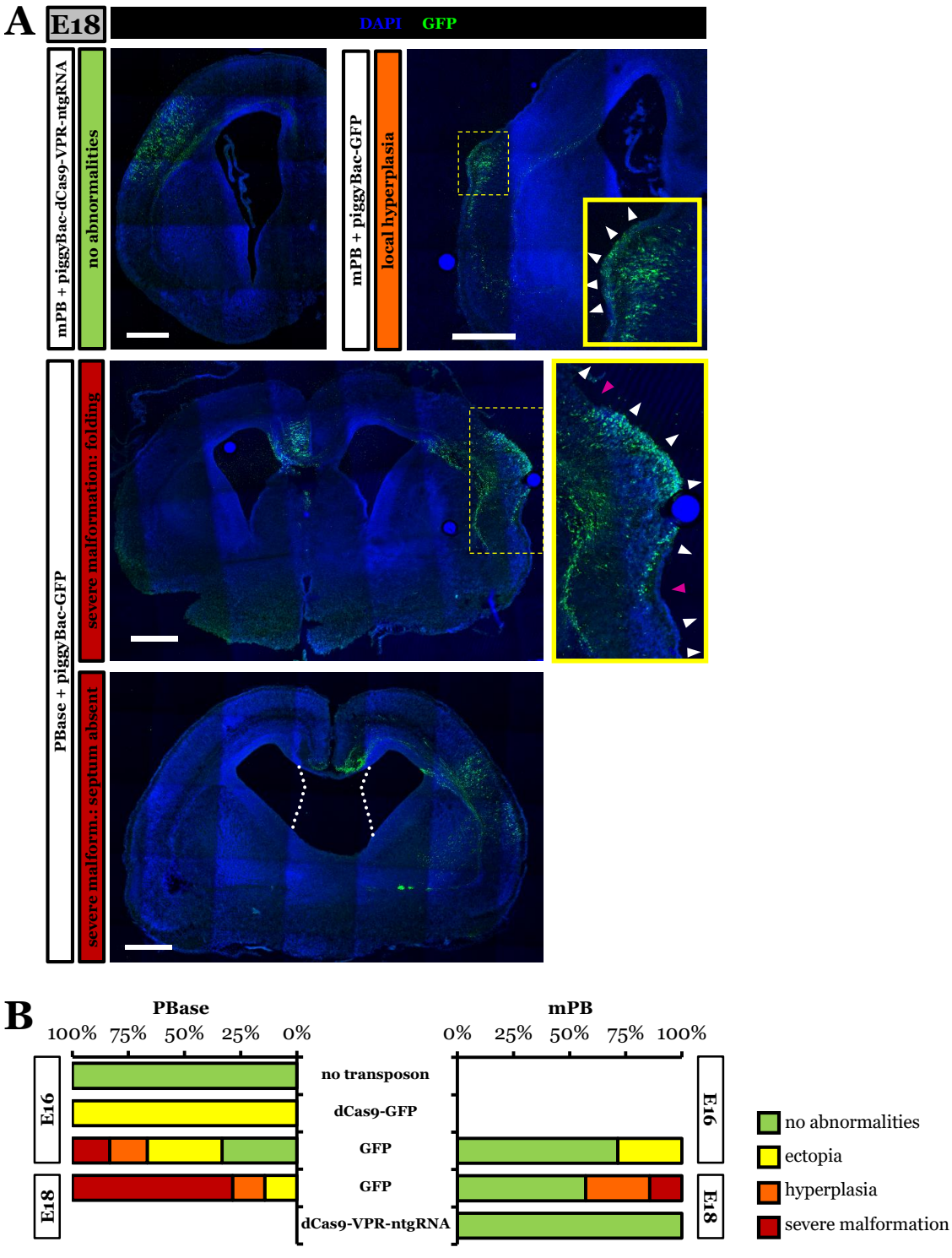

Figure 25: Exacerbated phenotypes after PBase-mediated transposition at five days post-IUE

A. *Representative fluorescence confocal images of E16 mouse brain with IHC for GFP, PAX6 and TBR2. Phenotypes five days post-IUE range from normal development to gross anatomical malformations. (Scale bars: 500 µm)* ***B.*** *Overview of the rate of abnormalities for different treatments. n=6 for PBase + GFP (E16), PBase + dCas9-GFP, and PBase + no transposon; n=7 for mPB + GFP (E16), mPB + GFP (E18), and PBase + GFP (E18); n=4 for mPB + dCas9-VPR-ntgRNA.*

3.3.2 Exploring possible causes for the differential effects of PBase/mPB

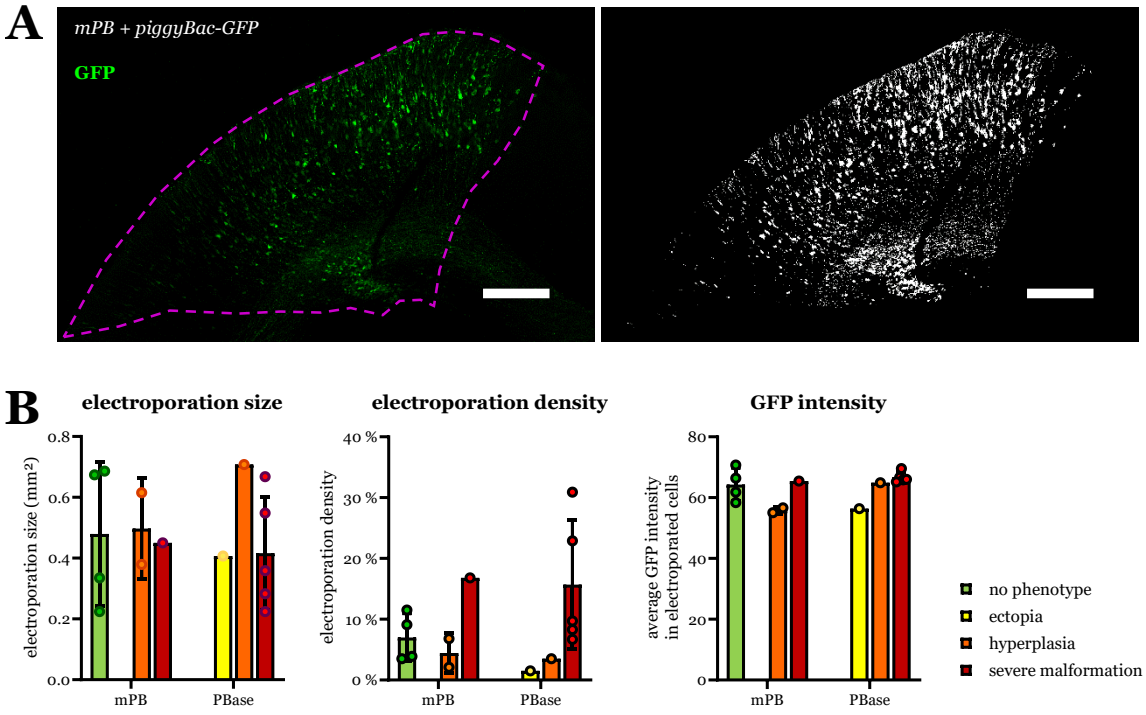

Figure 26: Electroporation size and density and GFP signal intensity in IUE brains with different phenotypes at E18

Fluorescent confocal images with IHC for GFP in E18 mouse brains, electroporated with piggyBac-GFP and PBase or mPB, were analyzed. ***A.*** *The area of electroporation was measured, and a thresholded mask was used to determine the area of GFP⁺ cells within the electroporation area (density). The mask was applied to the original image to measure average GFP intensity in electroporated cells. (Scale bars: 200 µm)* ***B.*** *Electroporation size, density and GFP intensity in different phenotypes and treatments.*

To determine a possible cause underlying the developmental abnormalities, the electroporation size and density as well as the GFP signal intensity were analyzed in E18 brains electroporated with PBase/mPB + *piggyBac-GFP* (Figure 26). Neither the electroporation size nor the GFP intensity seemed to be correlated to the severity of the phenotype. An increased electroporation density, i.e. the number of electroporated cells per area, was observed on the most severe phenotype. However, whether this is causal – i.e. more cells targeted during the electroporation leading to stronger effects – or a secondary effect of ectopic PAX6⁺/TBR2⁺ cells possibly proliferating, remains unclear.

Next, the effect on a cellular level was examined. As the non-codon optimized sequence of PBase is transcribed less effectively than a codon-optimized or endogenous one, this can lead to problems in the transcription machinery, such as ribosome collisions and the

ribotoxic stress response (RTR), which may ultimately lead to apoptosis (Wu et al. 2020). This impaired translation may also cause misfolding of the resulting proteins eliciting an unfolded protein response (UPR), which can not only lead to cell death, but its regulation has been linked to the regulation of neurogenesis (Cao and Kaufman 2012; Godin et al. 2016). Finally, the transposon integration itself, or incomplete or faulty transposition, might elicit DNA damage response (DDR), which may affect the cell cycle and also induce apoptosis (Sirbu and Cortez 2013; Li, G. M. 2013; Maréchal and Zou 2013; Ciccia and Elledge 2010).

To examine the phenotypes elicited by PBase, and find possible mechanisms by which the non-mouse codon optimized transposase acts differently on the cells than the mouse codon-optimized mPB, murine neural progenitor cells (mNPC) were used as an *in vitro* model system. These cells are prepared from embryonic cortex and stably retain a neural progenitor cell identity in culture (Pollard et al. 2006).

The cells were transfected with different combinations of PBase/mPB and *piggyBac*, or *piggyBac* alone, and the drug tunicamycin was used as a positive control for the UPR (Godin et al. 2016). Transfected cells were isolated by FACS three days post-transfection and gene expression was analyzed by qRT-PCR. (Figure 27A).

The expression of mPB in the cells was much higher than that of PBase (Figure 27B), as stated elsewhere (Cadiñanos and Bradley 2007), despite a putatively stronger promoter used in the PBase plasmid (Figure 24B). However, despite upregulation of UPR markers by the positive control tunicamycin, no regulation of genes related to RTR (Figure 27C), UPR (Figure 27D) or DDR (Figure 27E) were found in any of the transfection conditions, concluding that these pathways are not causal for observed phenotypes.

The exact mechanism that causes the phenotypic response of PBase/mPB-mediated transposon integration in the developing brain thus remains elusive for now.

Figure 27: mNPC as model for the cellular effects of PBase/mPB-mediated transposon integration *[see next page]*

A. *Experimental paradigm for transfecting mNPC with different plasmid combinations. Transfection itself had a similar effect on cell survival and morphology as Tunicamycin. (brightfield and fluorescent images taken directly before FACS, scale bars: 20 µm)* ***B.*** *qRT-PCR analysis for expression levels of PBase and mPB in mNPC upon transfection.* ***C.*** *Expression of selected marker genes for RTR,* ***D.*** *UPR and* ***E.*** *DDR. (Mean ± S.D.; n=5 for untransfected and mock transfection; n=4 for untransfected + Tunicamycin, PBase + GFP, mPB + GFP, and GFP; n=3 for PBase + dCas9-GFP and mPB + dCas9-GFP; n=2 for dCas9-GFP)*

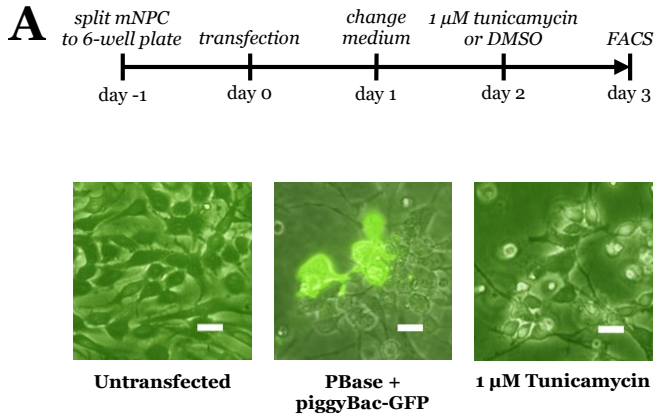
A
split mNPC to 6-well plate
transfection
change medium
1 µM tunicamycin or DMSO
FACS
day -1
day 0
day 1
day 2
day 3
Untransfected
PBase + piggyBac-GFP
1 µM Tunicamycin

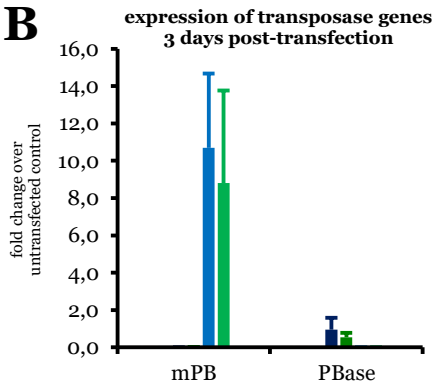
B
expression of transposase genes
3 days post-transfection
fold change over untransfected control
16,0
14,0
12,0
10,0
8,0
6,0
4,0
2,0
0,0
mPB
PBase

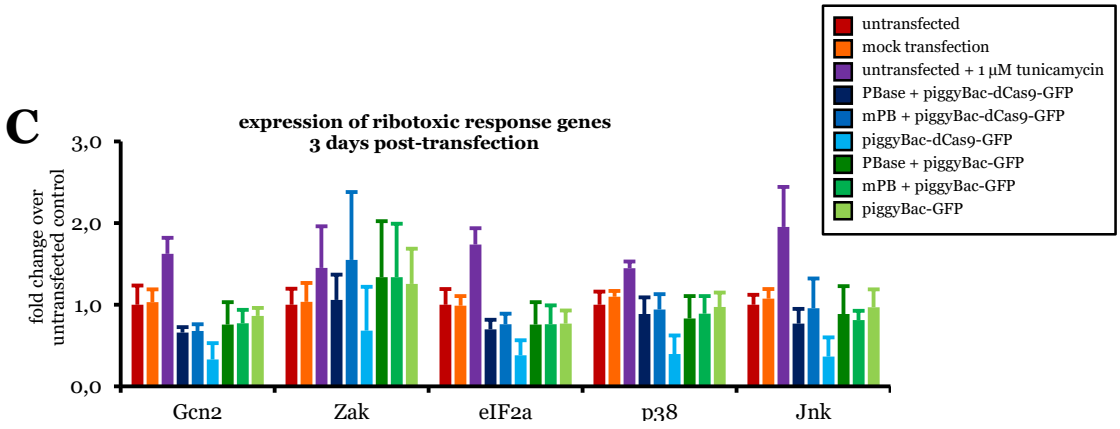
C
expression of ribotoxic response genes
3 days post-transfection
fold change over untransfected control
3,0
2,0
1,0
0,0
Gcn2
Zak
eIF2a
p38
Jnk
untransfected
mock transfection
untransfected + 1 µM tunicamycin
PBase + piggyBac-dCas9-GFP
mPB + piggyBac-dCas9-GFP
piggyBac-dCas9-GFP
PBase + piggyBac-GFP
mPB + piggyBac-GFP
piggyBac-GFP

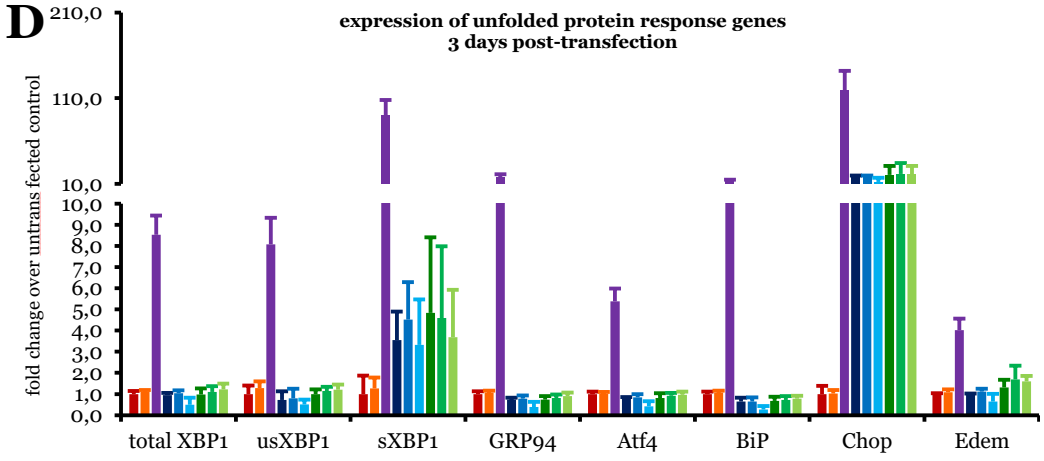
D
expression of unfolded protein response genes
3 days post-transfection
fold change over untrans fected control
210,0
110,0
10,0
10,0
9,0
8,0
7,0
6,0
5,0
4,0
3,0
2,0
1,0
0,0
total XBP1
usXBP1
sXBP1
GRP94
Atf4
BiP
Chop
Edem

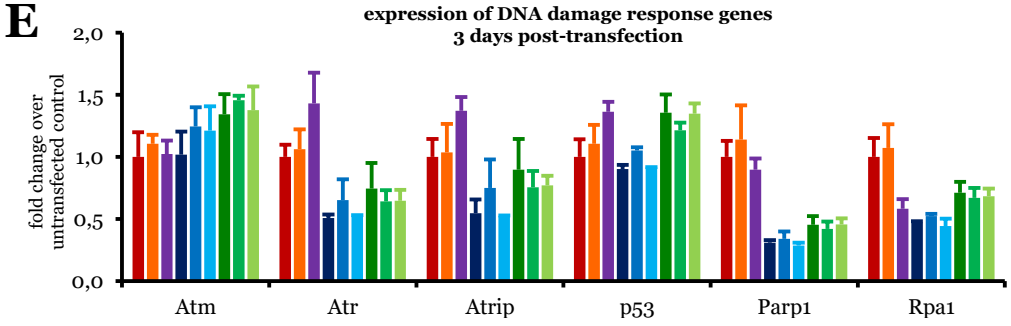
E
expression of DNA damage response genes
3 days post-transfection
fold change over untransfected control
2,0
1,5
1,0
0,5
0,0
Atm
Atr
Atrip
p53
Parp1
Rpa1

3.4 CONCURRENT ACTIVATION OF FATE DETERMINING FACTORS TO PROLONG NEUROGENIC POTENTIAL IN THE DEVELOPING MOUSE CORTEX

Declaration of author contributions: *Plasmid systems were developed and gRNA sequences chosen by Dr. Christopher Breunig and 4xgRNA cassettes subcloned in collaboration with Manpreet Kaur. The pcDNA-CMV-GFP-CMV-dCas9-VPR plasmid was kindly provided by Dr. Christopher Breunig and the pCMV-mPB plasmid by Rebeca Sánchez González. qRT-PCR primers for some of the candidate genes were provided by Dr. Stefan Stricker. All contributions are detailed in the Declaration of Author Contributions on page XXXIV.*

3.4.1 Establishing a system to concurrently manipulate the expression of multiple neurogenic factors

To change a transcriptomic network, it may be necessary to manipulate not only one, but several factors to achieve sufficient impact on the entire system. This is especially important to consider for genes that are part of a complex, like many chromatin remodelers, which may compensate for the manipulation of just one of its components. To prolong neurogenic potential in cortical stem cells, a promising approach is thus to activate several neurogenic and stem cell factors simultaneously to achieve a transcriptomic switch.

The approach to concurrently manipulate the expression of several factors is made possible by employing a dCas9-VPR fusion protein system, a strong transcriptional activator (Chavez et al. 2015), together with a multiplexing approach called STAgR (Breunig et al. 2018) that allows the generation of plasmids with up to eight gRNAs. This provides a powerful system for transcriptomic network manipulation.

To deliver the activation system into radial glia in vivo, with the goal of prolonging neurogenesis, it is necessary to use a system that genomically integrates the gRNA and activator sequences. A non-integrating systems would dilute over several cell divisions, which would be especially disadvantageous if a continued neurogenesis is indeed achieved, but then dampened again by loss of activation due to increased proliferation.

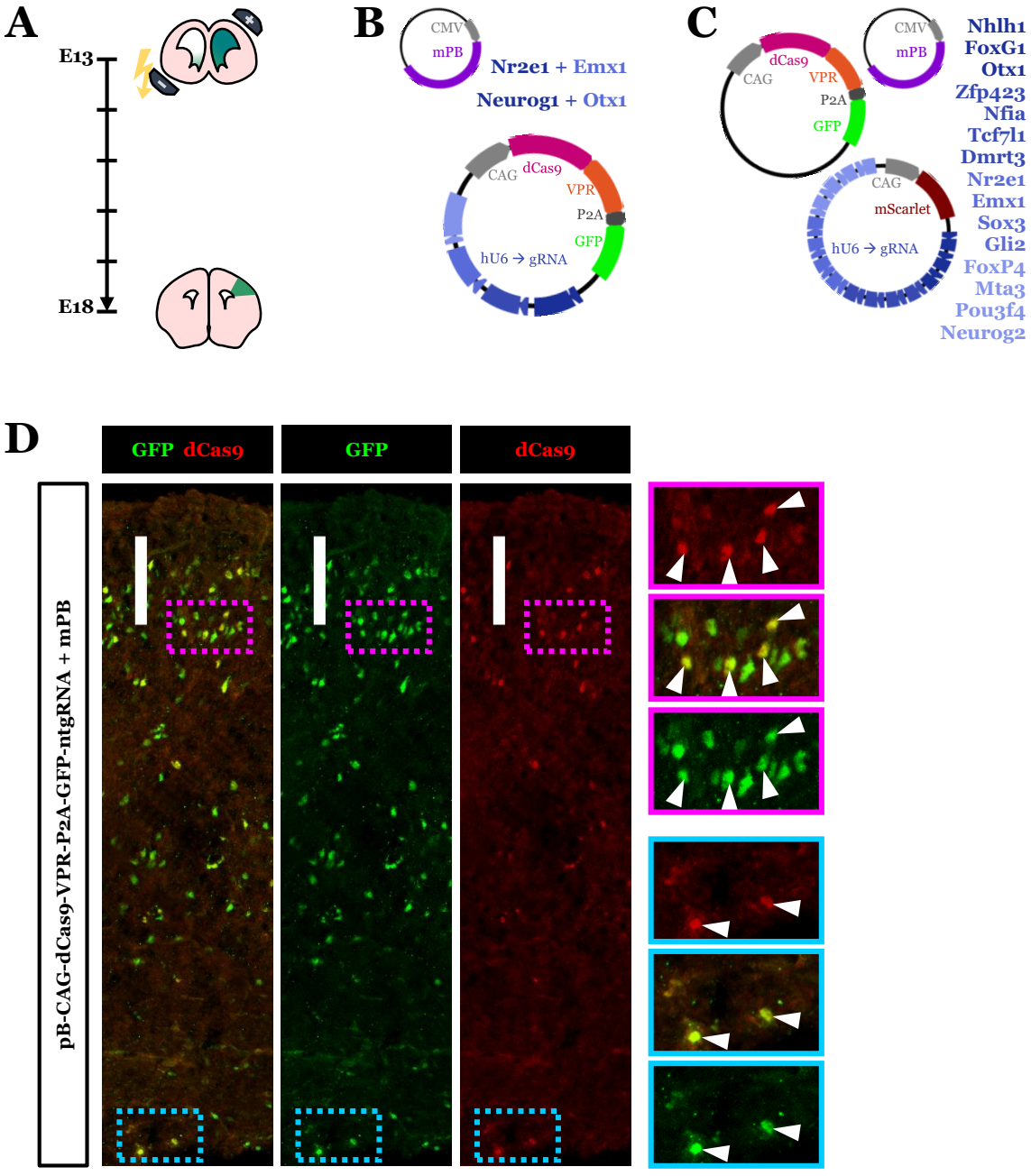

Figure 28: Multiplexing of gRNAs and dCas9-VPR into one piggyBac plasmid is a suitable delivery system for *in vivo* application

A. *Experimental paradigm of concurrent neurogenic factor application* in vivo. ***B.*** *Delivery system with dCas9-VPR and multiple gRNAs encoded in one integrating piggyBac transposon.* ***C.*** *Multiplexed vector with 15 gRNAs requires a two-plasmid system, with different reporters encoded on each piggyBac.* ***D.*** *Fluorescence confocal images of E18 mouse brain after IHC for GFP and dCas9. Application of the piggyBac system in vivo leads to expression of dCas9 protein in electroporated cells five days post-IUE. (Scale bars: 100 µm)*

The piggyBac transposon system lends itself to this purpose, as it can easily be delivered by IUE and can effectively transpose even large sequences (Ding et al. 2005; Li, M. A. et al. 2011). A piggyBac vector, encoding a dCas9-VPR fusion protein coupled to the GFP reporter by self-splicing P2A peptide (Liu et al. 2017) and the gRNA cassette in one plasmid, is used together with the transposase mPB (Figure 28B; see also Chapter 3.3). This system is applied *in vivo* by IUE at E13 during peak neurogenesis. At E18, the expression of dCas9 protein in electroporated was confirmed by immunohistochemistry (Figure 28D), thus allowing for transcriptomic activation with this system in the targeted cell *in vivo*.

Candidate genes were selected from a microarray previously performed in the lab (Pinto et al. 2008) as well as the transcriptomic data detailed in this thesis. To find candidate gRNAs with a suitable activation potential, two gRNAs for each gene were tested together in P19 cells by transfecting their STAgR plasmids together with a plasmid containing dCas9-VPR. Combinations were picked by putative gene function to neither contain too much of a proliferative nor neurogenic potential, to avoid uncontrolled proliferation and tumor formation on one hand, and premature differentiation of radial glia to neurons on the other hand. Rather, these two functions should be combined to achieve neurogenic cells with proliferative capacity, i.e. putative neurogenic stem cell-like cells.

In addition to combinations of two genes (with two gRNAs each, Figure 28B), a multiplexed vector containing gRNAs for 15 genes (one gRNA per gene, Figure 28C) was used. Due to the large size of this multiplex, the system is divided into two piggyBac plasmids, one containing the gRNA sequences and the other encoding the dCas9-VPR, with different fluorophores, that are transfected or electroporated together with mPB.

3.4.2 Effects of concurrent gene activation in vivo on neurogenesis and the neurogenic-to-gliogenic switch

To assess whether the concurrent activation of several of the candidate genes has a prolonging effect on neurogenesis or influences the neurogenic switch, the activation constructs were delivered by IUE at E13 during peak neurogenesis (experimental schematic see Figure 28A). To get a first idea whether this system could influence the cell fate progression, the analysis was performed five days post-IUE at E18, when the neurogenic-to-gliogenic switch has just occurred, to see if any effects on the physiological succession of neurogenesis are present, and if neurogenesis is still active at this stage.

Embryonic cortices at E18 were co-stained for the electroporated cells (GFP^+ or $GFP^+mScarlet^+$, respectively; see plasmid schematics in Figure 28B, C) and cell type markers PAX6 for neurogenic stem cells (Figure 29), TBR2 for intermediate progenitors, and KI-67 to assess the cell cycle activity (Figure 30).

The cells were quantified in five equidistant bins and the distribution of electroporated cells was examined, which gives a gross overview of cell types by expected localization (Figure 31A). Here, the activation of *Nr2e1* + *Emx1* leads to a significant (p=0.02) enrichment of cells in bin 2, representing the SVZ and IZ, where intermediate progenitors and migrating immature neurons would reside, hinting at either migration defects or impairment, retarded progression of neurogenesis, or a continuation of neurogenesis at this time point.

Activation of *Neurog1* + *Otx1* seemed to show, albeit not significantly, a slight reduction of the proportion of electroporated cells in the VZ (bin 1) and enrichment in deep-layer CP (bin 4) (Figure 31A). As the deep layers are first generated during neurogenesis, followed by the upper layers, this may hint at an adverse effect of initially accelerated differentiation or migration, and thus a depletion of the stem cell pool at the VZ.

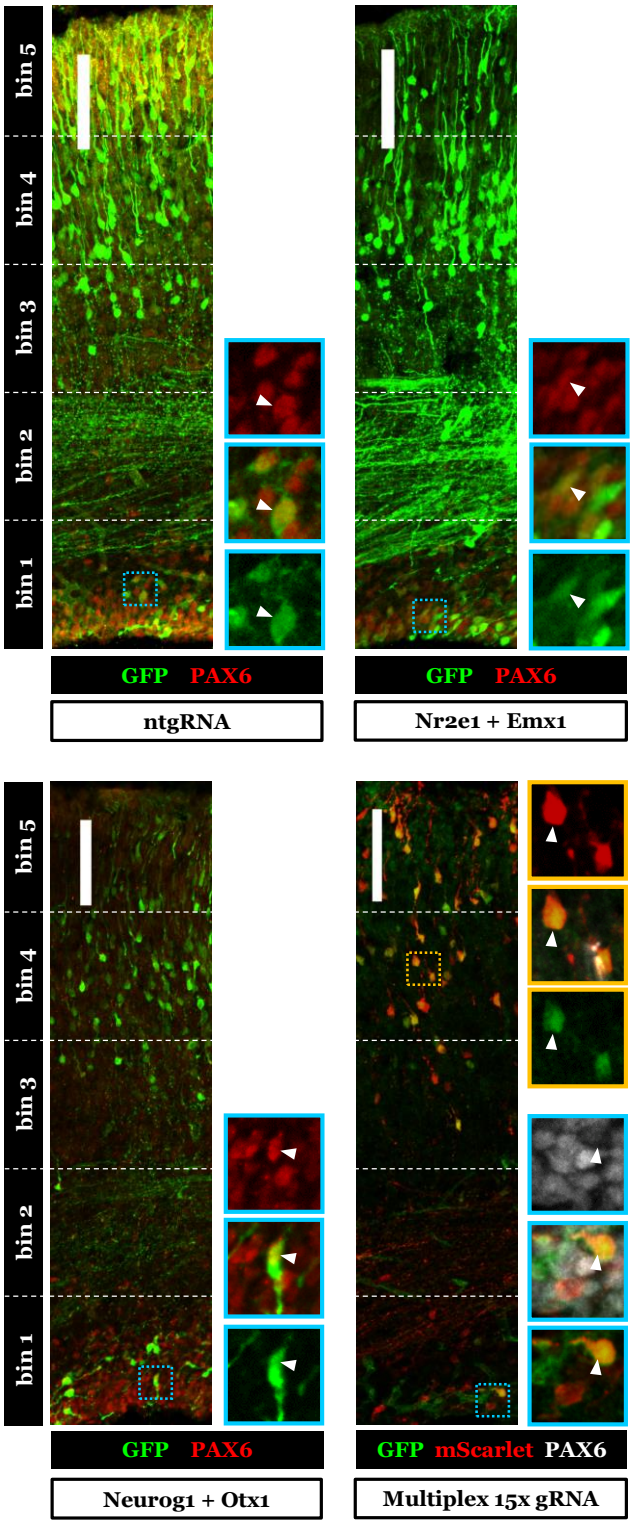

Figure 29: Cell distribution and PAX6 co-localization after concurrent activation of neurogenic gene transcription

Cortices of embryos at E18, five days post-IUE of different gRNA combinations, were quantified in five bins from VZ (bin 1) to CP (bin 5). GFP and mScarlet served as markers for electroporated cells, and co-immunostainings were performed for neurogenic stem cell marker PAX6. (Scale bars: 100 µm)

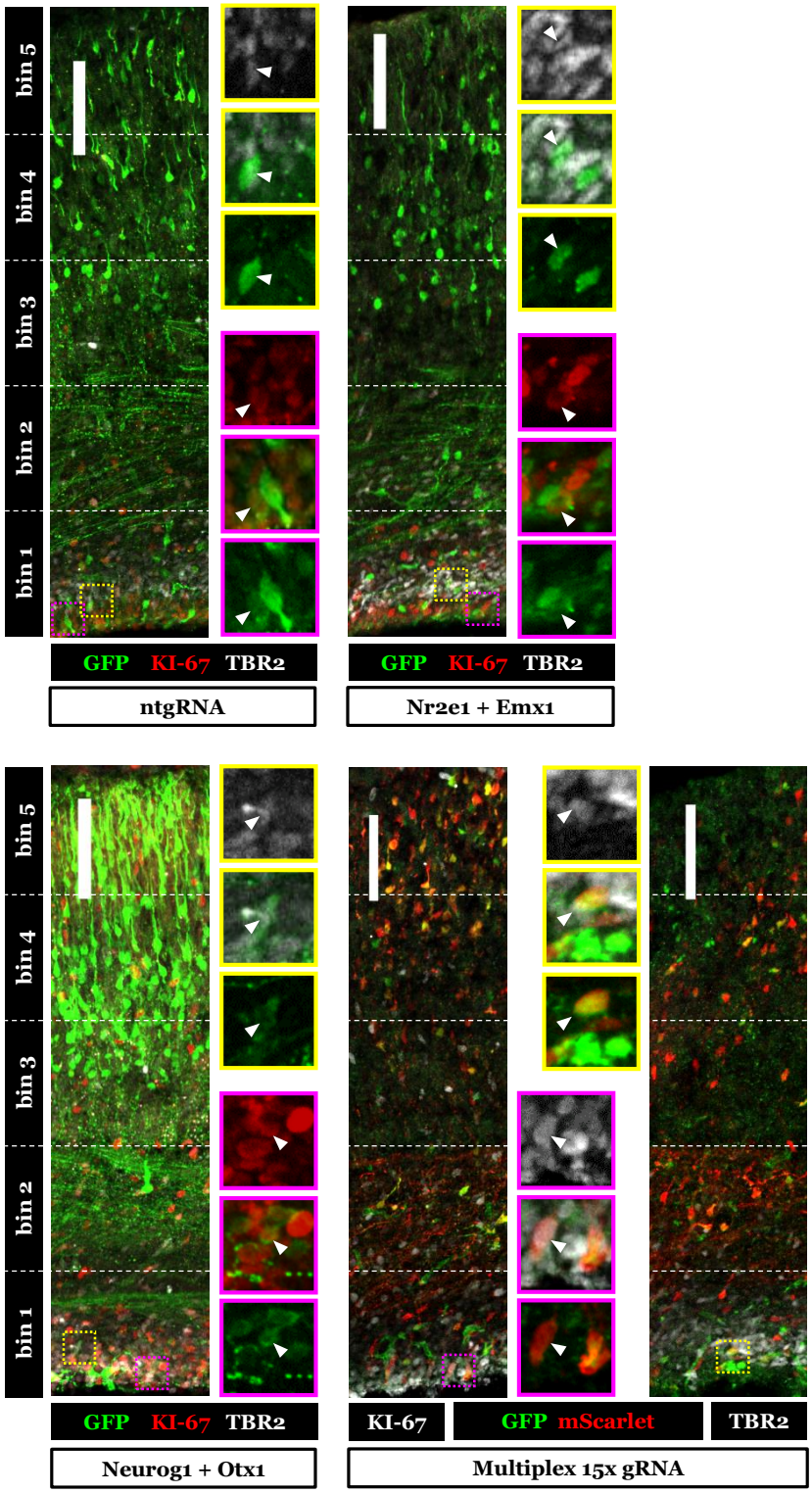

Figure 30: Cell distribution and co-localization with TBR2 and KI-67 after concurrent activation of neurogenic gene transcription

Cortices of embryos at E18, five days post-IUE of different gRNA combinations, were quantified for distribution of GFP⁺ (electroporated) cells and co-localization with bIP marker TBR2 and cell cycle marker KI-67. (Scale bars: 100 µm)

The concurrent activation of 15 genes leads to an, albeit not significant, enrichment of cells at the VZ (bin 1) (Figure 31A), where the stem cells would normally reside. In addition, the fractions of electroporated cells expressing the stem cell marker PAX6, as well as progenitor marker TBR2, seem to be higher (Figure 31B; not significant), hinting that at least some of the enriched cells at the VZ still assume a neurogenic identity. The expression of cell cycle marker KI-67, however, does not seem to be noticeably higher (Figure 31B), showing that the proliferation is not increased.

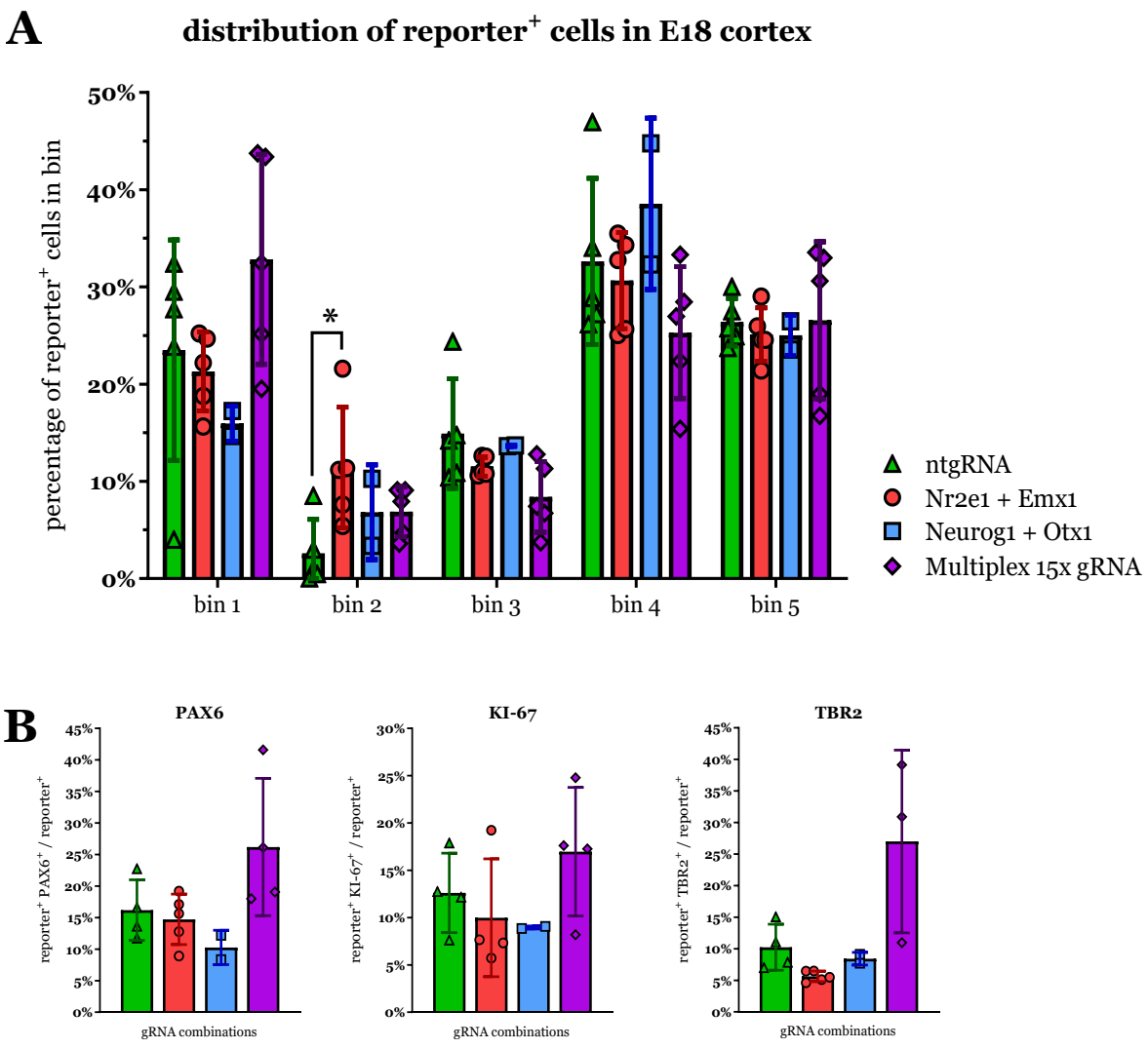

Figure 31: Quantification of electroporated cell distribution and marker colocalization five days post-IUE with neurogenic gene activation constructs.

A. *Distribution of electroporated cells across the cortex in five equidistant bins as fraction per bin of all electroporated cells (Mean ± S.D., biological replicates as scatter dot plot; Kruskal-Wallis ANOVA with Dunn's multiple comparisons test, * p=0.02).* ***B.*** *Colocalization of cell type markers with reporter+ cells as a fraction of all electroporated cells. (Mean ± S.D., biological replicates as scatter dot plot)*

4 DISCUSSION

4.1 DIFFERENTIAL PROTEIN LOCALIZATION AND MRNA EXPRESSION OF NURD SUBUNITS MTA3 AND GATAD2B

The subunits MTA3 and GATAD2B of the NuRD complex show very different localization in cortical development. MTA3 is expressed in both VZ cells, putatively aRGC and/or bIP, and in DL neurons at neurogenic stages (Figure 7), which is similar to the expression pattern reported for the NuRD core subunit MBD3 at the same stage (Knock et al. 2015). The expression in the stem cell layers is completely lost during gliogenic stages and only expression in DL neurons remains (Figure 8).

The expression of GATAD2B is limited to the cortical plate in both stages, and shows a similar expression pattern in several cortical layers at both time points (Figure 10, Figure 11). This diverging localization of complex subunits suggest that they are likely not active in the same assembly of the NuRD complex during neurogenesis.

In contrast to initial findings of differential expression between neurogenic and gliogenic cortical aRGC (Pinto et al. 2008), no regulation of mRNA levels could be detected for either *Mta3* or *Gatad2b* between the same cell states in the transcriptome detailed in Chapter 3.2 (not shown). For GATAD2B, this observation fits well to the protein expression, as it does not localize to the VZ in both stages.

Intriguingly, however, despite no significant difference and no regulatory trend in mRNA level, the protein expression of MTA3 in these cell states is clearly different between these time points, with a salt-and-pepper expression in the VZ at E14 but no protein detectable at E18 (Figure 7, Figure 8). This might point towards a post-transcriptional regulation of *Mta3* expression, in which the mRNA is constitutively present, but presence of MTA3 protein is differentially regulated.

This could be achieved by mRNA-based regulation, reducing the amount of protein produced, e.g. by mRNA decay or reduced translation initiation, which are common mechanisms in neural stem cells for ensuring rapid response to external stimuli (Kim 2016).

4.2 *IN VIVO* KNOCKDOWN OF NURD SUBUNITS REVEALS THE COMPLEXITY OF NEUROGENESIS REGULATION

In vivo knockdown of *Mta3* during neurogenesis leads to an increase in the proportion of cells remaining close to the VZ, while they are reduced in the CP (Figure 14). The effect is rather mild, which could hint at compensatory mechanisms by other MTA subunits with (partially) redundant function, as has been shown for catalytical subunits HDAC1 and HDAC2 (Montgomery et al. 2009). However, another layer of complexity is added by the expression of different *Mta3* transcript variants, which are expressed at very different levels in the neurogenic cortex (Figure 9). When designing the miRNAs used in this study, no sequence could be identified that would putatively knock down all isoforms equally, so a certain difference of the effect is to be expected. However, knockdown by a miRNA targeting the highest-expressed transcript variant 2, which was able to reduce total *Mta3* mRNA expression by about 88 % *in vitro*, had a milder phenotype than a miRNA that reduced levels only by 63 % *in vitro* while targeting the least-expressed transcript variants 3 and 4. This may point towards differential functions of the splice variants in the regulation of neurogenesis.

While the proportion of cells residing in the VZ is increased upon *Mta3* knockdown, the coexpression of stem cell and progenitor markers PAX6 and TBR2, which would identify resident cell types of the VZ, is not increased (Figure 14), suggesting a possible defect of the proper migration and differentiation behavior rather than maintenance of stem cell identity. This is reminiscent of the phenotypes of both MBD3 and CHD4 deletion, in which $PAX6^+$ radial glia undergo premature cell cycle exit without producing the proper $TBR2^+$ progenitors, causing a depletion in the progenitor pool and reduced neurogenesis, subsequent reduced cortical thickness and ectopia and misexpression of neuronal layer markers (Knock et al. 2015; Nitarska et al. 2016). This implies that some functions of the complex are impaired upon deficiency of one of its subunits, independent of their identity, by inhibiting the complex as such.

However, some subunits have NuRD-independent functions as well, such as the maintenance of stem cell identity by CHD4 alone (Zhao et al. 2017) or the function of RBBP proteins in other transcriptional regulator complexes (Kuzmichev et al. 2002), and CHD3, CHD4 and CHD5 have been shown to fulfill non-redundant, specialized roles in the progression of neurogenesis (Nitarska et al. 2016).

It is thus especially surprising that different human neurodevelopmental disorders reported for the three NuRD subunits GATAD2B, CHD3 and CHD4 (Vera et al. 2020; Weiss et al. 2016; Snijders Blok et al. 2018) have very similar symptoms, including intellectual disability, delayed speech, macrocephaly and distinct facial features, despite their putatively different function in neurogenesis.

4.3 MULTIDIMENSIONAL TRANSCRIPTOMIC ANALYSIS ALLOWS A MORE COMPREHENSIVE LOOK AT FATE DETERMINANTS IN THE DEVELOPING BRAIN

These findings once again pointed out the sophisticated complexity involved in the regulation of neurogenesis. To identify factors at the key points of these interwoven fate choices and progressions, the transcriptome presented in this study allows a broad look at different populations, which are the representatives of key fate switches in regional, temporal and cell type aspects of telencephalic development. While we confirmed several well-known neurogenic factors whose functions have been elucidated, these data also allow a more comprehensive overview to shed new light on putative networks and to help prioritize promising candidates for manipulation.

We could identify the chromatin remodelers as putatively important group in defining neurogenic cortical aRGC, and the transcriptome data provides indications that they may be determinants of maintaining plasticity and lineage potential in early versus late RGC of both the cortex and LGE (Figure 18). This is in accordance with functional investigations, in which the importance of chromatin state on a genome-wide scale was shown by manipulation of PrC components HMGA1 and HMGA2 (Kishi et al. 2012). Indeed, the expression of these chromatin remodelers, and the resulting accessibility of chromatin, strongly correlated with the plasticity and neurogenic stem cell potential of aRGC *in vivo*. The opposite effect on neurogenic potential was shown for PRC2 subunits RING1B, EZH2 and EED (Hirabayashi et al. 2009), with the latter two being found as well in the upstream factor ranking of neurogenic cortical RGC (Figure 18).

Notably, several of the identified putative upstream regulators of neurogenic cortical aRGC are either part of the NuRD complex (*Hdac2*, *Chd3*, *Chd4*, *Hdac1*) or have been shown or suggested to be able to interact with it (*Bcl11b* [*Ctip2*], *Sall1*, *Sall4*; see Miller et al. 2016; Lejon et al. 2011). This seems to confirm reports that suggest the defining function of NuRD in the proper execution of (neurogenic) lineage differentiation programs (see Chapter 2.3.5).

Differences between neurogenic aRGC in the cortex and LGE have also been emphasized by pathway overrepresentation analysis. According to the GO terms associated with the genes differentially regulated between the two regions, the later fate as consumptive or

continuous neurogenic region may already be specified at this early stage, with the LGE leaning towards cell cycle-related GO terms, while the cortical RGC gene expression is engaged in generation of projections and synaptic communication (Figure 21). While the aNSC for the SEZ, that are already set aside between E13 and E15, rather slow down their cell cycle (Furutachi et al. 2015; Fuentealba et al. 2015; Falk et al. 2017), this presumably small proportion of the population is not able to elicit a corresponding shift of functional annotation.

However, even with these findings, only a small proportion of the dataset created in this thesis has been analyzed in detail, with the comparison between cell types or the entirety of neuronal cell populations being neglected so far. These analyses will reveal a more comprehensive look towards the neuronal output of the examined populations, as well as differentiation processes. Other genes than TF and ChR have also not been considered, despite putatively having an important functions, such as metabolic or signaling genes, adhesion molecules or extracellular matrix proteins defining the niche.

4.4 IMPLICATION OF BASALLY LOCALIZED (ECTOPIC) PAX6⁺/TBR2⁺ CELLS UPON PBASE-MEDIATED TRANSPOSITION

Aiming to apply these newly identified factors for *in vivo* experiments, I also discovered an unexpected influence on bIP generation and neurogenesis: the piggyBac transposon system generated ectopic, basally localized PAX6⁺/TBR2⁺ cells, leading to cortical hyperplasia and folding, independent of any candidate gene manipulation.

The markers PAX6 and TBR2 are restricted to specific cell types and localizations in physiological murine cortex development; namely, PAX6 serves as a marker of cortical aRGC and staining signal is located at the VZ, whereas TBR2 marks bIP and localizes to the SVZ (Götz et al. 1998; Englund et al. 2005).

The ectopia elicited by PBase-mediated transposition is mainly localized in the IZ (Figure 24C), which would usually be devoid of those markers. However, it is tempting to compare this effect to the development of physiologically gyrified cortex. Here, the SVZ is extended into an iSVZ and oSVZ, with an enrichment of bRGC and bIP located there, which may express both PAX6 and TBR2 and greatly contribute to the amplification of the progenitor pool by repeated cell division (Namba and Huttner 2017; Hevner 2019). Of note, it has been shown that forced sustained PAX6 expression in mouse cortex increases bRGC production by altering the cleavage plane, and promotes cell cycle re-entry of bIP, with these forced-neurogenic cells localized in the IZ (Wong et al. 2015). These descriptions are reminiscent of the accumulation of PAX6⁺ and TBR2⁺ ectopic cells in the IZ after PBase-mediated transposition. If these cells strongly proliferate, similar to the bRGC in gyrified species, it may serve to explain the increased electroporation density in affected brains (Figure 26) as a secondary effect rather than initial targeting efficiency.

In gyrified species, these basal progenitor cells are especially localized below the emerging gyri, i.e. the areas of increased radial growth and resulting cortical thickness (Hevner 2019). Accordingly, upon transposition with PBase, and to a lesser extent, mPB, the most common malformation at late- to post-neurogenic stages included local hyperplasia at the IUE site or more global gyrus-like structures (Figure 25B), which may suggest similar radial expansion.

It is thus tempting to speculate that PBase-mediated transposition exerts similar effects as occur naturally in gyrified cortex development, namely increased proliferation of basally localized progenitor-like cells leading to local radial growth. However, if this is indeed a related mechanism or rather coincidental similarity remains to be understood. In addition, the non-cell autonomous manner of the observed phenotype is poorly defined, impeding a closer analysis of the underlying cellular mechanisms.

4.5 PUTATIVE EFFECT OF CODON USAGE ON TRANSLATION, PROTEIN FOLDING AND ENZYMATIC FUNCTION

While synonymous, or "silent", mutations and single nucleotide polymorphisms are often considered without relevance for protein function, this might not actually be the case; rather, codon usage can be exceedingly relevant for protein function. This includes examples for human diseases caused by synonymous mutations, such as Attention Deficit and Hyperactivity Disorder (ADHD, mutation in Neurotrophin 3) or hemophilia B (mutation in Factor IX) (Sauna and Kimchi-Sarfaty 2011).

Synonymous mutations have been implicated to affect splicing, miRNA-mediated knockdown via the 3' UTR, mRNA stability and formation of secondary RNA conformations, which modify translation initiation (Sauna and Kimchi-Sarfaty 2011). Ribosomal translation speed is partly controlled by codon usage, and improper usage can lead to ribosomes stalling in translation elongation. Subsequent ribosome collisions inhibit further translation initiation (Juszkiewicz et al. 2020), possibly explaining the lower expression of PBase in this study (Figure 27B), and may even elicit RTR (Wu et al. 2020).

By ribosome stalling and pausing, the peritranslational protein folding may also be impaired or altered, leading to misfolded proteins that in extreme cases may lead to misfolding of neighboring proteins, eliciting a cascade of proteotoxicity and UPR (Sauna and Kimchi-Sarfaty 2011; Cao and Kaufman 2012). By this misfolding, non-optimal codon usage can also severely alter or inhibit enzymatic function – however, this depends on the context, and exclusive usage of the most abundant, and thus "optimal", codons may decrease the performance even worse than exclusive usage of only the most atypical ones would (Agashe et al. 2013).

However, neither RTR nor UPR response could be detected in mNPC transfected with transposase and piggyBac transposon, thus excluding these pathways as primary cause of the observed phenotypes (Figure 27C, D). While global UPR was not elicited in bulk mNPC, rare misfolding events of non-codon optimized PBase are still possible, which may lead to irregular activity of the enzyme. This could include the cutting or nicking of DNA at integration or re-excision sites without proper re-ligation, or incomplete integration. While DDR elicited from these events was not found in the bulk mNPC (Figure 27E), each of these events naturally increases the chances of mutagenesis or stress responses (Ciccia and Elledge 2010).

However, the strongest hint that neither of these pathways directly derived from the improper codon usage of PBase are the main cause of the observed phenotype, is that it is not present without a transposon. Indeed, not only was the presence of a transposon necessary to elicit the phenotypical abnormalities, but the severity of the phenotype was correlated to the size of the transposon (Figure 25B, Figure 26B). Of note, the piggyBac transposon in which the abnormalities were completely mitigated, *piggyBac-dCas9-VPR-ntgRNA*, has a transposon size of about 9.5 kbp. This could result in decreased transposition efficiency, as this reportedly starts to decrease for transposons of 9 kbp and bigger (Ding et al. 2005).

This implies that the frequency of transposition and "locus hopping" may correlate with the emergence of abnormalities, as the probability for off-target effects, such as gene disruption or DNA damage, increases with every additional transposition event. This also points towards a stochastic effect, which may explain the high variability of the observed phenotypes.

This again is reminiscent of the role that endogenous retroviral elements (ERV) like long interspersed nuclear element 1 (LINE1) play in neurogenesis. LINE1 can retrotranspose during early stages of neuronal differentiation, and its deletions and insertions contribute to the genetic mosaicism of neurons especially observed in the human brain (Muotri et al. 2005; Linker et al. 2017). The LINE-1 retrotransposition tends to repressed in the murine brain (Muotri et al. 2010), and in contrast the abundance of ERV has increased in the primate neocortex in correlation to its size and gyrification (Linker et al. 2017). It is thus tempting to speculate that transposition of the piggyBac transposon may represent a similar pathway in eliciting a gyrification-like phenotype.

Of course, in the highly plastic embryonic brain, with proliferation rates remarkably high in the developing cortex, even the unintended detrimental manipulation of few cells can lead to a high number of impaired progeny and thus a visible phenotype. It is thus crucial to consider the limitation of genome editing methods, including any possible off-targets or side effects, and carefully verify the method of choice for each experimental system.

4.6 IDENTIFICATION OF POTENTIAL CANDIDATES TO PROLONG NEUROGENESIS *IN VIVO*

Based on the transcriptomic data (Chapter 3.2) and a previous analysis (Pinto et al. 2008), candidate genes were selected that are promising targets for manipulation to achieve a putative effect on the transcriptomic network of aRGC. These candidates were selected by their appearance in the different analyses as well as their known or putative functions.

One of the two key function of stemness is the ability to proliferate and self-renew. Thus, genes known for their promotion of proliferation and inhibition of differentiation were chosen. These included: *Foxg1*, a versatile factor known to promote proliferation and suppress premature differentiation by cell cycle regulation, but also ensure proper temporal progression through the genesis of different neuronal subtypes (Hou et al. 2020); *Zfp423*, which maintains proliferation and modifies retinoic acid-induced differentiation by *Notch*-mediated activation of *Hes5* (Masserdotti et al. 2010; Massimino et al. 2018); *Tcf7l1* (also known as *Tcf3*), which promotes proliferation and inhibits differentiation by repressing both *Wnt* signaling and the expression of proneural factor *Neurog1* (Kuwahara et al. 2014); *Nr2e1* (also known as *Tlx*), that regulates proliferation, stemness and timing of neuronal differentiation in embryonic aRGC as well as adult aNSC (Roy et al. 2004; Wang, T. and Xiong 2016); *Sox3*, an inhibitor of proneural bHLH transcription factors to maintain broad developmental potential (Wegner and Stolt 2005); and *Gli2*, which induces proliferation and self-renewal in pluripotent stem cells and in telencephalic development is activated by *Shh* signaling from the CSF via the primary cilium (Li, Y. et al. 2013; Agirman et al. 2017).

However, the activation of proliferation alone may lead to uncontrolled mitosis, causing overgrowth and essentially tumorigenesis. The second key function of stem cells has to be considered, namely the ability to produce differentiated progeny. Neuronal, proneural, differentiation or patterning factors were thus chosen in addition to elicit neurogenic potential and differentiation into correct neuronal subtypes. These candidates included *Otx1*, which regulates the onset of differentiation by cell cycle exit (Huang et al. 2018); *Nfia*, which induces the switch to differentiation by repressing *Hes1* (Piper et al. 2010); *Dmrt3*, which elicits dorso-ventral patterning by repressing ventralizing factors like

Gsx2 (Desmaris et al. 2018); *Emx1*, a cortical patterning factor that promotes self-renewal, but also the genesis of mainly glutamatergic neurons (Kobeissy et al. 2016; Weinandy et al. 2011); *Pou3f4* (also known as *Brn4*), which promotes neuronal differentiation of radial glia (Zhang et al. 2020); as well as *Neurog1* and *Neurog2*, two potent proneural factors in the cortex that initiate expression of neuronal genes and drive differentiation into different subtypes (Oproescu et al. 2021).

In addition, three factors were chosen whose function in neurogenesis has been at most implied, but not elucidated: *Nhlh1*, a bHLH factor that seems to initiate differentiation in neural crest cells (Bao et al. 2000; Lau et al. 2019); *Foxp4*, which is expressed in embryonic VZ/CP and lost at postnatal stages, but whose function has not been defined and may have to do with exit from proliferation (Co et al. 2020); and *Mta3*, whose knockdown may promote neuronal differentiation according to results presented in this thesis.

4.7 POTENTIAL EFFECTS OF CONCURRENT NEUROGENIC FACTOR ACTIVATION

With no neurogenic niche left after birth to supply cortical neurons, disease or injury which leads to their loss still has drastic implications, since neurons are not replaced by endogenous means. This is true not only for diseases typically affecting the older population, such as Alzheimer's disease, but also for injury or insult in early life. In fact, perinatal hypoxia is still a leading cause of infant death, with high mortality, but also high morbidity, causing e.g. cerebral palsy, epilepsy, and cognitive disabilities (Rocha-Ferreira and Hristova 2016). However, while it has been shown in mice that perinatal hypoxia can elicit generation of pyramidal neurons from activated local GFP+ cells (Bi et al. 2011), the high plasticity of the young postnatal brain can also be detrimental, leading to inflammation-related excessive connectivity which may cause epilepsy (Rocha-Ferreira and Hristova 2016).

However, in newborn humans as in postnatal mice, gliogenic radial glia are still active as stem cells (see Chapter 2.1.5). If it were possible to reactivate their neurogenic potential, lost neurons could potentially be replaced by an endogenous source. To achieve this reactivation, first the factors responsible for the switch between neurogenesis and gliogenesis have to be identified by examining if they are able to prolong the neurogenic phase by maintained expression.

To increase the chances of shifting the entire transcriptomic network towards the desired fate, several factors at once may have to be activated. For the concurrent activation of multiple target genes *in vivo*, a system of the combined expression of the dCas9-VPR fusion protein and the gRNAs (Figure 28) had to be established for an environment in which neither are present *a priori*. When both components are localized on the same large plasmid, activation is still possible *in vitro* and dCas9 expression can be observed *in vivo*, giving no indication of mutual inhibition of transcription.

The transcriptional activation of two or 15 genes during neurogenesis showed only mild effects at the analysis time point E18 (Figure 31), with *Nr2e1* + *Emx1* showing a slight enrichment of cells retained in the SVZ/IZ. While some of these are TBR2$^+$, which may

imply ongoing neurogenesis by presence of bIP, an overall increase of stem cell, proliferation or bIP markers was not present. The phenotype could thus also be caused by a delay or defect of migration, or general delay of normal neurogenesis progression.

For *Neurog1 + Otx1*, the population of cells in the VZ was slightly reduced, but slightly increased in the lower CP. This may indicate that a subpopulation of radial glia are prematurely differentiating at early stages, when DL neurons are being generated, depleting the stem cell pool. How this subpopulation is defined – e.g. by dosage effect – would need to be evaluated.

By the concurrent activation of 15 candidates, a non-significant accumulation of cells in the VZ could be observed, and the proportion of $PAX6^+$ and $TBR2^+$ cells was increased (not significant). This may hint that a higher number of radial glia with neurogenic potential still reside in the niche typical for earlier development. Cell cycle marker KI-67 was not increased, indicating the proliferating proportion of cells is not higher than in control.

However, these relatively mild phenotypes are elicited when neurogenesis in the cortex has only just come to an end. This is not unexpected, as these genes may have been highly expressed under physiological conditions until shortly before the analysis time point, and thus had little time to exert a notable effect when artificially activated. However, even at this early time point, a tendency towards desired effects, i.e. the enrichment of cells in the physiological niche of aRGC or bIP and increased expression of neurogenic stem cell and progenitor markers, or undesired effects, i.e. putative depletion of the stem cell pool, can already be observed. This validates the choice of time point as an early selection criterion for screening of different combinations of neurogenic candidate genes.

A much greater and potentially more significant and interesting effect may be expected for the analysis of later time points, when a longer time has passed since neurogenesis has concluded. Time points for consideration are in postnatal stages, when the brain development including the bulk of gliogenesis has been completed, or even adult stages, in which only the specific subtypes of adult neurogenesis as detailed in Chapter 2.2 would be present.

The effect of 15 gRNAs would not be expected to necessarily be equivalent to the additive effects of activation of only two candidates for several reasons. Firstly, the many different gRNAs may have unpredictable activity due to competition for the dCas9-VPR complex

(McCarty et al. 2020). A strong transcriptomic shift could also necessitate manipulation of multiple genes above a certain threshold, above which the effects of single gene regulation cannot be compensated by the network anymore. In addition, successfully activated genes may have competitive or synergistic effects on each other directly, or on converging or diverging networks and pathways (see also Chapter 2.3).

If the prolongation of neurogenesis by activation of specific factors would be successful, another interesting experiment would be to see if this effect can also overcome the hurdle of previously lost neurogenic potential. To this end, it may be intriguing to activate these factors only after the neurogenic-to-gliogenic switch has taken place (E18 or later). In addition, if the putative effects of the concurrent activation of 15 genes are confirmed at later stages, it remains to be determined if this is the effect of only one or few of these candidates, or if concerted action of a large group is necessary to elicit a prolonging or reactivating effect on neurogenesis.

Neocortical evolution has shown that continued neurogenesis can occur in different regions, even in the cortex, however minor (Akter et al. 2020). By using an approach to artificially create a neurogenic zone in the cerebral cortex, we may be able to understand the mechanisms by which regionally different, postnatal maintenance of neurogenesis is achieved. These finding may one day help in developing therapeutic strategies, i.e. for the treatment of childhood hypoxia, to replace lost neurons with new neurons of the proper identity, from an endogenous source.

5 METHODS

Declaration of author contributions: *Several collaborators provided materials or collaborated on technical execution of experiments, and their contributions are declared as such in the text. All contributions are detailed in the Declaration of Author Contributions on page XXXIV.*

5.1 ANIMALS, IN VIVO EXPERIMENTS AND TISSUE PROCESSING

All animal experiments, husbandry and handling were conducted in accordance with the German animal welfare laws (TierSchG) and guidelines of the GV-SOLAS (Gesellschaft für Versuchstierkunde / Society of Laboratory Animal Science), and under consultation of the responsible veterinarians and animal welfare officers (TierSchB).

5.1.1 Mouse husbandry and breeding

Animals were kept in the Core Facility Animal Models (CAM) of the BioMedical Center (Ludwig-Maximilians-Universität, Planegg-Martinsried) or the Core Facility Comparative Medicine (AVM) of the Helmholtz Center Munich (München-Neuherberg).

In both facilities, animals were kept in individually ventilated (IVC) cages under specified pathogen free (SPF) conditions, in a 12 hour light/dark cycle with constant *ad libitum* access to water and food, and standard cage enrichment.

Wild type C57BL/6J or BL/6 mixed background animals were used for all experiments. For the generation of embryos of a defined age, timed matings were performed. Matings were set up in the afternoon and females were examined for the presence of a mating plug on the next morning, which was considered E0.

At the desired embryonic day, mothers were sacrificed by cervical dislocation, the uterus exposed and embryos individually sacrificed by severing the neck with sharp scissors.

5.1.2 *In utero* electroporation

All animal experiments were performed as licensed by the Government of Upper Bavaria (ROB). *In utero* electroporation was performed as described previously (Esgleas et al. 2020).

In brief, timed-pregnant C57BL/6J mice at E13 were anesthetized by intraperitoneal (i.p.) injection of Medetomidine (0.5 mg/kg)/Midazolam (5 mg/kg)/Fentanyl (0.05mg/kg) and surgical tolerance was confirmed by interdigital and corneal reflex testing. The uterus was exposed through an incision in the abdomen along the linea alba, and 1 µl of plasmid solution, containing 0.01 % Fast Green dye for visualization, was injected into the lateral ventricle of the embryos by a glass capillary of approx. 10 µm diameter. Plasmids were directed into the lateral cortex by applying a pulsed current of 35 V along the anterior-posterior axis of the embryo. The uterus was then replaced into the abdominal cavity and the peritoneum and skin incision were sutured individually before anesthesia was antagonized by subcutaneous (s.c.) application of Atipamezole (2.5 mg/kg)/Flumazenil (0.5 mg/kg)/Buprenorphine (0.1 mg/kg). Post-surgical analgesia consisted of either Meloxicam (1 mg/kg i.p. or peroral [p.o.]) or Paracetamol (200 mg/kg p.o. via drinking water) and stress evaluation was performed daily for three days post-surgery.

At the analysis time point, mice were sacrificed as described in Chapter 5.1.1.

The plasmids used for IUE are listed in Table 1. Concentrations were determined in consideration of plasmid size and, in the case of co-electroporation, the molar ratio. Plasmids were prepared with a kit for endotoxin-free DNA (EndoFree® Plasmid Maxi Kit, Qiagen, cat. no. 12362) to avoid immune reaction in vivo and redissolved in medical-grade pure water. Plasmid solution was adjusted to isotonic level with sodium chloride (NaCl) and Fast Green dye was added for visualization before injection (Table 2).

Table 1: Plasmids used for IUE experiments

treatment identifier		*plasmid(s)*	*concentration*
NuRD knockdown	miRNA control	*pCAG-emGFP-miRNAcontrol*	500 ng/µl
	Gatad2b-miRNA2	*pCAG-emGFP-Gatad2b-miRNA2*	500 ng/µl
	Mta3-tv2-miRNA1	*pCAG-emGFP-Mta3-tv2-miRNA1*	500 ng/µl
	Mta3-tv3+4-miRNA	*pCAG-emGFP-Mta3-tv3+4-miRNA1*	500 ng/µl
piggyBac transposon	PBase + no transposon	*pCAG-PBase* *pCAG-IRES-GFP*	670 ng/µl 1000 ng/µl
	PBase + dCas9-GFP	*pCAG-PBase* *pB-CAG-dCas9-GFP-T2A-Blast*	670 ng/µl 1300 ng/µl
	PBase + GFP	*pCAG-PBase* *pB-CAG-GFP*	670 ng/µl 1000 ng/µl
	mPB + GFP	*pCMV-mPB* *pB-CAG-GFP*	760 ng/µl 1000 ng/µl
	mPB + dCas9-VPR-ntgRNA	*pCMV-mPB* *pB-CAG-dCas9-VPR-P2A-GFP-1xgRNA-control*	670 ng/µl 1350 ng/µl
neurogenic factor activation	ntgRNA	*pCAG-IRES-GFP*	150 ng/µl
	Nr2e1+Emx1	*pCMV-mPB* *pB-CAG-dCas9-VPR-P2A-GFP-4xgRNA-Nr2e1-Emx1* *pCAG-IRES-GFP*	670 ng/µl 1500 ng/µl 150 ng/µl
	Neurog1+Otx1	*pCMV-mPB* *pB-CAG-dCas9-VPR-P2A-GFP-4xgRNA-Ngn1-Otx1* *pCAG-IRES-GFP*	670 ng/µl 1500 ng/µl 150 ng/µl
	Multiplex 15xgRNA	*pCMV-mPB* *pB-CAG-dCas9-VPR-P2A-GFP* *pB-CAG-mScarlet-15xgRNA*	760 ng/µl 660 ng/µl 690 ng/µl

Table 2: Plasmid preparation for IUE

	component		*manufacturer*	*cat. no.*
0.01 % (w/v)	Fast Green dye	*(Fast Green FCF)*	Sigma-Aldrich	F7258
0.9 % (w/v)	NaCl	*(Sodium chloride)*	Sigma-Aldrich	S3014
	H_2O	*(Aqua B. Braun)*	B. Braun Melsungen	0082423E

5.1.3 Tissue processing for immunostaining

Brains were dissected from embryo and briefly washed in 1× phosphate-buffered saline (PBS, see Table 3). The tissue was immediately fixed in 4 % (w/v) paraformaldehyde (PFA, see Table 4) for 7 hours at 4 °C, washed for 5 min. in 1×PBS and then incubated in 30 % (w/v) sucrose (D(+)-Saccharose, Carl Roth, cat. no. 4621) in 1×PBS at 4 °C overnight for cryoprotection.

Table 3: Components of 10× PBS

	component		*manufacturer*	*cat. no.*
400 g	NaCl	*(Sodium chloride)*	Sigma-Aldrich	S3014
10 g	KCl	*(Potassium chloride)*	Carl Roth	6781
10 g	KH_2PO_4	*(Potassium dihydrogen phosphate)*	Merck	104873
58.75 g	Na_2HPO_4	*(Sodium phosphate dibasic dihydrate)*	Sigma-Aldrich	71645
ad 5000 ml	ddH_2O			
	→ for 1× PBS, dilute 1:10 in ddH2= and adjust pH to 7.4 with HCl			

Table 4: Components of 4 % PFA in PBS

	component		*manufacturer*	*cat. no.*
40 g	PFA	*(Paraformaldehyde, granulated)*	Carl Roth	0335
3 pellets	NaOH	*(Sodium hydroxide, pellets)*	Acros Organics	13407
100 ml	10× PBS	*(see Table 3)*		
ad 1000 ml	ddH_2O			
	→ adjust pH to 7.4 with HCl and store at 4 °C (short-term) or –20 °C (long-term)			

For cryosectioning, the brains were embedded in cutting medium (either Tissue-Tek® O.C.T.™ Compound, Sakura, cat. no. 4583 or Neg-50™ Frozen Section Medium, ThermoFisher, cat. no. 6502), frozen on dry ice and stored at –20 °C. The brains were sectioned on a cryostat (Leica CM3050 S or ThermoFisher Cryostar™ NX70) in coronal sections that were directly applied to adhesion object slides (SuperFrost Plus™, ThermoFisher, cat. no. 10149870). For expression analysis in wild type brains, section thickness was 40 µm. For electroporated brains, section thickness was 25 µm at E16 and 30 µm at E18.

5.1.4 RNA extraction from tissue

Embryonic brains were dissected into different regions and the tissue immediately snap frozen on dry ice. For phenol-chloroform RNA extraction, TRIzol™ Reagent (Invitrogen, cat. no. 15596) was used according to the manufacturer's protocol (for additional chemicals used see Table 5), with the tissue mechanically triturated with a syringe and progressively smaller needles. Extracted RNA was redissolved in RNase-free water and concentration was measured on a spectrophotometer (NanoDrop ND-1000 Spectrophotometer, Peqlab).

Table 5: Chemicals used for phenol-chloroform RNA extraction from tissue

component		*manufacturer*	*cat. no.*
Chloroform	*(Chloroform for analysis EMSURE®)*	Merck	102445
Isopropanol	*(2-Propanol, ROTIPURAN® ≥99,8 %, p.a.)*	Carl Roth	6752
Ethanol	*(Ethanol puriss. p.a., absolute)*	Sigma-Aldrich	32221
RNase-free water	*(Aqua B. Braun)*	B. Braun Melsungen	0082423E

5.2 CELL CULTURE METHODS

Murine cell lines were cultured in 37 °C, 5 % CO_2 conditions on tissue-culture treated plates and flasks. Cells intended for immunocytochemistry were plated on glass coverslips coated with Poly-D-Lysine (Sigma-Aldrich, cat. no. P1149; diluted 1:50 in H_2O) in 24-well plates.

5.2.1 Culture and transfection of P19 cells

P19 cells (ATCC, cat. no. CRL-1825) were cultured on uncoated plates in P19 maintenance medium based on Dulbecco's modified Eagle's medium (DMEM, see Table 6) and passaged by washing with PBS (Gibco, cat. no. 14190) and dissociation with 0.05 % Trypsin-EDTA (Gibco, cat. no. 25300). For cryopreservation, low-passage cells were frozen in maintenance medium with 10 % dimethyl sulfoxide (DMSO; Sigma-Aldrich, cat. no. D2438) and stored at −80 °C. Cultured cells were used up to passage 12, with the seeding of a freshly-thawed aliquot considered as passage 0.

Table 6: P19 cell culture maintenance medium

	component		***manufacturer***	***cat. no.***
	DMEM + GlutaMAX™	*(DMEM (1X) + GlutaMAX™, high glucose)*	Gibco	61965
+ 10 %	FBS	*(Fetal bovine serum premium)*	PAN Biotech	P30-3302
+ 1 %	Pen/Strep	*(Penicillin-Streptomycin [10,000 U/mL])*	Gibco	15140-122
+ 1 %	NEAA	*(MEM Non-Essential Amino Acids Solution)*	Gibco	11140-035

Transfection was performed on freshly seeded (floating) cells with the jetPRIME® DNA/siRNA transfection reagent (PolyPlus, cat. no. 114-15) according to the manufacturer's protocol. Untransfected cells and mock-transfected cells, which received the transfection reagents without plasmid DNA, were routinely included as experimental controls.

For testing of knockdown efficiency with miRNA plasmids, 750 000 cells were seeded per 6-well and transfected with 2 µg of miRNA plasmid per well, and knockdown efficiency analyzed by FACS isolation of the cells and qRT-PCR after 48 hours.

For testing the activation potential of gRNAs, 170 000 cells per 6-well or 1 400 000 cells per 10 cm dish were seeded and transfected with 2 µg or 10 µg of plasmid DNA, respectively. For the test of single-gene activation, a dCas9-VPR expressing plasmid (*pcDNA-CMV-GFP-CMV-dCas9-VPR*, Figure 3; kindly provided by Dr. Christopher Breunig) was co-transfected with one STAgR plasmid containing two gRNAs, or two STAgR plasmids containing one gRNA each. A molar ratio of gRNA : dCas9-VPR = 2 : 1 for each gRNA plasmid was chosen to ensure uptake of both gRNA plasmids in the latter case. Analysis by FACS isolation of the cells and qRT-PCR was performed after 72 hours.

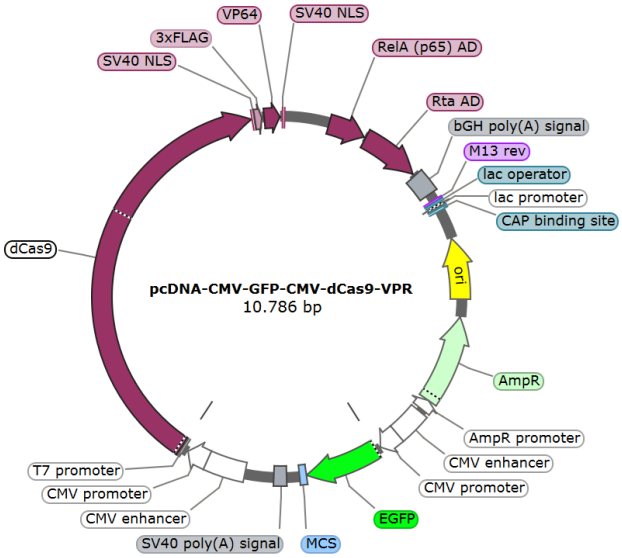

Figure 32: Plasmid map of pcDNA-CMV-GFP-CMV-dCas9-VPR

The dCas9-VPR fusion protein and the GFP reporter are each flanked by their own CMV promoter. (Plasmid map created with SnapGene® Viewer software [Insightful Science; snapgene.com]).

5.2.2 Culture and transfection of mNPC

Adherent mNPC were kindly provided by Andrea Neuner, and were derived from the cortex of wild type E14 mouse embryos as previously described (Pollard et al. 2006).

Thawed cells were cultured either in commercially optimized (NeuroCult™ Proliferation Kit [Mouse & Rat], StemCell Technologies, cat. no. 05702) or equivalent DMEM-based medium, with the components hEGF, hFGF and Laminin freshly added to both versions directly before use (Table 7). Cells were grown on Poly-D-Lysine (PDL; Sigma-Aldrich,

cat. no. P1149) coated plates and passaged by dissociation with Accutase (StemPro™ Accutase™ Cell Dissociation Reagent, Gibco, cat. no. A1110501), with the reaction stopped by mNPC washing medium (Table 8).

Table 7: DMEM-based proliferation medium for mNPC

		component	***manufacturer***	***cat. no.***
500 ml	DMEM/F-12 + GlutaMAX	*(DMEM/F-12 (1:1) (1X) + GlutaMAX™)*	Gibco	31331
10 ml	Pen/Strep	*(Penicillin-Streptomycin [10,000 U/mL])*	Gibco	15140-122
7.5 ml	Glucose	*(D-(+)-Glucose solution 45% in H_2O)*	Sigma	G8769
5 ml	NEAA	*(MEM Non-Essential Amino Acids Solution)*	Gibco	11140-035
2.25 ml	HEPES	*(HEPES [1M])*	Gibco	15630
5 ml	N2 supplement	*(N-2 Supplement [100X])*	Gibco	17502
0.8 ml	BSA (75 mg/ml in PBS)	*(Bovine Serum Albumin, powder)*	Sigma-Aldrich	A2153
		(DPBS, no calcium, no magnesium)	Gibco	14190
0.5 ml	β-mercaptoethanol	*(2-Mercaptoethanol)*	Sigma-Aldrich	805740
[1:500]	hEGF	*(Human Recombinant EGF [Epidermal growth factor])*	StemCell Technologies	78006
[1:1000]	hFGF	*(Recombinant Human FGF-basic)*	PeproTech	100-18B
[1:1000]	Laminin	*(Laminin from Engelbreth-Holm-Swarm murine sarcoma basement membrane)*	Sigma-Aldrich	L2020

Table 8: mNPC washing medium to inhibit Accutase digestion

		component	***manufacturer***	***cat. no.***
500 ml	DMEM/F-12 + GlutaMAX	*(DMEM/F-12 (1:1) (1X) + GlutaMAX™)*	Gibco	31331
5 ml	Pen/Strep	*(Penicillin-Streptomycin [10,000 U/mL])*	Gibco	15140-122
1 ml	BSA (75 mg/ml in PBS)	*(Bovine Serum Albumin, powder)*	Sigma-Aldrich	A2153
		(DPBS, no calcium, no magnesium)	Gibco	14190

mNPC were transfected with Lipofectamine™ 2000 (Invitrogen, cat. no. 11668) in Opti-MEM™ + GlutaMAX™ medium (Gibco, cat. no. 51985) according to the manufacturer's protocol, with untransfected control and mock transfection routinely included. For each 6-well, 750 000 cells were seeded 24 hours prior and transfected with a total of 3.2 µg plasmid DNA per well. Molarity of the plasmid combinations (see Figure 24B and Figure 27) was chosen as transposase : piggyBac = 1 : 1. Medium was changed after 16 hours, and

untransfected and mock transfected cells were split 1 : 2 - 1 : 4 after 24 hours, while increased cell death in transfected cells did not necessitate passaging. After 48 hours, one untransfected sample was treated with 1 µM Tunicamycin (Tunicamycin Ready Made Solution 5 mg/mL in DMSO, Sigma-Aldrich, cat. no. SML1287) as a positive control for UPR stress, and all other samples with DMSO (Sigma-Aldrich, cat. no. D2438) as treatment control. Cells were isolated by FACS and expression of selected genes analyzed by qRT-PCR 72 hours post-transfection.

5.3 MOLECULAR CLONING, PLASMID CONSTRUCTS AND SEQUENCES

Commonly established cloning methods, i.e. polymerase chain reaction (PCR), restriction digest, ligation, Gibson Assembly (GA) (Gibson et al. 2009), gel electrophoresis, plasmid preparation and other methods of DNA manipulation and amplification were performed, but will not be elaborated here due to their widespread and standard use. Reagents and kits used are detailed below in Table 9 through Table 14.

Table 9: Reagents used for PCR, restriction cloning, electrophoresis and purification

	component	*manufacturer*	*cat. no.*
PCR	Custom oligonucleotides/primers	Sigma/Merck (Darmstadt, Germany) Metabion (Planegg, Germany)	
	Phusion® High-Fidelity PCR Master Mix	New England Biolabs	M0531
	DMSO	New England Biolabs	B0515A
restriction cloning	Restriction enzymes (various)	New England Biolabs	—
	T4 DNA Ligase	New England Biolabs	M0202
agarose gel electrophoresis	Agarose, universal, peqGOLD	VWP Peqlab	35-1020
	SYBR™ Safe DNA Gel Stain	Invitrogen	533102
	GeneRuler 100 bp DNA Ladder	Thermo Scientific	SM0241
	GeneRuler 100 bp Plus DNA Ladder	Thermo Scientific	SM0321
	GeneRuler 1 kb DNA Ladder	Thermo Scientific	SM0311
	GeneRuler 1 kb Plus DNA Ladder	Thermo Scientific	SM1331
purification	GeneJET PCR Purification Kit	Thermo Scientific	K0702
	GeneJET Gel Extraction Kit	Thermo Scientific	K0692
	AMPure XP magnetic beads	BeckmannCoulter	A63881

Table 10: Components of 50× TAE buffer for agarose gel electrophoresis

	component		*manufacturer*	*cat. no.*
242.2 g	Tris-Base	*(Tris Base, Molecular Biology Grade)*	Merck Millipore	648310
37.2 g	EDTA	*(EDTA Disodium Salt 2-hydrate)*	PanReac AppliChem	131669.1211
57.1 g	Acetic acid	*(Acetic acid glacial)*	VWR Chemicals	20102.292
600 ml	ddH_2O			
	→ dilute 1 : 50 with ddH2O to use for casting and running agarose gels			

Table 11: Components of Gibson Assembly one-step isothermal reaction mix (Gibson et al. 2009)

5× isothermal reaction buffer			***manufacturer***	***cat. no.***
3 ml	Tris-HCl (1 M)	*(Trizma® hydrochloride)*	Sigma-Aldrich	T3253
300 µl	$MgCl_2$ (1 M)	*($MgCl_2$ Solution)*	New England Biolabs	B0510A
60 µl	dATP (100 mM)	*(dNTP Set, PCR Grade, 100 mM each)*	Qiagen	201913
60 µl	dTTP (100 mM)	*(dNTP Set, PCR Grade, 100 mM each)*	Qiagen	201913
60 µl	dCTP (100 mM)	*(dNTP Set, PCR Grade, 100 mM each)*	Qiagen	201913
60 µl	dGTP (100 mM)	*(dNTP Set, PCR Grade, 100 mM each)*	Qiagen	201913
300 µl	DTT (1 M)	*(DL-Dithiothreitol solution 1 M in H_2O)*	Supelco	646563
1.5 g	PEG-8000	*(Poly(ethylene glycol) BioUltra, 8000)*	Sigma-Aldrich	89510
300 µl	NAD (100 mM)	*(nicotinamide adenine dinucleotide)*	Carl Roth	AE11
ad 6 ml	ddH_2O	*(Aqua B. Braun)*	B. Braun Melsungen	0082423E
Gibson Assembly master mix			***manufacturer***	***cat. no.***
320 µl	5x isothermal reaction buffer			
3 µl	T5 exonuclease	*(T5 exonuclease, 10000 U/ml)*	New England Biolabs	M0663
3 µl	DNA Polymerase	*(Phusion® High-Fidelity DNA Polymerase)*	New England Biolabs	M0503
160 µl	*Taq* DNA ligase	*(Taq DNA ligase, 40000 U/ml)*	New England Biolabs	M0208
697 µl	ddH_2O	*(Aqua B. Braun)*	B. Braun Melsungen	0082423E
→ aliquots of both can be stored at –20 °C for at least 12 months				

Table 12: Bacterial strains and media/reagents for bacterial culture

	component		***manufacturer***	***cat. no.***
competent bacteria	*E. Coli* Top10	*(One Shot™ TOP10 Chemically Competent E. coli)*	Invitrogen	C4040
	E. Coli DH5α	*(NEB® 5-alpha Competent E. coli [High Efficiency])*	New England Biolabs	C2987
	E. Coli STABLE	*(NEB® Stable Competent E. coli [High Efficiency])*	New England Biolabs	C3040
growth medium	LB medium	*(Lysogeny Broth [Lennox])*	Carl Roth	X964
	Agar *(16 g/l)*	*(Agar-Agar, Kobe I)*	Carl Roth	5210
antibiotics	Ampicillin *(100 µg/ml)*	*(Ampicillin sodium salt)*	Carl Roth	K029
	Kanamycin *(50 µg/ml)*	*(Kanamycin sulphate)*	Carl Roth	T832
	Spectinomycin *(50 µg/ml)*	*(Spectinomycin dihydrochloride pentahydrate)*	Sigma-Aldrich	S4014

Table 13: Buffers for plasmid miniprep

Buffer P1 (resuspension buffer)			***manufacturer***	***cat. no.***
6.08 g	Tris-Base	*(Tris Base, Molecular Biology Grade)*	Merck Millipore	648310
3.72 g	EDTA	*(Ethylenediaminetetraacetic acid disodium salt dihydrate)*	Sigma-Aldrich	E5134
100 µg/ml	RNase	*(from GeneJET Plasmid Miniprep Kit)*	Thermo Scientific	K0503
ad 1000 ml	H_2O			
		→ adjust to pH 8.0 with HCl, store at 4 °C		
Buffer P2 (lysis buffer)			***manufacturer***	***cat. no.***
8.0 g	NaOH	*(Sodium hydroxide, pellets)*	Acros Organics	13407
10.0 g	SDS	*(Sodium dodecyl sulfate)*	Sigma-Aldrich	L3771
ad 1000 ml	H_2O			
Buffer P3 (neutralization buffer)			***manufacturer***	***cat. no.***
294 g	KAc	*(Potassium acetate)*	Carl Roth	T874
~75 ml	Acetic acid	*(Acetic acid glacial)*	VWR Chemicals	20102.292
ad 1000 ml	H_2O			
		→ adjust to pH 5.5 with acetic acid		
Precipitation and washing			***manufacturer***	***cat. no.***
100 %	Isopropanol	*(2-Propanol, ROTIPURAN® ≥99,8 %, p.a.)*	Carl Roth	6752
70 %	Ethanol	*(Ethanol puriss. p.a., absolute)*	Sigma-Aldrich	32221

Table 14: Commercially available kits for plasmid preparation

kit	***manufacturer***	***cat. no.***
GeneJET Plasmid Miniprep Kit	Thermo Scientific	K0503
PureLink™ HiPure Plasmid Maxiprep Kit	Invitrogen	K210007
EndoFree® Plasmid Maxi Kit	Qiagen	12362

5.3.1 miRNA knockdown plasmids and sequences

Sequences for the miRNAs (Table 16) were designed using the Block-iT™ RNAi Designer tool by Invitrogen (*rnaidesigner.thermofisher.com/rnaiexpress/)*. In cases where a higher number of putative miRNAs was suggested, the ones with the best predicted activity were selected, with binding in the open reading frame (ORF) or 3' untranslated region (UTR) of the target mRNA. The miRNA control sequence, which should not be able bind anywhere in the vertebrate genome, was derived from the BLOCK-iT™ Pol II miR RNAi Expression Vector Kit with EmGFP (Invitrogen, cat. no. K493600) and the finished miRNA control plasmid kindly provided by Dr. Adam O'Neill.

Table 15: Components of 10× miRNA Annealing Buffer

	component		***manufacturer***	***cat. no.***
100 mM	Tris-HCl, pH 7.5-8.0	*(Trizma® hydrochloride)*	Sigma-Aldrich	T3253
500 mM	NaCl	*(Sodium chloride)*	Sigma-Aldrich	S3014
10 mM	EDTA	*(Ethylenediaminetetraacetic acid disodium salt dihydrate)*	Sigma-Aldrich	E5134
in	ddH_2O	*(Aqua B. Braun)*	B. Braun Melsungen	0082423E
	→ dilute 1 : 10 in ddH_2O to obtain 1× Annealing Buffer			

The plasmid *pENTRY-GW-grandestuffer* (Figure 33A) was prepared by removing the insert with *BsaI* digestion, and single-strand oligonucleotides of the miRNA Top and Bottom strands were annealed in Annealing Buffer (Table 15) to form a double-stranded insert, which was ligated into the *pENTRY* backbone. Successful clones (Figure 33B), as determined by *PvuII* digestion, were then recombined into *pCAG-GS-DEST* (Figure 33C) by LR Gateway cloning using the Gateway™ LR Clonase™ II Enzyme mix (Invitrogen, cat. no. 11791020) according to the manufacturer's protocol to obtain the final miRNA plasmid, *pCAG-emGFP-miRNA* (Figure 33D).

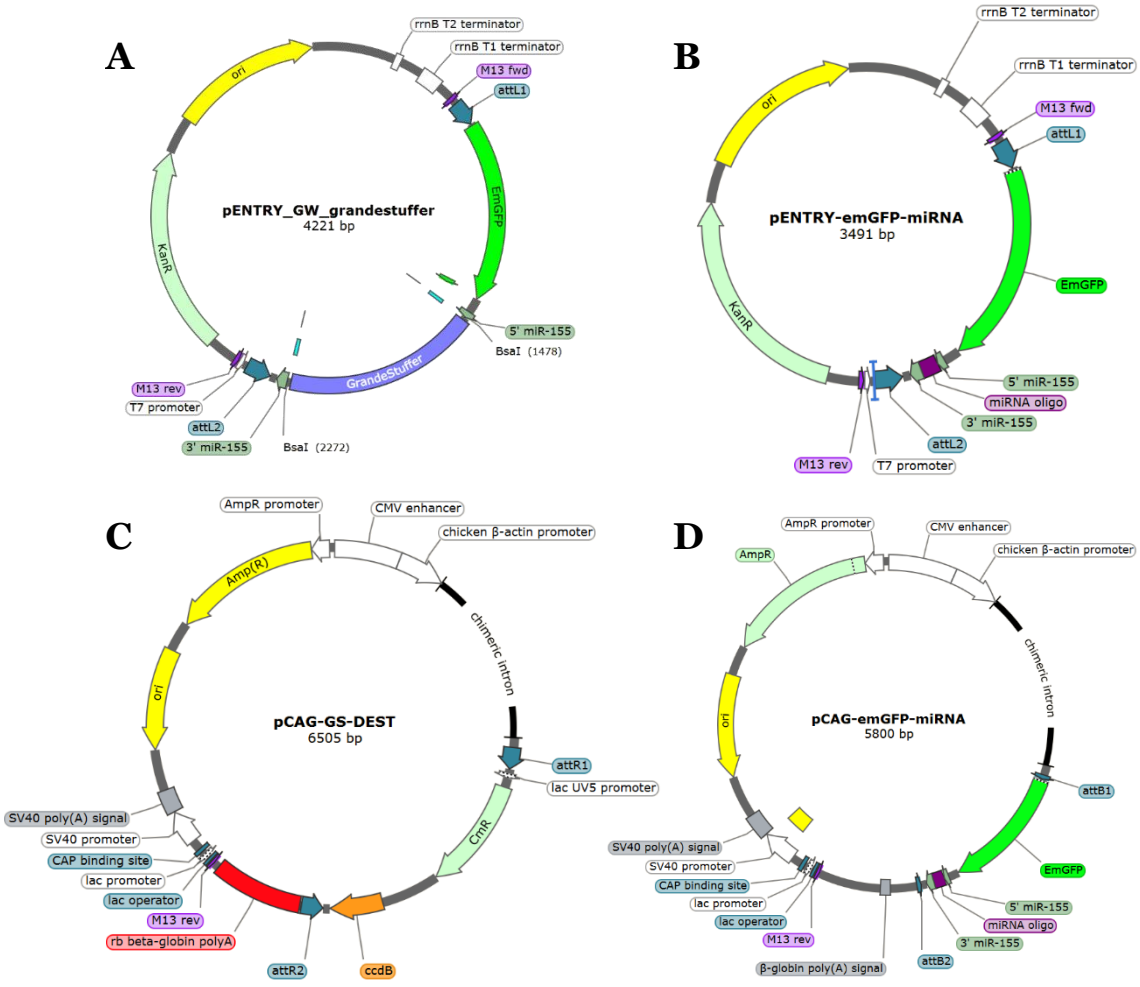

Figure 33: Plasmids used in miRNA cloning

Plasmid maps created with SnapGene® Viewer software (Insightful Science; snapgene.com). ***A.*** *pENTRY-GW-grandestuffer, the starting plasmid for the EmGFP-miRNA cassette.* ***B.*** *pENTRY with miRNA cassette ligated 3' to the EmGFP sequence.* ***C.*** *Destination vector for the EmGFP-miRNA cassette, containing a CAG promoter.* ***D.*** *Finished miRNA knockdown plasmid.*

Table 16: Sequences of miRNAs (5'→3')

miRNA	*mature miRNA sequence*	*binding region*	*ssOligonucleotide sequences*	
miRNA control	GAAATGTACTGCGCGTGGAGAC	none		
Gatad2b-miRNA1	TTCTTTAGCAGCACCAGGCGA	ORF	top	TGCTGTTCTTTAGCAGCACCAGGCGAGTTTTG GCCACTGACTGACTCGCCTGGCTGCTAAAGAA
			bottom	CCTGTTCTTTAGCAGCCAGGCGAGTCAGTCAG TGGCCAAAACTCGCCTGGTGCTGCTAAAGAAC
Gatad2b-miRNA2	TACAACTTCTTCCAAGCCTAC	ORF	top	TGCTGTACAACTTCTTCCAAGCCTACGTTTTG GCCACTGACTGACGTAGGCTTAAGAAGTTGTA
			bottom	CCTGTACAACTTCTTAAGCCTACGTCAGTCAG TGGCCAAAACGTAGGCTTGGAAGAAGTTGTAC
Gatad2b-miRNA3	TATTTCTGCCCACTGATGGAC	ORF	top	TGCTGTATTTCTGCCCACTGATGGACGTTTTG GCCACTGACTGACGTCCATCAGGGCAGAAATA
			bottom	CCTGTATTTCTGCCCTGATGGACGTCAGTCAG TGGCCAAAACGTCCATCAGTGGGCAGAAATAC
Gatad2b-miRNA4	ATTCAAGGATGGGCAGTACAA	3' UTR	top	CCTGATTCAAGGATGCAGTACAAGTCAGTCAG TGGCCAAAACTTGTACTGCCCATCCTTGAATC
			bottom	TGCTGATTCAAGGATGGGCAGTACAAGTTTTG GCCACTGACTGACTTGTACTGCATCCTTGAAT
Gatad2b-miRNA5	AATGGGTAAAGGATTCAAGGA	3' UTR	top	TGCTGAATGGGTAAAGGATTCAAGGAGTTTTG GCCACTGACTGACTCCTTGAACTTTACCCATT
			bottom	CCTGAATGGGTAAAGTTCAAGGAGTCAGTCAG TGGCCAAAACTCCTTGAATCCTTTACCCATTC
Gatad2b-miRNA6	TTTCCATGTATGGTAGGCACC	3' UTR	top	TGCTGTTTCCATGTATGGTAGGCACCGTTTTG GCCACTGACTGACGGTGCCTAATACATGGAAA
			bottom	CCTGTTTCCATGTATTAGGCACCGTCAGTCAG TGGCCAAAACGGTGCCTACCATACATGGAAAC
Mta3-tv1-miRNA1	ATAAGCAGGAGAGGACAGAGT	3' UTR	top	TGCTGATAAGCAGGAGAGGACAGAGTGTTTTG GCCACTGACTGACACTCTGTCCTCCTGCTTAT
			bottom	CCTGATAAGCAGGAGGACAGAGTGTCAGTCAG TGGCCAAAACACTCTGTCCTCTCCTGCTTATC
Mta3-tv1-miRNA2	TTAAATTGAGAAGTGAGCCCA	3' UTR	top	TGCTGTTAAATTGAGAAGTGAGCCCAGTTTTG GCCACTGACTGACTGGGCTCATCTCAATTTAA
			bottom	CCTGTTAAATTGAGATGAGCCCAGTCAGTCAG TGGCCAAAACTGGGCTCACTTCTCAATTTAAC
Mta3-tv2-miRNA1	TTCTGTCTCATTCAGCAGGGC	ORF	top	TGCTGTTCTGTCTCATTCAGCAGGGCGTTTTG GCCACTGACTGACGCCCTGCTATGAGACAGAA
			bottom	CCTGTTCTGTCTCATAGCAGGGCGTCAGTCAG TGGCCAAAACGCCCTGCTGAATGAGACAGAAC
Mta3-tv2-miRNA2	TTCCAATACAGCCAACAGGTC	ORF	top	TGCTGTTCCAATACAGCCAACAGGTCGTTTTG GCCACTGACTGACGACCTGTTCTGTATTGGAA
			bottom	CCTGTTCCAATACAGAACAGGTCGTCAGTCAG TGGCCAAAACGACCTGTTGGCTGTATTGGAAC
Mta3-tv3+4-miRNA1	AAAGAGAGAGCGAGGGAGAGA	3' UTR	top	TGCTGAAAGAGAGAGCGAGGGAGAGAGTTTTG GCCACTGACTGACTCTCTCCCGCTCTCTCTTT
			bottom	CCTGAAAGAGAGAGCGGGAGAGAGTCAGTCAG TGGCCAAAACTCTCTCCCTCGCTCTCTCTTTC

5.3.2 gRNA plasmids (STAgR) and sequences and subcloning into piggyBac transposon vectors

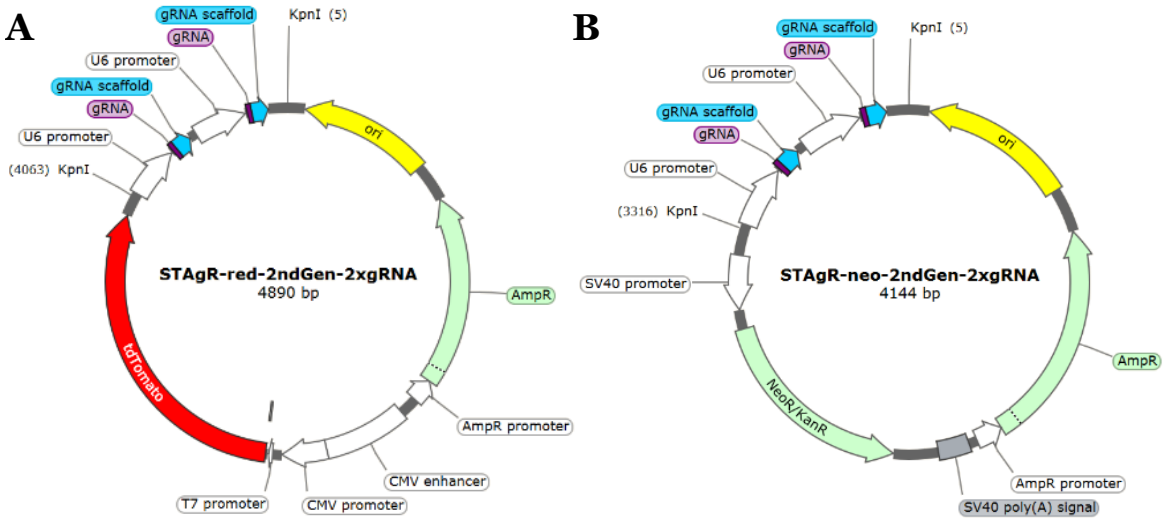

Figure 34: Plasmid map of tdTomato and neomycin STAgR plasmids with two gRNAs

Plasmid maps created with SnapGene® Viewer software (Insightful Science; snapgene.com). ***A.*** *STAgR red with fluorescent reporter tdTomato and two gRNAs with scaffold, flanked by hU6 promoters.* ***B.*** *The equivalent STAgR plasmid with neomycin resistance cassette.*

For testing transcription activation potential of gRNAs, STAgR plasmids containing one or two gRNAs were cloned into backbones encoding either for the fluorescent reporter tdTomato or a Neomycin selection cassette (Figure 34) as previously described (Breunig et al. 2018). A multiplexed vector with 15 consecutive gRNA cassettes was developed by Dr. Christopher Breunig and synthetized by Life Technologies GmbH (Darmstadt, Germany; Construct no. 19AEWLAC). This multiplexed plasmid contains one gRNA per gene, and the gRNA closer to the TSS was chosen (gRNA1). All gRNA sequences are listed in Table 17.

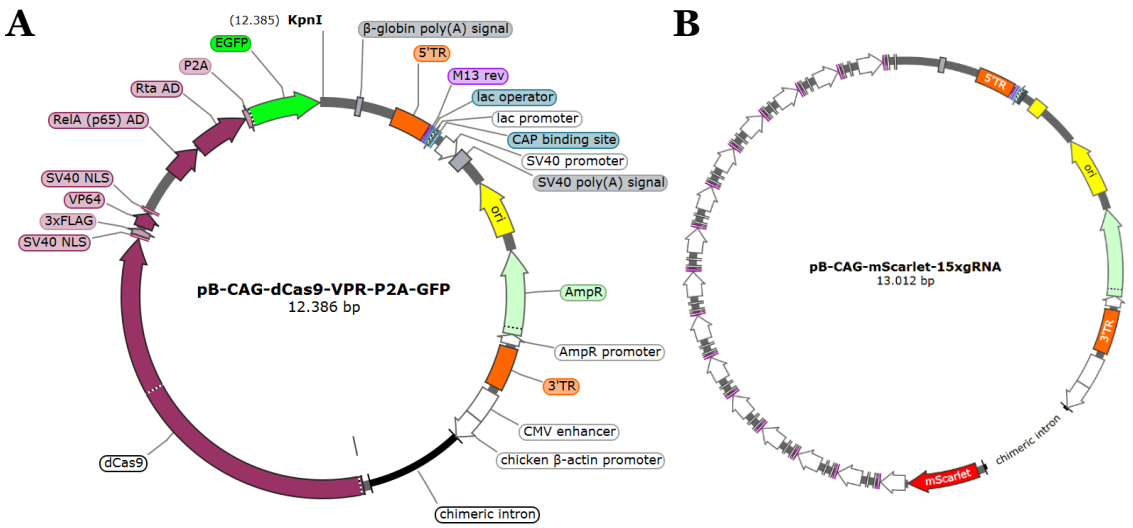

Figure 35: piggyBac plasmids for in vivo expression of dCas9-VPR and gRNAs

Plasmid maps created with SnapGene® Viewer software (Insightful Science; snapgene.com). A. piggyBac plasmid encoding for dCas9-VPR and GFP reporter. gRNA cassettes were subcloned from STAgR plasmids into the KpnI restriction site. B. Multiplexed piggyBac vector with 15x gRNA and CAG-mScarlet reporter.

For subcloning into piggyBac vectors for in vivo application, STAgR plasmids containing four gRNAs with MS2 stem loops were cloned and the entire cassette, cut at KpnI restriction sites, inserted into the piggyBac backbone *pB-CAG-dCas9-VPR-P2A-GFP* (Figure 35A), randomly integrating sense or antisense (in collaboration with Manpreet Kaur). The multiplexed 15x gRNA cassette was subcloned into the empty piggyBac backbone and a *CAG-mScarlet* reporter cassette inserted by Gibson assembly to obtain the *pB-CAG-mScarlet-15xgRNA* plasmid (Figure 35B).

Table 17: gRNA sequences (5' → 3') for neurogenic candidate activation

The gRNA1 of candidates numbered from 1 to 15 are included in the multiplexed 15x gRNA vectors from 5' → 3' in the noted order. For initial testing of activation potential, two gRNAs were used.

candidate		*gRNA1*	*gRNA2*
	ntgRNA	ACCAATTCAGTCGACTGCCC	
1.	**Nhlh1**	GATGTTTAATATTGATGAGG	
2.	**FoxG1**	CAAGGCCTTTAAAAAGATCG	
3.	**Otx1**	CCTGTCACTCAGTCCGCTCT	GTTAGCGCGCGACCGGGGCG
4.	**Zfp423**	GTGCAAAGTTTGCAGGCGTC	GGAGCCCGTAGGGTCTCAGG
5.	**Nfia**	GCAATCTGAGCCATATGTAT	GCGGCGAGGTTCGAGCCGGC
6.	**Tcf7l1**	GCAGTTCGCCTGGTTCCGAG	
7.	**Dmrt3**	GAGGCCAGGCTGCAGGTGGC	
8.	**Nr2e1**	GAGTTGGGGGAAAAGCTAAG	GAGAGCGCTTGCATTTTCTT
9.	**Emx1**	AGTGGCCCAACTCGGTGTTA	GTGAGTGCATGTGCCAGGCT
10.	**Sox3**	GCTCAGATCCGGGAGGGTTG	GGTCTGGAGGGTGAACGAAA
11.	**Gli2**	CGCCATCCCAGAGACGCTGA	
12.	**FoxP4**	AGGGAGCGCGCCGAGCGACA	
13.	**Mta3**	CCCGCTCGGCGTCGCTCTGC	
14.	**Pou3f4**	ACTAACAGCCTTGTAGTCTC	
15.	**Neurog2**	TGGATGGCCAGGCCAGGGGA	AAACAATCAGATCTGCCCCG
	Neurog1	ATTCACCCGCGCCGCCTCGG	CCGGCCTCCCTCGCTTGATC

5.4 BIOCHEMICAL ASSAYS AND IMAGING

5.4.1 Fluorescence-activated cell sorting (FACS) of cell culture

Cultured cells were dissociated from the plate as described in Chapter 5.2. P19 cells were washed once in PBS (DPBS, no calcium, no magnesium, Gibco, cat. no. 14190) and re-suspended in PBS for sorting. mNPC are more susceptible to damage and were thus directly resuspended in PBS with 5 % BSA solution (75 mg/ml in PBS, see Chapter 5.2.2). The cell suspension was filtered through a cell strainer (pluriStrainer Mini 40 µm, PluriSelect, cat. no. 43-10040-60) into suitable sample tubes (Falcon™ Round-Bottom Polypropylene Test Tubes With Cap, Falcon, cat. no. 352063) to avoid clogging the fluidics system with cell aggregates.

Samples were sorted on a FACSAria™ III Cell Sorter (BD Biosciences) with the FACSDiva software (version 6.1.3, BD Biosciences). The first gate was set to isolate live cells from small debris and high granularity (unhealthy) cells by forward (FSC) and side scatter (SSC), respectively. A second gate (FSC-area/FSC-width) separated single cells from doublets or aggregates. The sorting gate analyzed fluorescence single or double positive cells by the laser lines 582/15 (tdTomato or mScarlet) and/or 530/30 (GFP), with the cutoff set in a way that a maximum of 0.1 % of the parent population was detected as positive in the mock transfected sample.

Cells were collected for RNA extraction in PBS (P19) or culture medium (mNPC), pelleted by centrifugation and either snap frozen on dry ice or immediately lysed with the RNA extraction buffer (see also Chapter 5.4.2). P19 cells for re-plating were collected in maintenance medium.

5.4.2 RNA extraction from cells, cDNA synthesis and quantitative real-time PCR (qRT-PCR)

RNA was extracted from cells with different commercially available kits (Table 18) depending on the number of cells and the expected RNA yield, according to the manufacturers' protocols including on-column DNase digestion (for RNA extraction from tissue

see Chapter 5.1.4). RNA concentration and quality was assessed by spectrophotometry (NanoDrop ND-1000 Spectrophotometer, Peqlab). Complementary DNA (cDNA) was synthetized with a commercial kit (Table 18) from 20-1000 ng of RNA according to the manufacturer's protocol and diluted 1:5 to 1:30 for qRT-PCR. Reactions were prepared in 384-well format with ready-to-use SYBR green reaction mix to detect gene amplification (Table 18). qRT-PCR was performed on the QuantStudio® 6 Flex real-time PCR system (ThermoFisher) with the associated software.

Table 18: Kits, reagents and equipment used for RNA extraction, cDNA synthesis and qRT-PCR

application	*kit / component*	*manufacturer*	*cat. no.*
RNA extr.	RNeasy® Mini Kit	Qiagen	74106
	PicoPure™ RNA Isolation Kit	Applied Biosystems	KIT0204
	2-Mercaptoethanol	Sigma-Aldrich	805740
	On-Column DNase I digestion set	Sigma-Aldrich	DNASE70
cDNA synth.	Maxima First Strand cDNA Synthesis Kit for RT-qPCR	Thermo Scientific	K1642
qRT-PCR	Hard-Shell 480 PCR Plates 384-Well CLR/CLR	Bio-Rad	HSR-4801
	Microseal 'B' PCR Plate Sealing Film, adhesive, optical	Bio-Rad	MSB1001
	PowerUp™ SYBR™ Green Master Mix	Applied Biosystems	A25742

Custom-made primers for detection were mostly designed using the NCBI Primer Designing Tool (*www.ncbi.nlm.nih.gov/tools/primer-blast/index.cgi*), and were made to span an exon-exon junction wherever possible, to avoid amplification of genomic DNA residues. Custom oligonucleotides were ordered from Sigma/Merck (Darmstadt, Germany) and Metabion (Planegg, Germany). All qRT-PCR primers used in this thesis are listed in Table 19.

Table 19: qRT-PCR primer sequences

Primers are listed by project. Initials mark primers designed or provided from other sources: StS, Dr. Stefan Stricker; SN, Sonia Najas Sales; GC, Dr. Germán Camargo Ortega; Stock, common primers of the laboratory.

	target		*forward primer*	*reverse primer*
house-keeping	Actb	*Stock*	TTGCTGACAGGATGCAGAAG	ACATCTGCTGGAAGGTGGAC
	GAPDH	*Stock*	GTGTTCCTACCCCCAATGTGT	ATTGTCATACCAGGAAATGAGCTT
	Rpl27	*GC*	ACAACCACCTCATGCCCACA	CTGGCCTTGCGCTTCAAA
NuRD complex subunits	Gatad2a		TGAACTTCTTGCCCAGTGCT	GAAATCCTGCCTGCTTGTGTC
	Gatad2b	*Stock*	TGGTGTCAAGGGTTATGAAG	ATTATGTCTGGGGAAGGAGT
	Mta1	*Stock*	TCTTGATGCCCAGTAGGG	TTCGGTGGCCATGTAAAATA
	Mta2	*Stock*	TTTCTAGTAGCCTCAACAGC	AGATGTCTGTCTCGTTCAAG
	Mta3	*Stock*	ACCAAATCCCAACCAAATCT	GTCTACACTGCATGTTAGGT
	Mta3_tv1		GGAGCCTCCTTCTCTGACGG	CTTCATGCCCTTACCGGCTC
	Mta3_tv2		ACATATCAGGGGGAAGTGCAG	ATCTGAGTCTTCTGGTAGCATGTC
	Mta3_tv3+4		AGACGGCCGTTTGTTGCTAT	CAAGGAGCGGAACGCGG
neurogenesis candidates (gRNA activation test)	Dmrt3		GCGCAGCTTGCTAAACCAG	CCTCTGATCGGTGTCTTTGTCA
	Emx1	*StS*	GCTAAGCGGGGTTTCACCATA	CCTGAGCGGTTCCTCTGATG
	FoxG1		CTGATTGGTTCGGCAGTAGGA	CGAGGCTAGGAGACAGCGAT
	FoxP4		GCTGTTACTGCTACCTCGTTT	CTGTCTCTCCGAGATGTGAGC
	Gli2		CAACGCCTACTCTCCCAGAC	GAGCCTTGATGTACTGTACCAC
	Mta3		(see above)	
	Neurog1	*StS*	CCAGCGACACTGAGTCCTG	CGGGCCATAGGTGAAGTCTT
	Neurog2	*Stock*	ACCGCATGCACAACCTAAAC	AGCGCCCAGATGTAATTGTG
	Nfia	*StS*	TTCCAACGTCACCCATCATCC	CAGCATCAGGACAGACAAGTT
	Nhlh1		GAGTCCTTCTAGGCTCCAGGC	AAATGCGGATCCTCTCCCCA
	Nr2e1	*StS*	GGGAAGCACTACGGGGTCTA	GTGTCTTGTCTACGGGGCAT
	Otx1	*StS*	ATGTCTTACCTCAAACAACCC	GTAGCGAGTCTTTGCGAACAG
	Pou3f4	*StS*	CTGCCTCGAATCCCTACAGC	CTGCAAGTAGTCACTTTGGAGAA
	Sox3	*StS*	GCCGACTGGAAACTGCTGA	CGTAGCGGTGCATCTGAGG
	Tcf7l1		TCCAGCACACTTGTCCAACAAA	TTTGGGTCGATCTCTGGGGA
	Zfp423	*StS*	TGGCCTGGGATTCCTCTGT	CTCTTGACTTGTCACGCTGTT

(cont. on next page)

	target		*forward primer*	*reverse primer*
trans-posase	PBase		GGAACACAGACCAACGGAGT	CTCGCGTTTGTTTGATCGCA
	mPB		GGGAGAGCATGACCGGC	TGTGGTTGTCCTTCCTCACG
RTR	eIF2a		TGGGACGCCTAACCTACAAC	TGACCAGGAAGGACACCAATTT
	Gcn2		AGTCGTTTCTCAGCGAGCAT	TGGAGGATTTCACGTTGCTCC
	Jnk		GCCGTCTCCTTTAGGTGCAG	TGTATCCGAGGCCAAAGTCG
	p38		CGACGACCACGTTCAGTTTC	GGGCTTTAGGTCCCTGTGAA
	Zak		GAGGCGGAATGTTCAACTCC	AACGTCCACAAAATCTGGCTC
UPR	Atf4	*SN*	GGGTTCTGTCTTCCACTCCA	AAGCAGCAGAGTCAGGCTTTC
	BiP	*SN*	TTCAGCCAATTATCAGCAAACTCT	TTTTCTGATGTATCCTCTTCACCAGT
	Chop	*SN*	CCACCACACCTGAAAGCAGAA	AGGTGAAAGGCAGGGACTCA
	Edem	*SN*	CTACCTGCGAAGAGGCCG	GTTCATGAGCTGCCCACTGA
	GRP94	*SN*	AAGAATGAAGGAAAAACAGGACAAAA	CAAATGGAGAAGATTCCGCC
	total XBP1	*SN*	TGGCCGGGTCTGCTGAGTCC	GTCCATGGGAAGATGTTCTGG
	usXBP1	*SN*	CAGCACTCAGACTATGTGCA	GTCCATGGGAAGATGTTCTGG
	sXBP1	*SN*	CTGAGTCCGAATCAGGTGCAG	GTCCATGGGAAGATGTTCTGG
DDR	Atm		TGGCATTGTGGTGAAGCTAGT	CACCTTCCGACAGCCTCTAA
	Atr		AAGAAGATCAGCAAGAGGTTTATGC	GGTGAGATGGTCAAGCACAGA
	Atrip		CGTCTCCCACGTCAGTCCTA	TGGAAGAGAGGCGTGTTAGC
	p53		GTATTTCACCCTCAAGATCCGC	CTTCAGGTAGCTGGAGTGAGC
	Parp1		CGAGTGGAGTACGCGAAGAG	TCGAACATGGGTGACTGCAC
	Rpa1		ACTTGTGGATGAAAGCGGTGA	TGTTAGCGATCTTCAGGGCG

(Table 19 cont. from previous page)

5.4.3 Immunohistochemistry and immunocytochemistry

For immunocytochemistry (ICC), cells on glass coverslips were fixed in 4 % PFA (see Table 4) for 10 minutes at RT, and stored in PBS (see Table 3) with 0.1 % (w/v) sodium azide (Carl Roth, cat. no. K305) at 4 °C to avoid contamination with microorganisms. (For preparation of tissue for immunohistochemistry (IHC), see Chapter 5.1.3.)

Cells and tissue were stained with the same standard protocol. In brief, samples were washed twice in PBS for 5 minutes at room temperature (RT) and incubated with primary antibodies in staining solution (see Table 20) at 4 °C overnight. They were then washed twice in PBS (as above) before incubating for 1-2 hours at RT with secondary antibodies and 0.1 mg/ml DAPI (4′,6-Diamidino-2-phenylindole dihydrochloride, Sigma-Aldrich, cat. no. D9542) as a counterstain for nuclear DNA. Finally, samples were again washed twice in PBS and coverslips mounted on slides with mounting medium (Aqua-Poly/Mount, Polysciences, cat. no. 18606). Antibodies used are listed in Table 21.

Table 20: Components of standard staining solution for IHC/ICC

	component	***manufacturer***	***cat. no.***
	1× PBS	*(see Table 3)*	
10 %	NGS	*(Normal Goat Serum, New Zealand Origin)* Gibco	16210
0.5 %	Triton-X100	*(Triton® X 100)* Carl Roth	3051

For staining with MTA3 antibody, epitope retrieval had to be performed. For this, samples were treated after the initial washing steps with 2 N hydrochloric acid (Hydrochloric acid standard solution, Carl Roth, cat. no. 0281.1) for 45 minutes at RT, followed by two 15 minute neutralization steps with 0.1 M sodium borate, pH 8.5 (di-Sodium tetraborate, Merck, cat. no. 106306) at room temperature. They were washed twice in PBS before incubation with the primary antibodies. Triton X-100 in the staining solution was replaced by Tween20® (Carl Roth, cat. no. 9127) at the same concentration for all steps.

Staining of GFP in neurogenic candidate IUE had to be amplified due to weak signal especially in cells at the apical side. For experiments with *ntgRNA*, *Nr2e1 + Emx1* and *Neurog1 + Otx1*, this was achieved by biotin-streptavidin amplification. A biotin-adsorbed secondary antibody was incubated with other secondary antibodies as stated above, followed by two additional washing steps in PBS and another 1-2 hour incubation with

streptavidin-coupled fluorochrome in staining solution at RT, followed by final washing steps and mounting as above.

For sections of IUE with the Multi 15xgRNA plasmid, a stronger amplification was achieved with a TSA system (TSA Fluorescein System, Akoya Biosciences, cat. no. NEL701A001KT). For this, after the initial washing step, slides were incubated in 0.3 % hydrogen peroxide (Carl Roth, cat. no. 8070) in PBS for 60 minutes at RT to deactivate endogenous peroxidases. This was followed by standard washing steps and incubation with primary and secondary antibodies, with a biotinylated secondary antibody used for the GFP staining at a dilution of 1:100. After two washing steps, slides were incubated with streptavidin-coupled horseradish peroxidase (Strept-HRP, included in TSA system) in staining solution for 1 hour at RT, and then again washed twice. The amplification step was performed by 10 minutes of incubation with Fluorescein reagent diluted 1:70 in Amplification Diluent, followed by final washing steps and mounting.

Table 21: Primary and secondary antibodies for ICC and IHC

Antibodies produced by the Core Facility Monoclonal Antibodies of the Helmholtz Center Munich are listed as HMGU MAB.

Primary antibodies			
target	***host and clonality***	***manufacturer***	***cat. no.***
Cas9 (dCas9)	rat IgG2a monoclonal [8G4-1-1]	HMGU MAB	—
DCX	guinea pig polyclonal	Merck/Millipore	AB2253
GATAD2B	rabbit polyclonal	Sigma	HPA017015
GFP	chicken polyclonal	Aves Labs	GFP-1020
KI-67	rat IgG2a monoclonal [SolA15]	eBioscience	14-5698-82
MTA3	rabbit polyclonal	Proteintech	14682-1-AP
NESTIN	mouse IgG1 monoclonal [rat-401]	Millipore	MAB353
PAX6	rabbit polyclonal	Merck/Millipore	AB2237
PAX6	mouse IgG1 monoclonal [P3U1]	DSHB / HMGU MAB	AB_528427
RFP (mScarlet)	rabbit polyclonal	Rockland	600-401-379
RFP (mScarlet)	rat IgG2a monoclonal [5F8]	HMGU MAB	—
TBR2	rabbit monoclonal [EPR19012]	Abcam	ab183991
Secondary antibodies			
target species and preadsorption	***host***	***manufacturer***	***cat.no.***
chicken-AlexaFluor 488	goat	Invitrogen	A-11039
chicken-biotin	goat	Dianova	103-065-155
guinea pig-AlexaFluor 633	goat	Invitrogen	A-21105
mouse IgG1-AlexaFluor 488	goat	Invitrogen	A-21131
mouse IgG1-AlexaFluor 546	goat	Invitrogen	A-21123
rabbit-AlexaFluor 488	donkey	Invitrogen	A-21206
rabbit-AlexaFluor 546	goat	Invitrogen	A-11010
rabbit-AlexaFluor 633	goat	Invitrogen	A-21070
rat-AlexaFluor 546	goat	Invitrogen	A-11081
rat-AlexaFluor 633	goat	Invitrogen	A-21094
Streptavidin-AlexaFluor 488	—	Invitrogen	S-11223

5.4.4 Fluorescence microscopy, quantification and statistics

Tissue sections with IHC staining were imaged on a confocal microscope (LSM710, Zeiss) with laser lines of 405 nm (blue), 488 nm (green), 561 nm (red) and 633 nm (far red) used. Immunostained cells were imaged on the same confocal microscope or an inverted epifluorescent microscope (Axio Observer Z1, Zeiss). The software used for acquisition in both cases was ZEN (ZEN black v2.3 SP1, Carl Zeiss). Live cells were imaged on an inverted epifluorescent and brightfield microscope (DM IL LED, Leica) with corresponding acquisition software (Leica Application Suite v4.6.1, Leica).

Cell distribution and marker colocalization was analyzed in ImageJ Fiji v1.53 (Rueden et al. 2017; Schindelin et al. 2012) using the region of interest (ROI) manager and Multi-Point tool and cells counted by colocalization of reporter with nuclear staining (DAPI) or marker staining. For cell culture, at least three random fields of view were quantified. For IUE sections, one optical slice per tissue section was quantified by creating a column of five equidistant bins across the cortex. As IUE areas tend to have conical shape with width increasing from VZ to CP, the column was no wider than the electroporation site at the VZ. At least three sections per animal were quantified. Statistical analysis was performed in GraphPad Prism v8.3.0 (GraphPad Software, LLC) using the Kruskal-Wallis ANOVA with Dunn's post-hoc multiple comparisons test to compare each treatment to control, with $p<0.05$ considered significant.

To determine electroporation area, density and GFP intensity in ImageJ Fiji, one section per animal was selected in the putative rostro-caudal center of the IUE area and a Z-Stack was recorded. Quantification was performed on maximum intensity projections by selecting the IUE area containing all GFP^+ cell bodies as ROI. A threshold was applied to the GFP channel which excluded background with an intensity below 35 and a mask was created which contained all areas (cells) with intensity >35, allowing the measurement of GFP^+ area per total IUE area (IUE density). The mask was then applied back to the original image and average GFP intensity was measured within the cells.

5.5 RNA-SEQUENCING

5.5.1 Extraction and dissociation of cells from embryonic brain

Wild type C57/Bl6J embryos at E14 and E18 were used for the RNA sequencing experiments, with tissue of one litter/mother being pooled and considered one biological replicate. Brains were dissected in 1× HBSS (Gibco, cat. no. 14025) with 10 mM HEPES (Gibco, cat. no. 15630). Lateral cortex from the mediolateral to the cortex-LGE border, and LGE without overlying ventrolateral cortex, were dissected and centrifuged at 1000 rpm, 4 °C for five minutes. Dissection buffer was aspirated and tissue was enzymatically dissociated with 1 ml of 0.05 % Trypsin/EDTA (Gibco, cat. no. 25300) for 15 minutes at 37 °C. Digestion was inhibited by adding 2 ml DMEM (Gibco, cat. no. 61965) with 10 % FBS (PAN Biotech, cat. no. P30-3302) and tissue was further mechanically dissociated with a fire-polished glass Pasteur pipette coated with DMEM + 10 % FBS to obtain a single-cell suspension. The suspension was centrifuged at 1000 rpm, 4 °C for 5 minutes, the supernatant aspirated and the cells resuspended in 1× Staining Solution (Table 22).

Table 22: Components of 1× Staining Solution for live cell staining

Solution I			***manufacturer***	***cat. no.***
50 ml	HBSS (10×)	*(HBSS (10X), calcium, magnesium, no phenol red)*	Gibco	14065
9.0 ml	Glucose	*(D-(+)-Glucose solution 45% in H2O)*	Sigma	G8769
7.5 ml	HEPES (1 M)	*(HEPES [1 M])*	Gibco	15630
ad 500 ml	ddH_2O	*(Aqua B. Braun)*	B. Braun Melsungen	0082423E
		→ adjust pH to 7.5 and store at –20 °C		
2× Staining Solution			***manufacturer***	***cat. no.***
5 ml	FBS	*(Fetal bovine serum premium)*	PAN Biotech	P30-3302
100 µl	NaN_3 (0.1 % w/v in PBS)	*(Sodium azide)*	Carl Roth	K305
2 ml	EDTA (1 mM)	*(EDTA disodium salt dihydrate)*	Sigma-Aldrich	E5134
ad 50 ml	DMEM-F12	*(DMEM/F-12 [1:1] [1X])*	Gibco	21331
1× Staining Solution				
		→ mix Solution I and 2× Staining Solution at equal volumes and store at 4 °C		

5.5.2 Live cell staining and FACS

The cell suspension was divided into three samples for unstained control (75 µl), isotype control (75 µl) and stained sample (850 µl). Volume was adjusted to 750 µl (unstained and isotype) and 1500 µl (stained), respectively, with 1× Staining Solution (Table 22). Preadsorbed antibodies were added to the stained sample, mCD133-PE at 1:500 dilution (Anti-Mouse-CD133-PE [13A4], eBioscience/Invitrogen, cat. no. 12-1331-82) and PSA-NCAM-APC at 1:750 dilution (Anti-PSA-NCAM-APC [human, mouse, rat], Miltenyi Biotec, cat. no. 130-093-273). Corresponding isotype control antibodies (Rat IgG1 κ Isotype Control PE [eBIRG1], eBioscience/Invitrogen, cat. no. 12-4301-81; Mouse IgM-APC, Miltenyi Biotec, cat. no. 130-093-176) were added to the isotype control sample in the same dilutions. Cells were incubated at 4 °C in the dark for 25 minutes, then DAPI (1:1000 dilution of 1 mg/ml stock; Sigma-Aldrich, cat. no. D9542) was added followed by another 5 minutes of incubation. To wash the cells, the suspension was filled up to 10 ml with PBS (Gibco, cat. no. 14190) and centrifuged at 1000 rpm, 4 °C for 5 minutes. The supernatant was aspirated, cells were resuspended in 1000 µl (stained) or 300 µl (unstained/isotype control) PBS and filtered through a cell strainer (pluriStrainer Mini 40 µm, PluriSelect, cat. no. 43-10040-60) into suitable sample tubes (Falcon™ Round-Bottom Polypropylene Test Tubes With Cap, Falcon, cat. no. 352063).

Cells were sorted on a FACSAria™ III Cell Sorter (BD Biosciences) with FACSDiva software (version 6.1.3, BD Biosciences). To separate the populations (see also Figure 15), the first gate was set to separate small debris (low FSC) and dead or damaged cells, which were $DAPI^+$ (high 450/40 signal). The second gate was set to remove doublets or cell aggregates by FSC-area/FSC-width. The third gate separated the stained populations by the laser lines 582/15 and 660/20 for PE and APC, respectively, with the gate set so that max. 0.1 % of the parent population in the isotype control was detected as single or double positive.

Sorted cells were collected in PBS and centrifuged at 1000 rpm, 4 °C for 10 minutes. The supernatant was aspirated and cells were immediately lysed in RNA extraction buffer.

5.5.3 RNA extraction and library generation

Total RNA extraction was performed with the PicoPure™ RNA Isolation Kit (Applied Biosystems, cat. no. KIT0204) according to the manufacturer's protocol with on-column DNase digestion (On-Column DNase I digestion set, Sigma-Aldrich, cat. no. DNASE70). RNA concentration and quality were evaluated on the Bioanalyzer (Model 2100, Agilent) using the RNA 6000 Pico Kit (Agilent, cat. no. 5067-1513) according to the manufacturer's protocol. Samples with an RNA Integrity number (RIN) <8.0 were excluded from library preparation.

First-strand cDNA was prepared from 2 ng RNA per sample with the SmartSeq v4 Ultra Low Input RNA Kit for Sequencing (TaKaRa/Clontech, cat. no. 634897) according to the manufacturer's instructions. Number of amplification cycles for each sample was determined with a side qRT-PCR reaction performed after the first 4 amplification cycles (Table 23) to avoid over-amplification bias. With this, the number of required total amplification cycles for each sample corresponded to the cycle number at ¼ of the maximum fluorescence signal (Rn).

Table 23: Side qRT-PCR reaction for cDNA amplification

Reaction				***manufacturer***	***cat. no.***
5 µl	pre-amplified DNA (4 cycles)				
1.5 µl	ddH_2O				
1.0 µl	primer PCR_SMARTer II A	*5´-AAGCAGTGGTATCAACGCAGAGT-3´*			
7.5 µl	2× PCR master mix	*(SensiMix™ SYBR® No-ROX Kit)*		Bioline	QT650
15 µl	total volume				
Cycler program					
	95 °C	10 min			
	98 °C	10 sec	35 cycles		
	65 °C	30 sec			
	68 °C	3 min			
	72 °C	10 min			
	4 °C	pause			

The amplified cDNA was purified using AMPure XP magnetic beads (Beckmann Coulter, cat. no. QT650) and quality and quantity analyzed by Bioanalyzer (High Sensitivity DNA Kit, Agilent, cat. no. 5067-4626) and Qubit Assay (Qubit™ dsDNA HS Assay Kit and tubes, Invitrogen, cat. nos. Q32854/Q32856). Purified DNA was fragmented by ultrasonic shearing on the Covaris AFA S220 system using corresponding tubes (microTube AFA Fiber Pre-Slit Snap-Cap 6x16mm, Covaris, cat. no. 520045), resulting in approximately 200 bp – 500 bp long fragments that were purified by ethanol precipitation.

Samples were evaluated again on the Bioanalyzer (HS DNA assay) before proceeding to the library preparation with the MicroPlex Library Preparation Kit v2 (Diagenode, cat. no. C05010014) according to the manufacturer's instructions, using 10 ng of DNA per sample. Following the library amplification, DNA concentration was verified by Qubit assay and the libraries were purified over AMPure XP magnetic beads.

Quality and quantity of these final libraries was evaluated by Bioanalyzer HS DNA assay and samples were multiplexed at 5nM each in two pools consisting of uniquely barcoded libraries, which were again evaluated on the Bioanalyzer before sequencing.

Next generation sequencing was performed at the NGS facility, Institute of Human Genetics, Helmholtz Center Munich on an Illumina HiSeq 4000system as 100-bp paired-end deep sequencing. Pool 1, consisting of 21 samples, was run on three lanes and pool 2, 15 samples, on two lanes, resulting in an average of approximately 50 million reads per sample.

5.5.4 Analysis of transcriptomic data

Processing and initial analysis was performed by Dr. Pawel Smialowski: Reads were aligned to the mouse genome (mm10, UCSC Genome Browser) with STAR v2.5.3a (Dobin et al. 2013), with approximately 28 million reads per sample (~56 %) uniquely mapped on average. Genes and isoforms were quantified with RSEM v1.3 (Li, B. and Dewey 2011) and differential gene expression analysis was performed with the help of the DESeq2 algorithm (Love et al. 2014) running in R environment (*www.r-project.org*, R Foundation for Statistical Computing, Vienna, Austria).

The identification of most characteristic regulated genes between E14 and E18 cortical RGC (Figure 17) was performed by Dr. Pawel Smialowski. These consisted of the genes whose regulation was strongest, i.e. whose Log2 fold change was among the Top 20. Additional criteria for biological relevance were added by the normalized read counts, which must be higher than 45 in the upregulated condition to ensure sufficient expression levels for presumed biological relevance. On the other hand, they must not be higher than 450 in the downregulated condition, as this would imply functional relevance for the gene in both up- and downregulated condition, implying a more modulating property rather than being characteristic for the cell fate switch. The heatmap was plotted using the rLog normalized read counts.

Identification of upstream factors (Figure 18B) was performed by Dr. Pawel Smialowski as described previously (Angerilli et al. 2018).

For evaluating the role of TF and ChR in maintaining stemness and plasticity (Figure 18A, Figure 23), all mouse TF and ChR were identified by filtering for the corresponding GO terms (Table 24) in AmiGO drill-down ontology (AmiGO v2.5, *amigo.geneontology.org/amigo/dd_browse*). The proportion of these genes among all regulated genes between two compared cell states, or the intersections between cell states, was determined by list overlap.

Table 24: AmiGO drill-down GO terms to identify TF and ChR

AmiGO drill-down GO terms		
transcription factors (TF)	GO:0140110	transcription regulator activity
chromatin remodelers (ChR)	GO:0034724	DNA replication-independent nucleosome organization
	GO:0031497	chromatin assembly
	GO:0031498	chromatin disassembly
	GO:0034401	chromatin organization involved in regulation of transcription
	GO:0006338	chromatin remodeling
	GO:0016569	covalent chromatin modification
	GO:0090202	gene looping
	GO:0070828	heterochromatin organization
	GO:0034728	nucleosome organization
	GO:0006342	chromatin silencing

Pathway overrepresentation analysis was performed with PANTHER v14 (*pantherdb.org*, overrepresentation test: release of 12.07.2019). Lists of regulated genes were compared against the mouse genome as a background reference with Fisher/Bonferroni statistical test with $p<0.05$ being considered significant. Annotation was chosen as *GO: biological process full*.

APPENDIX

REFERENCES

Agashe, Martinez-Gomez, Drummond, and Marx. 2013. "Good Codons, Bad Transcript: Large Reductions in Gene Expression and Fitness Arising from Synonymous Mutations in a Key Enzyme." *Molecular Biology and Evolution* 30 (3): 549–60. https://doi.org/10.1093/molbev/mss273.

Agirman, Broix, and Nguyen. 2017. "Cerebral Cortex Development: An Outside-in Perspective." *FEBS Letters* 591 (24): 3978–92. https://doi.org/10.1002/1873-3468.12924.

Akter, Kaneko, and Sawamoto. 2020. "Neurogenesis and Neuronal Migration in the Postnatal Ventricular-Subventricular Zone: Similarities and Dissimilarities between Rodents and Primates." *Neuroscience Research*. https://doi.org/10.1016/j.neures.2020.06.001.

Allen, Wade, and Kutateladze. 2013. "The NuRD Architecture." *Cellular and Molecular Life Sciences* 70 (19): 3513–24. https://doi.org/10.1007/s00018-012-1256-2.

Alqarni, Murthy, Zhang, Przewloka, Silva, Watson, Lejon, Pei, Smits, Kloet, Wang, Shepherd, Stokes, Blobel, Vermeulen, Glover, Mackay, and Laue. 2014. "Insight into the Architecture of the NuRD Complex: Structure of the RbAp48-MTA1 Subcomplex." *Journal of Biological Chemistry* 289 (32): 21844–55. https://doi.org/10.1074/jbc.M114.558940.

Amaral, Scharfman, and Lavenex. 2007. "The Dentate Gyrus: Fundamental Neuroanatomical Organization (Dentate Gyrus for Dummies)." In *Progress in Brain Research*, 163:3–790. https://doi.org/10.1016/S0079-6123(07)63001-5.

Angerilli, Smialowski, and Rupp. 2018. "The Xenopus Animal Cap Transcriptome: Building a Mucociliary Epithelium." *Nucleic Acids Research* 46 (17): 8772–87. https://doi.org/10.1093/nar/gky771.

Arai, Pulvers, Haffner, Schilling, Nüsslein, Calegari, and Huttner. 2011. "Neural Stem and Progenitor Cells Shorten S-Phase on Commitment to Neuron Production." *Nature Communications* 2 (1). https://doi.org/10.1038/ncomms1155.

Artegiani and Calegari. 2013. "Lentiviruses Allow Widespread and Conditional Manipulation of Gene Expression in the Developing Mouse Brain." *Development (Cambridge)* 140 (13): 2818–22. https://doi.org/10.1242/dev.093823.

Bansod, Kageyama, and Ohtsuka. 2017. "Hes5 Regulates the Transition Timing of Neurogenesis and Gliogenesis in Mammalian Neocortical Development." *Development (Cambridge)* 144 (17): 3156–67. https://doi.org/10.1242/dev.147256.

Bao, Talmage, Role, and Gautier. 2000. "Regulation of Neurogenesis by Interactions between HEN1 and Neuronal LMO Proteins." *Development* 127 (2): 425–35.

Barker, Götz, and Parmar. 2018. "New Approaches for Brain Repair - from Rescue to Reprogramming." *Nature* 557 (7705): 329–34. https://doi.org/10.1038/s41586-018-0087-1.

Barkho, Song, Aimone, Smrt, Kuwabara, Nakashima, Gage, and Zhao. 2006. "Identification of Astrocyte-Expressed Factors That Modulate Neural Stem/Progenitor Cell Differentiation." *Stem Cells and Development* 15 (3): 407–21. https://doi.org/10.1089/scd.2006.15.407.

Beckervordersandforth, Tripathi, Ninkovic, Bayam, Lepier, Stempfhuber, Kirchhoff, Hirrlinger, Haslinger, Lie, Beckers, Yoder, Irmler, and Götz. 2010. "In Vivo Fate Mapping and Expression Analysis Reveals Molecular Hallmarks of Prospectively Isolated Adult Neural Stem Cells." *Cell Stem Cell* 7 (6): 744–58. https://doi.org/10.1016/j.stem.2010.11.017.

Behringer, Gertsenstein, Vintersten Nagy, and Nagy. 2017. "Reprogramming Mouse Fibroblasts with PiggyBac Transposons." *Cold Spring Harbor Protocols* 2017 (10): 827–30. https://doi.org/10.1101/pdb.prot092627.

Berg, Su, Jimenez-Cyrus, Patel, Huang, Morizet, Lee, Shah, Ringeling, Jain, Epstein, Wu, Canzar, Ming, Song, and Bond. 2019. "A Common Embryonic Origin of Stem Cells Drives Developmental and Adult Neurogenesis." *Cell* 177 (3): 654-668.e15. https://doi.org/10.1016/j.cell.2019.02.010.

Bi, Salmaso, Komitova, Simonini, Silbereis, Cheng, Kim, Luft, Ment, Horvath, Schwartz, and Vaccarino. 2011. "Cortical Glial Fibrillary Acidic Protein-Positive Cells Generate Neurons after Perinatal Hypoxic Injury." *The Journal of Neuroscience : The Official Journal of the Society for Neuroscience* 31 (25): 9205–21. https://doi.org/10.1523/JNEUROSCI.0518-11.2011.

Bode, Yu, Tate, Pardo, and Choudhary. 2016. "Characterization of Two Distinct Nucleosome Remodeling and Deacetylase (NuRD) Complex Assemblies in Embryonic Stem Cells." *Molecular & Cellular Proteomics* 15 (3): 878–91. https://doi.org/10.1074/mcp.M115.053207.

Bonaguidi, Wheeler, Shapiro, Stadel, Sun, Ming, and Song. 2011. "In Vivo Clonal Analysis Reveals Self-Renewing and Multipotent Adult Neural Stem Cell Characteristics." *Cell* 145 (7): 1142–55. https://doi.org/10.1016/j.cell.2011.05.024.

Bowen, Fujita, Kajita, and Wade. 2004. "Mi-2/NuRD: Multiple Complexes for Many Purposes." *Biochimica et Biophysica Acta (BBA) - Gene Structure and Expression* 1677 (1–3): 52–57. https://doi.org/10.1016/j.bbaexp.2003.10.010.

Brackertz, Gong, Leers, and Renkawitz. 2006. "P66alpha and P66beta of the Mi-2/NuRD Complex Mediate MBD2 and Histone Interaction." *Nucleic Acids Research* 34 (2): 397–406. https://doi.org/10.1093/nar/gkj437.

Breunig, Durovic, Neuner, Baumann, Wiesbeck, Köferle, Götz, Ninkovic, and Stricker. 2018. "One Step Generation of Customizable GRNA Vectors for Multiplex CRISPR Approaches through String Assembly GRNA Cloning (STAgR)." Edited by Knut Stieger. *PLOS ONE* 13 (4): e0196015. https://doi.org/10.1371/journal.pone.0196015.

Brusés and Rutishauser. 2001. "Roles, Regulation, and Mechanism of Polysialic Acid Function during Neural Development." *Biochimie* 83 (7): 635–43. https://doi.org/10.1016/s0300-9084(01)01293-7.

Buchsbaum, Kielkowski, Giorgio, O'Neill, Giaimo, Di, Kyrousi, Khattak, Sieber, Robertson, and Cappello. 2020. "ECE2 Regulates Neurogenesis and Neuronal Migration during Human Cortical Development." *EMBO Reports* 21 (5): e48204. https://doi.org/10.15252/embr.201948204.

Burgold, Barber, Kloet, Cramard, Gharbi, Floyd, Kinoshita, Ralser, Vermeulen, Reynolds, Dietmann, and Hendrich. 2019. "The Nucleosome Remodelling and Deacetylation Complex Suppresses Transcriptional Noise during Lineage Commitment." *The EMBO Journal* 38 (12): 1–18. https://doi.org/10.15252/embj.2018100788.

Cadiñanos and Bradley. 2007. "Generation of an Inducible and Optimized PiggyBac Transposon System." *Nucleic Acids Research* 35 (12): e87. https://doi.org/10.1093/nar/gkm446.

Camargo Ortega, Falk, Johansson, Peyre, Broix, Sahu, Hirst, et al. 2019. "The Centrosome Protein AKNA Regulates Neurogenesis via Microtubule Organization." *Nature* 567 (7746): 113–17. https://doi.org/10.1038/s41586-019-0962-4.

Cao and Kaufman. 2012. "Unfolded Protein Response." *Current Biology* 22 (16): R622–26. https://doi.org/10.1016/j.cub.2012.07.004.

Carleton, Petreanu, Lansford, Alvarez-Buylla, and Lledo. 2003. "Becoming a New Neuron in the Adult Olfactory Bulb." *Nature Neuroscience* 6 (5): 507–18. https://doi.org/10.1038/nn1048.

Cary, Goebel, Corsaro, Wang, Rosen, and Fraser. 1989. "Transposon Mutagenesis of Baculoviruses: Analysis of Trichoplusia Ni Transposon IFP2 Insertions within the FP-Locus of Nuclear Polyhedrosis Viruses." *Virology* 172 (1): 156–69. https://doi.org/10.1016/0042-6822(89)90117-7.

Chavez, Scheiman, Vora, Pruitt, Tuttle, P R Iyer, Lin, et al. 2015. "Highly Efficient Cas9-Mediated Transcriptional Programming." *Nature Methods* 12 (4): 326–28. https://doi.org/10.1038/nmeth.3312.

Chew. 2018. "Immunity to CRISPR Cas9 and Cas12a Therapeutics." *Wiley Interdisciplinary Reviews: Systems Biology and Medicine* 10 (1): 1–23. https://doi.org/10.1002/wsbm.1408.

Ciccia and Elledge. 2010. "The DNA Damage Response: Making It Safe to Play with Knives." *Molecular Cell* 40 (2): 179–204. https://doi.org/10.1016/j.molcel.2010.09.019.

Co, Anderson, and Konopka. 2020. "FOXP Transcription Factors in Vertebrate Brain Development, Function, and Disorders." *Wiley Interdisciplinary Reviews: Developmental Biology* 9 (5): 1–25. https://doi.org/10.1002/wdev.375.

Desmaris, Keruzore, Saulnier, Ratié, Assimacopoulos, Clercq, De, Nan, et al. 2018. "DMRT5, DMRT3, and EMX2 Cooperatively Repress GSX2 at the Pallium–Subpallium Boundary to Maintain Cortical Identity in Dorsal Telencephalic Progenitors." *Journal of Neuroscience* 38 (42): 9105–21. https://doi.org/10.1523/JNEUROSCI.0375-18.2018.

Dimou and Gallo. 2015. "NG2-Glia and Their Functions in the Central Nervous System." *Glia* 63 (8): 1429–51. https://doi.org/10.1002/glia.22859.

Ding, Wu, Li, Han, Zhuang, and Xu. 2005. "Efficient Transposition of the PiggyBac (PB) Transposon in Mammalian Cells and Mice." *Cell* 122 (3): 473–83. https://doi.org/10.1016/j.cell.2005.07.013.

Dobin, Davis, Schlesinger, Drenkow, Zaleski, Jha, Batut, Chaisson, and Gingeras. 2013. "STAR: Ultrafast Universal RNA-Seq Aligner." *Bioinformatics (Oxford, England)* 29 (1): 15–21. https://doi.org/10.1093/bioinformatics/bts635.

Doudna and Charpentier. 2014. "The New Frontier of Genome Engineering with CRISPR-Cas9." *Science* 346 (6213). https://doi.org/10.1126/science.1258096.

Egan, Nyman, Skotte, Streubel, Turner, O'Connell, Rraklli, Dolan, Chadderton, Hansen, Farrar, Helin, Holmberg, and Bracken. 2013. "CHD5 Is Required for Neurogenesis and Has a Dual Role in Facilitating Gene Expression and Polycomb Gene Repression." *Developmental Cell* 26 (3): 223–36. https://doi.org/10.1016/j.devcel.2013.07.008.

Elick. 1996. "Excision of the Piggy Bac Transposable Element in Vitro Is a Precise Event That Is Enhanced by the Expression of Its Encoded Transposase." *Genetica* 98 (1): 33–41. https://doi.org/10.1007/BF00120216.

Englund, Fink, Lau, Pham, Daza, Bulfone, Kowalczyk, and Hevner. 2005. "Pax6, Tbr2, and Tbr1 Are Expressed Sequentially by Radial Glia, Intermediate Progenitor Cells, and Postmitotic Neurons in Developing Neocortex." *The Journal of Neuroscience : The Official Journal of the Society for Neuroscience* 25 (1): 247–51. https://doi.org/10.1523/JNEUROSCI.2899-04.2005.

Eriksson, Perfilieva, Björk-Eriksson, Alborn, Nordborg, Peterson, and Gage. 1998. "Neurogenesis in the Adult Human Hippocampus." *Nature Medicine* 4 (11): 1313–17. https://doi.org/10.1038/3305.

Ernst, Alkass, Bernard, Salehpour, Perl, Tisdale, Possnert, Druid, and Frisén. 2014. "Neurogenesis in the Striatum of the Adult Human Brain." *Cell* 156 (5): 1072–83. https://doi.org/10.1016/j.cell.2014.01.044.

Esgleas, Falk, Forné, Thiry, Najas, Zhang, Mas-Sanchez, Geerlof, Niessing, Wang, Imhof, and Götz. 2020. "Trnp1 Organizes Diverse Nuclear Membrane-Less Compartments in Neural Stem Cells." *The EMBO Journal* 39 (16): e103373. https://doi.org/10.15252/embj.2019103373.

Falk, Bugeon, Ninkovic, Pilz, Postiglione, Cremer, Knoblich, and Götz. 2017. "Time-Specific Effects of Spindle Positioning on Embryonic Progenitor Pool Composition and Adult Neural Stem Cell Seeding." *Neuron* 93 (4): 777-791.e3. https://doi.org/10.1016/j.neuron.2017.02.009.

Falk and Götz. 2017. "Glial Control of Neurogenesis." *Current Opinion in Neurobiology* 47 (Figure 1): 188–95. https://doi.org/10.1016/j.conb.2017.10.025.

Fuentealba, Rompani, Parraguez, Obernier, Romero, Cepko, and Alvarez-Buylla. 2015. "Embryonic Origin of Postnatal Neural Stem Cells." *Cell* 161 (7): 1644–55. https://doi.org/10.1016/j.cell.2015.05.041.

Furutachi, Miya, Watanabe, Kawai, Yamasaki, Harada, Imayoshi, Nelson, Nakayama, Hirabayashi, and Gotoh. 2015. "Slowly Dividing Neural Progenitors Are an Embryonic Origin of Adult Neural Stem Cells." *Nature Neuroscience* 18 (5): 657–65. https://doi.org/10.1038/nn.3989.

Gao, Postiglione, Krieger, Hernandez, Wang, Han, Streicher, Papusheva, Insolera, Chugh, Kodish, Huang, Simons, Luo, Hippenmeyer, and Shi. 2014. "Deterministic Progenitor Behavior and Unitary Production of Neurons in the Neocortex." *Cell* 159 (4): 775–88. https://doi.org/10.1016/j.cell.2014.10.027.

García-Marqués and López-Mascaraque. 2013. "Clonal Identity Determines Astrocyte Cortical Heterogeneity." *Cerebral Cortex (New York, N.Y. : 1991)* 23 (6): 1463–72. https://doi.org/10.1093/cercor/bhs134.

Ge, Miyawaki, Gage, Jan, and Jan. 2012. "Local Generation of Glia Is a Major Astrocyte Source in Postnatal Cortex." *Nature* 484 (7394): 376–80. https://doi.org/10.1038/nature10959.

Geha, Pallud, Junier, Devaux, Leonard, Chassoux, Chneiweiss, Daumas-Duport, and Varlet. 2010. "NG2+/Olig2+ Cells Are the Major Cycle-Related Cell Population of the Adult Human Normal Brain." *Brain Pathology (Zurich, Switzerland)* 20 (2): 399–411. https://doi.org/10.1111/j.1750-3639.2009.00295.x.

Gibson, Young, Chuang, Venter, Hutchison, and Smith. 2009. "Enzymatic Assembly of DNA Molecules up to Several Hundred Kilobases." *Nature Methods* 6 (5): 343–45. https://doi.org/10.1038/nmeth.1318.

Godin, Creppe, Laguesse, and Nguyen. 2016. "Emerging Roles for the Unfolded Protein Response in the Developing Nervous System." *Trends in Neurosciences* 39 (6): 394–404. https://doi.org/10.1016/j.tins.2016.04.002.

Gong, Brackertz, and Renkawitz. 2006. "SUMO Modification Enhances P66-Mediated Transcriptional Repression of the Mi-2/NuRD Complex." *Molecular and Cellular Biology* 26 (12): 4519–28. https://doi.org/10.1128/MCB.00409-06.

Goodwin and Picketts. 2018. "The Role of ISWI Chromatin Remodeling Complexes in Brain Development and Neurodevelopmental Disorders." *Molecular and Cellular Neurosciences* 87 (June 2017): 55–64. https://doi.org/10.1016/j.mcn.2017.10.008.

Götz and Huttner. 2005. "The Cell Biology of Neurogenesis." *Nature Reviews. Molecular Cell Biology* 6 (10): 777–88. https://doi.org/10.1038/nrm1739.

Götz, Sirko, Beckers, and Irmler. 2015. "Reactive Astrocytes as Neural Stem or Progenitor Cells: In Vivo Lineage, In Vitro Potential, and Genome-Wide Expression Analysis." *Glia* 63 (8): 1452–68. https://doi.org/10.1002/glia.22850.

Götz, Stoykova, and Gruss. 1998. "Pax6 Controls Radial Glia Differentiation in the Cerebral Cortex." *Neuron* 21 (5): 1031–44. https://doi.org/10.1016/s0896-6273(00)80621-2.

Grade and Götz. 2017. "Neuronal Replacement Therapy: Previous Achievements and Challenges Ahead." *Npj Regenerative Medicine* 2 (1). https://doi.org/10.1038/s41536-017-0033-0.

Guezennec, Le, Vermeulen, Brinkman, Hoeijmakers, Cohen, Lasonder, and Stunnenberg. 2006. "MBD2/NuRD and MBD3/NuRD, Two Distinct Complexes with Different Biochemical and Functional Properties." *Molecular and Cellular Biology* 26 (3): 843–51. https://doi.org/10.1128/MCB.26.3.843-851.2006.

Han, Dennis, Balakrishnan, Dixit, Britz, Zinyk, Touahri, Olender, Brand, Guillemot, Kurrasch, and Schuurmans. 2018. "A Non-Canonical Role for the Proneural Gene Neurog1 as a Negative Regulator of Neocortical Neurogenesis." *Development (Cambridge)* 145 (19). https://doi.org/10.1242/dev.157719.

Harris, Rigo, Stiehl, Gaber, Austin, Masdeu, Edwards, Urbán, Marciniak-Czochra, and Guillemot. 2021. "Coordinated Changes in Cellular Behavior Ensure the Lifelong Maintenance of the Hippocampal Stem Cell Population." *Cell Stem Cell*, February, 1–14. https://doi.org/10.1016/j.stem.2021.01.003.

Haubensak, Attardo, Denk, and Huttner. 2004. "Neurons Arise in the Basal Neuroepithelium of the Early Mammalian Telencephalon: A Major Site of Neurogenesis." *Proceedings of the National Academy of Sciences of the United States of America* 101 (9): 3196–3201. https://doi.org/10.1073/pnas.0308600100.

Hevner. 2019. "Intermediate Progenitors and Tbr2 in Cortical Development." *Journal of Anatomy* 235 (3): 616–25. https://doi.org/10.1111/joa.12939.

Hirabayashi, Suzki, Tsuboi, Endo, Toyoda, Shinga, Koseki, Vidal, and Gotoh. 2009. "Polycomb Limits the Neurogenic Competence of Neural Precursor Cells to Promote Astrogenic Fate Transition." *Neuron* 63 (5): 600–613. https://doi.org/10.1016/j.neuron.2009.08.021.

Hochgerner, Zeisel, Lönnerberg, and Linnarsson. 2018. "Conserved Properties of Dentate Gyrus Neurogenesis across Postnatal Development Revealed by Single-Cell RNA Sequencing." *Nature Neuroscience* 21 (2): 290–99. https://doi.org/10.1038/s41593-017-0056-2.

Hou, Hailín, Vogel, and Hanashima. 2020. "Transcription and Beyond: Delineating FOXG1 Function in Cortical Development and Disorders." *Frontiers in Cellular Neuroscience* 14 (February): 1–14. https://doi.org/10.3389/fncel.2020.00035.

Huang, Li, Tu, Zhao, Zhu, Feng, Si, and Chen. 2018. "OTX1 Regulates Cell Cycle Progression of Neural Progenitors in the Developing Cerebral Cortex." *Journal of Biological Chemistry* 293 (6): 2137–48. https://doi.org/10.1074/jbc.RA117.001249.

Ivics, Hackett, Plasterk, and Izsvá. 1997. "Molecular Reconstruction of Sleeping Beauty, a Tc1-like Transposon from Fish, and Its Transposition in Human Cells Its Original Location and Promotes Its Reintegration Else- Where in the Genome (Plasterk, 1996). Autonomous Mem- Bers of a Transposon." *Cell* 91: 501–10.

Jinek, East, Cheng, Lin, Ma, and Doudna. 2013. "RNA-Programmed Genome Editing in Human Cells." *ELife* 2013 (2): 1–9. https://doi.org/10.7554/eLife.00471.

Jurkowski, Bettio, K. Woo, Patten, Yau, and Gil-Mohapel. 2020. "Beyond the Hippocampus and the SVZ: Adult Neurogenesis Throughout the Brain." *Frontiers in Cellular Neuroscience* 14 (September): 1–36. https://doi.org/10.3389/fncel.2020.576444.

Juszkiewicz, Slodkowicz, Lin, Freire-Pritchett, Peak-Chew, and Hegde. 2020. "Ribosome Collisions Trigger Cis-Acting Feedback Inhibition of Translation Initiation." *ELife* 9. https://doi.org/10.7554/eLife.60038.

Kageyama, Shimojo, and Ohtsuka. 2019. "Dynamic Control of Neural Stem Cells by BHLH Factors." *Neuroscience Research* 138: 12–18. https://doi.org/10.1016/j.neures.2018.09.005.

Kempermann, Gage, Aigner, Song, Curtis, Thuret, Kuhn, Jessberger, Frankland, Cameron, Gould, Hen, Abrous, Toni, Schinder, Zhao, Lucassen, and Frisén. 2018. "Human Adult Neurogenesis: Evidence and Remaining Questions." *Cell Stem Cell* 23 (1): 25–30. https://doi.org/10.1016/j.stem.2018.04.004.

Kim. 2016. "Post-Transcriptional Regulation of Gene Expression in Neural Stem Cells." *Cell Biochemistry and Function* 34 (4): 197–208. https://doi.org/10.1002/cbf.3181.

Kishi, Fujii, Hirabayashi, and Gotoh. 2012. "HMGA Regulates the Global Chromatin State and Neurogenic Potential in Neocortical Precursor Cells." *Nature Neuroscience* 15 (8): 1127–33. https://doi.org/10.1038/nn.3165.

Kloet, Baymaz, Makowski, Groenewold, Jansen, Berendsen, Niazi, Kops, and Vermeulen. 2015. "Towards Elucidating the Stability, Dynamics and Architecture of the Nucleosome Remodeling and Deacetylase Complex by Using Quantitative Interaction Proteomics." *FEBS Journal* 282 (9): 1774–85. https://doi.org/10.1111/febs.12972.

Knock, Pereira, Lombard, Dimond, Leaford, Livesey, and Hendrich. 2015. "The Methyl Binding Domain 3/Nucleosome Remodelling and Deacetylase Complex Regulates Neural Cell Fate Determination and Terminal Differentiation in the Cerebral Cortex." *Neural Development* 10 (1): 13. https://doi.org/10.1186/s13064-015-0040-z.

Kobeissy, Hansen, Neumann, Fu, Jin, and Liu. 2016. "Deciphering the Role of Emx1 in Neurogenesis: A Neuroproteomics Approach." *Frontiers in Molecular Neuroscience* 9 (OCT2016). https://doi.org/10.3389/fnmol.2016.00098.

Komor, Kim, Packer, Zuris, and Liu. 2016. "Programmable Editing of a Target Base in Genomic DNA without Double-Stranded DNA Cleavage." *Nature* 533 (7603): 420–24. https://doi.org/10.1038/nature17946.

Kriegstein and Alvarez-Buylla. 2009. "The Glial Nature of Embryonic and Adult Neural Stem Cells." *Annual Review of Neuroscience* 32 (1): 149–84. https://doi.org/10.1146/annurev.neuro.051508.135600.

Kumar and Wang. 2016. "Structure, Expression and Functions of MTA Genes." *Gene* 582 (2): 112–21. https://doi.org/10.1016/j.gene.2016.02.012.

Kuwahara, Sakai, Xu, Itoh, Hirabayashi, and Gotoh. 2014. "Tcf3 Represses Wnt-β-Catenin Signaling and Maintains Neural Stem Cell Population during Neocortical Development." *PLoS ONE* 9 (5): 1–12. https://doi.org/10.1371/journal.pone.0094408.

Kuzmichev, Nishioka, Erdjument-Bromage, Tempst, and Reinberg. 2002. "Histone Methyltransferase Activity Associated with a Human Multiprotein Complex Containing the Enhancer of Zeste Protein." *Genes and Development* 16 (22): 2893–2905. https://doi.org/10.1101/gad.1035902.

Lau, Li, Pui-Ling Lai, Nga-Chu Lui, Li, Munera, Pan, Mahe, Hui, Wells, and Sau-Wai Ngan. 2019. "Activation of Hedgehog Signaling Promotes Development of Mouse and Human Enteric Neural Crest Cells, Based on Single-Cell Transcriptome Analyses." *Gastroenterology* 157 (6): 1556-1571.e5. https://doi.org/10.1053/j.gastro.2019.08.019.

Lee, Conboy, Park, Jiang, Kim, Dewitt, Mackley, et al. 2017. "Nanoparticle Delivery of Cas9 Ribonucleoprotein and Donor DNA in Vivo Induces Homology-Directed DNA Repair." *Nature Biomedical Engineering* 1 (11): 889–901. https://doi.org/10.1038/s41551-017-0137-2.

Lejon, Thong, Murthy, AlQarni, Murzina, Blobel, Laue, and Mackay. 2011. "Insights into Association of the NuRD Complex with FOG-1 from the Crystal Structure of an RbAp48·FOG-1 Complex." *Journal of Biological Chemistry* 286 (2): 1196–1203. https://doi.org/10.1074/jbc.M110.195842.

Lennon, Jones, Lovelace, Guillemin, and Brew. 2017. "Bcl11b-A Critical Neurodevelopmental Transcription Factor-Roles in Health and Disease." *Frontiers in Cellular Neuroscience* 11 (March): 89. https://doi.org/10.3389/fncel.2017.00089.

Li, Bo and Dewey. 2011. "RSEM: Accurate Transcript Quantification from RNA-Seq Data with or without a Reference Genome." *BMC Bioinformatics* 12 (August): 323. https://doi.org/10.1186/1471-2105-12-323.

Li, G. M. 2013. "DNA Mismatch Repair and the DNA Damage Response." *Encyclopedia of Biological Chemistry: Second Edition*, 51–53. https://doi.org/10.1016/B978-0-12-378630-2.00238-3.

Li, Meng Amy, Pettitt, Eckert, Ning, Rice, Cadiñanos, Yusa, Conte, and Bradley. 2013. "The PiggyBac Transposon Displays Local and Distant Reintegration Preferences and Can Cause Mutations at Noncanonical Integration Sites." *Molecular and Cellular Biology* 33 (7): 1317–30. https://doi.org/10.1128/MCB.00670-12.

Li, Meng Amy, Turner, Ning, Yusa, Liang, Eckert, Rad, Fitzgerald, Craig, and Bradley. 2011. "Mobilization of Giant PiggyBac Transposons in the Mouse Genome." *Nucleic Acids Research* 39 (22). https://doi.org/10.1093/nar/gkr764.

Li, X, Harrell, Handler, Beam, Hennessy, and Fraser. 2005. "PiggyBac Internal Sequences Are Necessary for Efficient Transformation of Target Genomes." *Insect Molecular Biology* 14 (1): 17–30. https://doi.org/10.1111/j.1365-2583.2004.00525.x.

Li, Yanzhen, Drnevich, Akraiko, Band, Li, Wang, Matoba, and Tanaka. 2013. "Gene Expression Profiling Reveals the Heterogeneous Transcriptional Activity of Oct3/4 and Its Possible Interaction with Gli2 in Mouse Embryonic Stem Cells." *Genomics* 102 (5–6): 456–67. https://doi.org/10.1016/j.ygeno.2013.09.004.

Linker, Marchetto, Narvaiza, Denli, and Gage. 2017. "Examining Non-LTR Retrotransposons in the Context of the Evolving Primate Brain." *BMC Biology* 15 (1): 68. https://doi.org/10.1186/s12915-017-0409-z.

Liu, Chen, Wall, Zheng, Zhou, Wang, Vaseghi, Qian, and Liu. 2017. "Systematic Comparison of 2A Peptides for Cloning Multi-Genes in a Polycistronic Vector." *Scientific Reports* 7 (1): 2193. https://doi.org/10.1038/s41598-017-02460-2.

Llorca and Marín. 2021. "Orchestrated Freedom: New Insights into Cortical Neurogenesis." *Current Opinion in Neurobiology* 66: 48–56. https://doi.org/10.1016/j.conb.2020.09.004.

Love, Huber, and Anders. 2014. "Moderated Estimation of Fold Change and Dispersion for RNA-Seq Data with DESeq2." *Genome Biology* 15 (12): 550. https://doi.org/10.1186/s13059-014-0550-8.

Luo, Zou, Tan, Zhang, Guo, Zeng, Zhang, Tan, Wei, Hu, Zheng, Liang, and Wu. 2017. "Novel GATAD2B Loss-of-Function Mutations Cause Intellectual Disability in Two Unrelated Cases." *Journal of Human Genetics* 62 (4): 513–16. https://doi.org/10.1038/jhg.2016.164.

Malatesta, Hartfuss, and Götz. 2000. "Isolation of Radial Glial Cells by Fluorescent-Activated Cell Sorting Reveals a Neuronal Lineage." *Development (Cambridge, England)* 127 (24): 5253–63. http://www.ncbi.nlm.nih.gov/pubmed/11076748.

Maréchal and Zou. 2013. "DNA Damage Sensing by the ATM and ATR Kinases." *Cold Spring Harbor Perspectives in Biology* 5 (9): 1–18. https://doi.org/10.1101/cshperspect.a012716.

Masserdotti, Badaloni, Green, Croci, Barili, Bergamini, Vetter, and Consalez. 2010. "ZFP423 Coordinates Notch and Bone Morphogenetic Protein Signaling, Selectively up-Regulating Hes5 Gene Expression." *Journal of Biological Chemistry* 285 (40): 30814–24. https://doi.org/10.1074/jbc.M110.142869.

Massimino, Flores-Garcia, Stefano, Di, Colasante, Icoresi-Mazzeo, Zaghi, Hamilton, and Sessa. 2018. "TBR2 Antagonizes Retinoic Acid Dependent Neuronal Differentiation by Repressing Zfp423 during Corticogenesis." *Developmental Biology* 434 (2): 231–48. https://doi.org/10.1016/j.ydbio.2017.12.020.

McBurney. 1993. "P19 Embryonal Carcinoma Cells." *The International Journal of Developmental Biology* 37 (1): 135–40. https://doi.org/10.1387/ijdb.8507558.

McCarty, Graham, Studená, and Ledesma-Amaro. 2020. "Multiplexed CRISPR Technologies for Gene Editing and Transcriptional Regulation." *Nature Communications* 11 (1): 1–13. https://doi.org/10.1038/s41467-020-15053-x.

Merkle, Mirzadeh, and Alvarez-Buylla. 2007. "Mosaic Organization of Neural Stem Cells in the Adult Brain." *Science (New York, N.Y.)* 317 (5836): 381–84. https://doi.org/10.1126/science.1144914.

Merkle, Tramontin, García-Verdugo, and Alvarez-Buylla. 2004. "Radial Glia Give Rise to Adult Neural Stem Cells in the Subventricular Zone." *Proceedings of the National Academy of Sciences of the United States of America* 101 (50): 17528–32. https://doi.org/10.1073/pnas.0407893101.

Methot, Soubannier, Hermann, Campos, Li, and Stifani. 2018. "Nuclear Factor-KappaB Regulates Multiple Steps of Gliogenesis in the Developing Murine Cerebral Cortex." *Glia* 66 (12): 2659–72. https://doi.org/10.1002/glia.23518.

Millard, Varma, Saleh, Morris, Watson, Bottrill, Fairall, Smith, and Schwabe. 2016. "The Structure of the Core NuRD Repression Complex Provides Insights into Its Interaction with Chromatin." *ELife* 5 (APRIL2016): e13941. https://doi.org/10.7554/eLife.13941.

Miller, Ralser, Kloet, Loos, Nishinakamura, Bertone, Vermeulen, and Hendrich. 2016. "Sall4 Controls Differentiation of Pluripotent Cells Independently of the Nucleosome Remodelling and Deacetylation (NuRD) Complex." *Development (Cambridge)* 143 (17): 3074–84. https://doi.org/10.1242/dev.139113.

Mirzadeh, Merkle, Soriano-Navarro, Garcia-Verdugo, and Alvarez-Buylla. 2008. "Neural Stem Cells Confer Unique Pinwheel Architecture to the Ventricular Surface in Neurogenic Regions of the Adult Brain." *Cell Stem Cell* 3 (3): 265–78. https://doi.org/10.1016/j.stem.2008.07.004.

Mitra, Fain-Thornton, and Craig. 2008. "PiggyBac Can Bypass DNA Synthesis during Cut and Paste Transposition." *EMBO Journal* 27 (7): 1097–1109. https://doi.org/10.1038/emboj.2008.41.

Miyata, Kawaguchi, Saito, Kawano, Muto, and Ogawa. 2004. "Asymmetric Production of Surface-Dividing and Non-Surface-Dividing Cortical Progenitor Cells." *Development (Cambridge, England)* 131 (13): 3133–45. https://doi.org/10.1242/dev.01173.

Montgomery, Hsieh, Barbosa, Richardson, and Olson. 2009. "Histone Deacetylases 1 and 2 Control the Progression of Neural Precursors to Neurons during Brain Development." *Proceedings of the National Academy of Sciences of the United States of America* 106 (19): 7876–81. https://doi.org/10.1073/pnas.0902750106.

Mor, Rais, Sheban, Peles, Aguilera-Castrejon, Zviran, Elinger, et al. 2018. "Neutralizing Gatad2a-Chd4-Mbd3/NuRD Complex Facilitates Deterministic Induction of Naive Pluripotency." *Cell Stem Cell* 23 (3): 412-425.e10. https://doi.org/10.1016/j.stem.2018.07.004.

Moreno-Jiménez, Flor-García, Terreros-Roncal, Rábano, Cafini, Pallas-Bazarra, Ávila, and Llorens-Martín. 2019. "Adult Hippocampal Neurogenesis Is Abundant in Neurologically Healthy Subjects and Drops Sharply in Patients with Alzheimer's Disease." *Nature Medicine* 25 (4): 554–60. https://doi.org/10.1038/s41591-019-0375-9.

MuhChyi, Juliandi, Matsuda, and Nakashima. 2013. "Epigenetic Regulation of Neural Stem Cell Fate during Corticogenesis." *International Journal of Developmental Neuroscience : The Official Journal of the International Society for Developmental Neuroscience* 31 (6): 424–33. https://doi.org/10.1016/j.ijdevneu.2013.02.006.

Mukhtar and Taylor. 2018. "Untangling Cortical Complexity During Development." *Journal of Experimental Neuroscience* 12 (Figure 1). https://doi.org/10.1177/1179069518759332.

Muotri, Chu, Marchetto, Deng, Moran, and Gage. 2005. "Somatic Mosaicism in Neuronal Precursor Cells Mediated by L1 Retrotransposition." *Nature* 435 (7044): 903–10. https://doi.org/10.1038/nature03663.

Muotri, Marchetto, Coufal, Oefner, Yeo, Nakashima, and Gage. 2010. "L1 Retrotransposition in Neurons Is Modulated by MeCP2." *Nature* 468 (7322): 443–46. https://doi.org/10.1038/nature09544.

Naldini, Blömer, Gage, Trono, and Verma. 1996. "Efficient Transfer, Integration, and Sustained Long-Term Expression of the Transgene in Adult Rat Brains Injected with a Lentiviral Vector." *Proceedings of the National Academy of Sciences of the United States of America* 93 (21): 11382–88. https://doi.org/10.1073/pnas.93.21.11382.

Namba and Huttner. 2017. "Neural Progenitor Cells and Their Role in the Development and Evolutionary Expansion of the Neocortex." *Wiley Interdisciplinary Reviews. Developmental Biology* 6 (1). https://doi.org/10.1002/wdev.256.

Ninkovic and Götz. 2013. “Fate Specification in the Adult Brain--Lessons for Eliciting Neurogenesis from Glial Cells.” *BioEssays : News and Reviews in Molecular, Cellular and Developmental Biology* 35 (3): 242–52. https://doi.org/10.1002/bies.201200108.

Nishiyama, Komitova, Suzuki, and Zhu. 2009. “Polydendrocytes (NG2 Cells): Multifunctional Cells with Lineage Plasticity.” *Nature Reviews. Neuroscience* 10 (1): 9–22. https://doi.org/10.1038/nrn2495.

Nitarska, Smith, Sherlock, Hillege, Nott, Barshop, Vashisht, Wohlschlegel, Mitter, and Riccio. 2016. “A Functional Switch of NuRD Chromatin Remodeling Complex Subunits Regulates Mouse Cortical Development.” *Cell Reports* 17 (6): 1683–98. https://doi.org/10.1016/j.celrep.2016.10.022.

Noctor, Martínez-Cerdeño, Ivic, and Kriegstein. 2004. “Cortical Neurons Arise in Symmetric and Asymmetric Division Zones and Migrate through Specific Phases.” *Nature Neuroscience* 7 (2): 136–44. https://doi.org/10.1038/nn1172.

Obernier and Alvarez-Buylla. 2019. “Neural Stem Cells: Origin, Heterogeneity and Regulation in the Adult Mammalian Brain.” *Development (Cambridge)* 146 (4). https://doi.org/10.1242/dev.156059.

Ohtsuka and Kageyama. 2019. “Regulation of Temporal Properties of Neural Stem Cells and Transition Timing of Neurogenesis and Gliogenesis during Mammalian Neocortical Development.” *Seminars in Cell and Developmental Biology* 95 (September 2018): 4–11. https://doi.org/10.1016/j.semcdb.2019.01.007.

Oproescu, Han, and Schuurmans. 2021. “New Insights Into the Intricacies of Proneural Gene Regulation in the Embryonic and Adult Cerebral Cortex.” *Frontiers in Molecular Neuroscience* 14 (February): 642016. https://doi.org/10.3389/fnmol.2021.642016.

Paez-Gonzalez, Abdi, Luciano, Liu, Soriano-Navarro, Rawlins, Bennett, Garcia-Verdugo, and Kuo. 2011. “Ank3-Dependent SVZ Niche Assembly Is Required for the Continued Production of New Neurons.” *Neuron* 71 (1): 61–75. https://doi.org/10.1016/j.neuron.2011.05.029.

Parisi, Piscitelli, Passaro, and Russo. 2020. "HMGA Proteins in Stemness and Differentiation of Embryonic and Adult Stem Cells." *International Journal of Molecular Sciences* 21 (1). https://doi.org/10.3390/ijms21010362.

Pereira, Sansom, Smith, Dobenecker, Tarakhovsky, and Livesey. 2010. "Ezh2, the Histone Methyltransferase of PRC2, Regulates the Balance between Self-Renewal and Differentiation in the Cerebral Cortex." *Proceedings of the National Academy of Sciences of the United States of America* 107 (36): 15957–62. https://doi.org/10.1073/pnas.1002530107.

Pilz, Shitamukai, Reillo, Pacary, Schwausch, Stahl, Ninkovic, Snippert, Clevers, Godinho, Guillemot, Borrell, Matsuzaki, and Götz. 2013. "Amplification of Progenitors in the Mammalian Telencephalon Includes a New Radial Glial Cell Type." *Nature Communications* 4: 2125. https://doi.org/10.1038/ncomms3125.

Pinto, Mader, Irmler, Gentilini, Santoni, Drechsel, Blum, Stahl, Bulfone, Malatesta, Beckers, and Götz. 2008. "Prospective Isolation of Functionally Distinct Radial Glial Subtypes—Lineage and Transcriptome Analysis." *Molecular and Cellular Neuroscience* 38 (1): 15–42. https://doi.org/10.1016/j.mcn.2008.01.012.

Piper, Barry, Hawkins, Mason, Lindwall, Little, Sarkar, Smith, Moldrich, Boyle, Tole, Gronostajski, Bailey, and Richards. 2010. "NFIA Controls Telencephalic Progenitor Cell Differentiation through Repression of the Notch Effector Hes1." *Journal of Neuroscience* 30 (27): 9127–39. https://doi.org/10.1523/JNEUROSCI.6167-09.2010.

Piras, Riba, Petrillo, Lazarevic, Cuccovillo, Bartolaccini, Stupka, Gentner, Cittaro, Naldini, and Kajaste-Rudnitski. 2017. "Lentiviral Vectors Escape Innate Sensing but Trigger P53 in Human Hematopoietic Stem and Progenitor Cells." *EMBO Molecular Medicine* 9 (9): 1198–1211. https://doi.org/10.15252/emmm.201707922.

Pollard, Conti, Sun, Goffredo, and Smith. 2006. "Adherent Neural Stem (NS) Cells from Fetal and Adult Forebrain." *Cerebral Cortex* 16 (SUPPL. 1). https://doi.org/10.1093/cercor/bhj167.

Qi, Larson, Gilbert, Doudna, Weissman, Arkin, and Lim. 2013. "Repurposing CRISPR as an RNA-Guided Platform for Sequence-Specific Control of Gene Expression." *Cell* 152 (5): 1173–83. https://doi.org/10.1016/j.cell.2013.02.022.

Rabin, Millan, Cabrera-Luque, and Pappas. 2018. "Intellectual Disability Due to Monoallelic Variant in GATAD2B and Mosaicism in Unaffected Parent." *American Journal of Medical Genetics. Part A* 176 (12): 2907–10. https://doi.org/10.1002/ajmg.a.40667.

Reynolds, Latos, Hynes-Allen, Loos, Leaford, O'Shaughnessy, Mosaku, Signolet, Brennecke, Kalkan, Costello, Humphreys, Mansfield, Nakagawa, Strouboulis, Behrens, Bertone, and Hendrich. 2012. "NuRD Suppresses Pluripotency Gene Expression to Promote Transcriptional Heterogeneity and Lineage Commitment." *Cell Stem Cell* 10 (5): 583–94. https://doi.org/10.1016/j.stem.2012.02.020.

Reynolds, Salmon-Divon, Dvinge, Hynes-Allen, Balasooriya, Leaford, Behrens, Bertone, and Hendrich. 2012. "NuRD-Mediated Deacetylation of H3K27 Facilitates Recruitment of Polycomb Repressive Complex 2 to Direct Gene Repression." *The EMBO Journal* 31 (3): 593–605. https://doi.org/10.1038/emboj.2011.431.

Rocha-Ferreira and Hristova. 2016. "Plasticity in the Neonatal Brain Following Hypoxic-Ischaemic Injury." *Neural Plasticity* 2016. https://doi.org/10.1155/2016/4901014.

Roy, Kuznicki, Wu, Sun, Bock, Schutz, Vranich, and Monaghan. 2004. "The Tlx Gene Regulates the Timing of Neurogenesis in the Cortex." *Journal of Neuroscience* 24 (38): 8333–45. https://doi.org/10.1523/JNEUROSCI.1148-04.2004.

Rueden, Schindelin, Hiner, DeZonia, Walter, Arena, and Eliceiri. 2017. "ImageJ2: ImageJ for the next Generation of Scientific Image Data." *BMC Bioinformatics* 18 (1): 529. https://doi.org/10.1186/s12859-017-1934-z.

Sakaki-Yumoto, Kobayashi, Sato, Fujimura, Matsumoto, Takasato, Kodama, Aburatani, Asashima, Yoshida, and Nishinakamura. 2006. "The Murine Homolog of SALL4, a Causative Gene in Okihiro Syndrome, Is Essential for Embryonic Stem Cell Proliferation, and Cooperates with Sall1 in Anorectal, Heart, Brain and Kidney Development." *Development (Cambridge, England)* 133 (15): 3005–13. https://doi.org/10.1242/dev.02457.

Sauna and Kimchi-Sarfaty. 2011. "Understanding the Contribution of Synonymous Mutations to Human Disease." *Nature Reviews Genetics* 12 (10): 683–91. https://doi.org/10.1038/nrg3051.

Schindelin, Arganda-Carreras, Frise, Kaynig, Longair, Pietzsch, Preibisch, Rueden, Saalfeld, Schmid, Tinevez, White, Hartenstein, Eliceiri, Tomancak, and Cardona. 2012. "Fiji: An Open-Source Platform for Biological-Image Analysis." *Nature Methods* 9 (7): 676–82. https://doi.org/10.1038/nmeth.2019.

Sen, Gui, and Kumar. 2014. "Physiological Functions of MTA Family of Proteins." *Cancer Metastasis Reviews* 33 (4): 869–77. https://doi.org/10.1007/s10555-014-9514-4.

Shinmyo and Kawasaki. 2017. "CRISPR/Cas9-Mediated Gene Knockout in the Mouse Brain Using in Utero Electroporation." *Current Protocols in Neuroscience* 2017: 3.32.1-3.32.11. https://doi.org/10.1002/cpns.26.

Sirbu and Cortez. 2013. "DNA Damage Response: Three Levels of DNA Repair Regulation." *Cold Spring Harbor Perspectives in Biology* 5 (8). https://doi.org/10.1101/cshperspect.a012724.

Smits, Jansen, Poser, Hyman, and Vermeulen. 2013. "Stoichiometry of Chromatin-Associated Protein Complexes Revealed by Label-Free Quantitative Mass Spectrometry-Based Proteomics." *Nucleic Acids Research* 41 (1): e28–e28. https://doi.org/10.1093/nar/gks941.

Snijders Blok, Rousseau, Twist, Ehresmann, Takaku, Venselaar, Rodan, et al. 2018. "CHD3 Helicase Domain Mutations Cause a Neurodevelopmental Syndrome with Macrocephaly and Impaired Speech and Language." *Nature Communications* 9 (1): 1–12. https://doi.org/10.1038/s41467-018-06014-6.

Snyder. 2019. "Recalibrating the Relevance of Adult Neurogenesis." *Trends in Neurosciences* 42 (3): 164–78. https://doi.org/10.1016/j.tins.2018.12.001.

Sorrells, Paredes, Cebrian-Silla, Sandoval, Qi, Kelley, James, et al. 2018. "Human Hippocampal Neurogenesis Drops Sharply in Children to Undetectable Levels in Adults." *Nature* 555 (7696): 377–81. https://doi.org/10.1038/nature25975.

Spalding, Bergmann, Alkass, Bernard, Salehpour, Huttner, Boström, Westerlund, Vial, Buchholz, Possnert, Mash, Druid, and Frisén. 2013. "Dynamics of Hippocampal Neurogenesis in Adult Humans." *Cell* 153 (6): 1219–27. https://doi.org/10.1016/j.cell.2013.05.002.

Spassky, Merkle, Flames, Tramontin, García-Verdugo, and Alvarez-Buylla. 2005. "Adult Ependymal Cells Are Postmitotic and Are Derived from Radial Glial Cells during Embryogenesis." *The Journal of Neuroscience : The Official Journal of the Society for Neuroscience* 25 (1): 10–18. https://doi.org/10.1523/JNEUROSCI.1108-04.2005.

Spruijt, Luijsterburg, Menafra, Lindeboom, Jansen, Edupuganti, Baltissen, Wiegant, Voelker-Albert, Matarese, Mensinga, Poser, Vos, Stunnenberg, Attikum, van, and Vermeulen. 2016. "ZMYND8 Co-Localizes with NuRD on Target Genes and Regulates Poly(ADP-Ribose)-Dependent Recruitment of GATAD2A/NuRD to Sites of DNA Damage." *Cell Reports* 17 (3): 783–98. https://doi.org/10.1016/j.celrep.2016.09.037.

Staahl, Benekareddy, Coulon-Bainier, Banfal, Floor, Sabo, Urnes, Munares, Ghosh, and Doudna. 2017. "Efficient Genome Editing in the Mouse Brain by Local Delivery of Engineered Cas9 Ribonucleoprotein Complexes." *Nature Biotechnology* 35 (5): 431–34. https://doi.org/10.1038/nbt.3806.

Stenman, Toresson, and Campbell. 2003. "Identification of Two Distinct Progenitor Populations in the Lateral Ganglionic Eminence: Implications for Striatal and Olfactory Bulb Neurogenesis." *The Journal of Neuroscience : The Official Journal of the Society for Neuroscience* 23 (1): 167–74. https://doi.org/10.1523/jneurosci.23-01-00167.2003.

Stepien, Naumann, Holtz, Helppi, Huttner, and Vaid. 2020. "Lengthening Neurogenic Period during Neocortical Development Causes a Hallmark of Neocortex Expansion." *Current Biology* 30 (21): 4227-4237.e5. https://doi.org/10.1016/j.cub.2020.08.046.

Sultan, Brown, and Shi. 2013. "Production and Organization of Neocortical Interneurons." *Frontiers in Cellular Neuroscience* 7 (NOV): 221. https://doi.org/10.3389/fncel.2013.00221.

Suzuki, Tsunekawa, Hernandez-Benitez, Wu, Zhu, Kim, Hatanaka, et al. 2016. "In Vivo Genome Editing via CRISPR/Cas9 Mediated Homology-Independent Targeted Integration." *Nature* 540 (7631): 144–49. https://doi.org/10.1038/nature20565.

Taverna, Götz, and Huttner. 2014. *The Cell Biology of Neurogenesis: Toward an Understanding of the Development and Evolution of the Neocortex*. *Annual Review of Cell and Developmental Biology*. Vol. 30. https://doi.org/10.1146/annurev-cellbio-101011-155801.

Torchy, Hamiche, and Klaholz. 2015. "Structure and Function Insights into the NuRD Chromatin Remodeling Complex." *Cellular and Molecular Life Sciences : CMLS* 72 (13): 2491–2507. https://doi.org/10.1007/s00018-015-1880-8.

Trubnykova, Bazalar Montoya, Serna-Infantes, La, Vásquez Sotomayor, Castro Mujica, and Abarca Barriga. 2019. "GATAD2B Gene Microdeletion Causing Intellectual Disability Autosomal Dominant Type 18: Case Report and Review of the Literature." *Molecular Syndromology* 10 (4): 186–94. https://doi.org/10.1159/000499209.

Tsunekawa, Britto, Takahashi, Polleux, Tan, and Osumi. 2012. "Cyclin D2 in the Basal Process of Neural Progenitors Is Linked to Non-Equivalent Cell Fates." *EMBO Journal* 31 (8): 1879–92. https://doi.org/10.1038/emboj.2012.43.

Ueda, Yanagi, Kaname, and Okamoto. 2019. "A Novel Mutation in the GATAD2B Gene Associated with Severe Intellectual Disability." *Brain & Development* 41 (3): 276–79. https://doi.org/10.1016/j.braindev.2018.10.003.

Uzquiano, Gladwyn-Ng, Nguyen, Reiner, Götz, Matsuzaki, and Francis. 2018. "Cortical Progenitor Biology: Key Features Mediating Proliferation versus Differentiation." *Journal of Neurochemistry* 146 (5): 500–525. https://doi.org/10.1111/jnc.14338.

Vera, Sorlin, Delplancq, Lecoquierre, Brasseur-Daudruy, Petit, Smol, et al. 2020. "Clinical and Molecular Description of 19 Patients with GATAD2B-Associated Neurodevelopmental Disorder (GAND)." *European Journal of Medical Genetics* 63 (10): 104004. https://doi.org/10.1016/j.ejmg.2020.104004.

Wang, Tao and Xiong. 2016. "The Orphan Nuclear Receptor TLX/NR2E1 in Neural Stem Cells and Diseases." *Neuroscience Bulletin* 32 (1): 108–14. https://doi.org/10.1007/s12264-015-0004-7.

Wang, Wei, Lin, Lu, Ning, Cox, Melvin, Wang, Bradley, and Liu. 2008. "Chromosomal Transposition of PiggyBac in Mouse Embryonic Stem Cells." *Proceedings of the National Academy of Sciences of the United States of America* 105 (27): 9290–95. https://doi.org/10.1073/pnas.0801017105.

Wegner and Stolt. 2005. "From Stem Cells to Neurons and Glia: A Soxist's View of Neural Development." *Trends in Neurosciences* 28 (11): 583–88. https://doi.org/10.1016/j.tins.2005.08.008.

Weinandy, Ninkovic, and Götz. 2011. "Restrictions in Time and Space--New Insights into Generation of Specific Neuronal Subtypes in the Adult Mammalian Brain." *The European Journal of Neuroscience* 33 (6): 1045–54. https://doi.org/10.1111/j.1460-9568.2011.07602.x.

Weiss, Terhal, Cohen, Bruccoleri, Irving, Martinez, Rosenfeld, et al. 2016. "De Novo Mutations in CHD4, an ATP-Dependent Chromatin Remodeler Gene, Cause an Intellectual Disability Syndrome with Distinctive Dysmorphisms." *American Journal of Human Genetics* 99 (4): 934–41. https://doi.org/10.1016/j.ajhg.2016.08.001.

Willemsen, Nijhof, Fenckova, Nillesen, Bongers, Castells-Nobau, Asztalos, et al. 2013. "GATAD2B Loss-of-Function Mutations Cause a Recognisable Syndrome with Intellectual Disability and Are Associated with Learning Deficits and Synaptic Undergrowth in Drosophila." *Journal of Medical Genetics* 50 (8): 507–14. https://doi.org/10.1136/jmedgenet-2012-101490.

Witzel, Petersheim, Fan, Bahrami, Racek, Rohlfs, Puchałka, et al. 2017. "Chromatin-Remodeling Factor SMARCD2 Regulates Transcriptional Networks Controlling Differentiation of Neutrophil Granulocytes." *Nature Genetics* 49 (5): 742–52. https://doi.org/10.1038/ng.3833.

Woltjen, Michael, Mohseni, Desai, Mileikovsky, Hämäläinen, Cowling, Wang, Liu, Gertsenstein, Kaji, Sung, and Nagy. 2009. "PiggyBac Transposition Reprograms Fibroblasts to Induced Pluripotent Stem Cells." *Nature* 458 (7239): 766–70. https://doi.org/10.1038/nature07863.

Wong, Fei, Mora-Bermúdez, Taverna, Haffner, Fu, Anastassiadis, Stewart, and Huttner. 2015. "Sustained Pax6 Expression Generates Primate-like Basal Radial Glia in Developing Mouse Neocortex." *PLoS Biology* 13 (8): e1002217. https://doi.org/10.1371/journal.pbio.1002217.

Wu, Peterson, Zinshteyn, Regot, and Green. 2020. "Ribosome Collisions Trigger General Stress Responses to Regulate Cell Fate." *Cell* 182 (2): 404-416.e14. https://doi.org/10.1016/j.cell.2020.06.006.

Xu, Qi, Du, Zou, Gao, Feng, Lu, Li, An, Zhang, Wu, Liu, Li, Capecchi, and Wu. 2017. "PiggyBac Mediates Efficient in Vivo CRISPR Library Screening for Tumorigenesis in Mice." *Proceedings of the National Academy of Sciences of the United States of America* 114 (4): 722–27. https://doi.org/10.1073/pnas.1615735114.

Yoshida, Akagi, Misawa, Kokubu, Takeda, and Horie. 2017. "Chromatin States Shape Insertion Profiles of the PiggyBac, Tol2 and Sleeping Beauty Transposons and Murine Leukemia Virus." *Scientific Reports* 7 (January): 1–18. https://doi.org/10.1038/srep43613.

Yusa, Zhou, Li, Bradley, and Craig. 2011. "A Hyperactive PiggyBac Transposase for Mammalian Applications." *Proceedings of the National Academy of Sciences of the United States of America* 108 (4): 1531–36. https://doi.org/10.1073/pnas.1008322108.

Zhang, Zhang, Zhang, Xu, Wang, Zhu, and Xia. 2020. "Brn4 Promotes the Differentiation of Radial Glial Cells into Neurons by Inhibiting CtBP2." *Life Sciences* 254: 116866. https://doi.org/10.1016/j.lfs.2019.116866.

Zhao, Han, Liu, Gu, Tang, Wei, and Jin. 2017. "The Chromatin Remodeler Chd4 Maintains Embryonic Stem Cell Identity by Controlling Pluripotency- and Differentiation-Associated Genes." *The Journal of Biological Chemistry* 292 (20): 8507–19. https://doi.org/10.1074/jbc.M116.770248.

Zhou and Anderson. 2002. "The BHLH Transcription Factors OLIG2 and OLIG1 Couple Neuronal and Glial Subtype Specification." *Cell* 109 (1): 61–73. https://doi.org/10.1016/s0092-8674(02)00677-3.

ABBREVIATIONS

(v/v)	volume per volume
(w/v)	weight per volume
µl	microliter
µm	micrometer
µM	micromolar
ADHD	attention deficit and hyperactivity disorder
ANOVA	analysis of variance
aNSC	adult neural stem cell
APC	Allophycocyanin
aRGC	apical radial glial cell
aRGL	apical radial glia-like
Ascl1	achaete-scute family bHLH transcription factor 1
AVM	Core facility Comparative Medicine (Abteilung für Vergleichende Medizin)
Baz1a	bromodomain adjacent to zinc finger domain 1A
Bcl11b	B-Cell CLL/Lymphoma 11B (see *Ctip2*)
bHLH	basic helix-loop-helix
bIP	basal intermediate progenitor
Blbp	brain lipid-binding protein
BMP	bone morphogenic protein
bRGC	basal radial glial cells
Brn4	Brain-4 (see *Pou3f4*)
BSA	bovine serum albumine
CAM	Core facility Animal Models
Cas9	CRISPR associated protein 9
cDNA	complementary DNA
CGE	caudal ganglionic eminence
Chd	chromodomain helicase DNA binding protein
ChR	chromatin remodeler/remodeling factor
CO_2	carbon dioxide

CP	cortical plate
CR1	complement receptor 1
CRISPR	Clustered Regularly Interspaced Short Palindromic Repeats
CRISPRi	CRISPR interference
CSF	cerebrospinal fluid
Ctip2	COUP-TF-interacting protein 2 (see *Bcl11b*)
CTX	cortex
DAPI	4′,6-Diamidin-2-phenylindol
dCas9	"dead" (enzymatically deactivated) Cas9
DDR	DNA damage response
DG	dentate gyrus, gyrus dentatus of the hippocampus
dH_2O/ddH_2O	distilled/double distilled water
DL	deep-layer
Dll1	delta-like canonical Notch ligand 1
DMEM	Dulbecco's modified Eagle's medium
Dmrt3	doublesex and Mab-3 related transcription factor 3
DMSO	dimethyl sulfoxide
DNA	deoxyribonucleic acid
DNase	deoxyribonuclease
DTT	dithiothreitol
E*	embryonic day (e.g. E14)
E. coli	Escherichia coli
EDTA	ethylenediaminetetraacetic acid
Eed	embryonic ectoderm development protein
emGFP	emerald green fluorescent protein
Emx1	empty spiracles homeobox 1
Eomes	Eomesodermin (see *Tbr2*)
ERV	endogenous retroviral elements
ESC	embryonic stem cell
Etv6	ETS variant transcription factor 6
Ezh2	enhancer of zeste 2
FACS	fluorescence-activated cell sorting

FBS	fetal bovine serum
FGF	fibroblast growth factor
Foxg1	forkhead box G1
Foxp2	forkhead box P2
Foxp4	forkhead box P4
FSC(-A/-W)	forward scatter (area/width)
GA	Gibson assembly
GABA	γ-aminobutyric acid
Gatad2a/b	GATA zinc finger domain containing 2a/b
GC	granule cell
GE	ganglionic eminence
Gfap	glial fibrillary acidic protein
GFP	green fluorescent protein
Glast	sodium-dependent glutamate/aspartate transporter
Gli2	GLI family zinc finger 2
GO	gene ontology
gRNA	guide RNA
GV-SOLAS	Gesellschaft für Versuchstierkunde / Society of Laboratory Animal Science
HBSS	Hank's balanced salt solution
HCl	hydrochloric acid
Hdac	Histone deacetylase
HDR	homology-directed repair
hEGF	human epithelial growth factor
HEPES	2-(4-(2-Hydroxyethyl)-1-piperazinyl)-ethansulfonic acid
Hes	hairy and enhancer of Split
hFGF	human fibroblast growth factor
Hmga1/2	high mobility group A 1/2
Hopx	HOP [homeodomain-only protein] homeobox
i.p.	intraperitoneal
ICC	immunocytochemistry
IGF	insulin-like growth factor
IHC	immunohistochemistry

INM	interkinetic nuclear migration
Insc	inscuteable homolog
ISF	Institute of Stem Cell Research (Institut für Stammzellforschung)
ISF-N	Institute of Stem Cell Research, research group neural stem cells
iSVZ	inner subventricular zone
ISWI	imitation SWI
IUE	in utero electroporation
IVC	individually ventilated cages
IZ	intermediate zone
KAc	potassium acetate
kbp	kilo-base pairs
KCl	potassium chloride
kg	kilogram
KH_2PO_4	potassium dihydrogen phosphate
LB	lysogeny broth
LGE	lateral ganglionic eminence
LINE1	long interspersed nuclear element 1
M	molar (mol/l)
Mbd2/3	methyl-CpG-binding domain protein 2/3
MEM	modified Eagle's medium
mg	milligram
$MgCl_2$	magnesium chloride
MGE	medial ganglionic eminence
miRNA	micro-RNA
mM	millimolar
mNPC	murine neural progenitor cells
mPB	mouse codon-optimized piggyBac transposase
mRNA	messenger RNA
Mta1/2/3	metastasis-associated protein 1/2/3
n	number of biological replicates
Na_2HPO_4	sodium phosphate dibasic dihydrate
NaCl	sodium chloride

NAD	nicotinamide adenine dinucleotide
NaN_3	sodium azide
NaOH	sodium hydroxide
nbIP	neurogenic basal intermediate progenitor
NEAA	non-essential amino acids
NEC	neuroepithelial cell
Neurog1/2	neurogenin 1/2
Nfia	nuclear factor I A
NF-κB	Nuclear Factor Kappa B
ng	nanogram
NGS	normalized goat serum
NHEJ	non-homologous end joining
Nhlh1	nescient helix-loop-helix 1
nm	nanometer
Nr2e1	nuclear receptor subfamily 2 group E member 1 (see *Tlx*)
ntgRNA	non-targeted gRNA
NuRD (complex)	nucleosome remodeling and deacetylase (complex)
OB	olfactory bulb
Olig1/2	oligodendrocyte transcription factor 1/2
OPC	oligodendrocyte progenitor cell
ORF	open reading frame
oSVZ	outer subventricular zone
Otx1	orthodenticle homeobox 1
p	p-value
p.o.	peroral
p_{adj}	adjusted p-value
Pax6	paired box 6
PBase	piggyBac transposase
pbIP	proliferating basal intermediate progenitor
PBS	phosphate buffered saline
PCR	polymerase chain reaction
PDL	poly-D-lysine

PE	Phycoerythrin
Pen/Strep	Penicillin/Streptomycin
PFA	paraformaldehyde
Pou3f4	POU class 3 homeobox 4 (see *Brn4*)
PrC	Polycomb repressor complex
PRC2	Polycomb repressor complex 2
PSA-NCAM	polysialylated neural cell adhesion molecule
qRT-PCR	quantitative real-time polymerase chain reaction
Rbbp4/7	retinoblastoma binding protein 4/7
RGC	radial glial cell
Ring1b	RING finger protein 1B
RMS	rostral migratory stream
RNA	ribonucleic acid
RNase	ribonuclease
RNP	ribonucleoprotein complex
ROB	Regierung von Oberbayern (Government of Upper Bavaria)
ROI	region of interest
rpm	rotations per minute
RT	room temperature
RTR	ribotoxic stress response
s.c.	subcutaneous
S.D.	standard deviation
S100β	S 100 calcium binding protein B
Sall1/4	Spalt-like transcription factor 1/4
SAP	subapical progenitor
SDS	sodium dodecyl sulfate
SEZ	subependymal zone
SGZ	subgranular zone
Shh	Sonic hedgehog
Smarcd2	SWI/SNF related, matrix associated, actin dependent regulator of chromatin, subfamily D, member 2
SNP	short neural precursor cell

Sox3	SRY-box transcription factor 3
SPF	specified pathogen-free
SSC	side scatter
STAgR	string assembly gRNA (cloning)
SUMO	Small Ubiquitin-like Modifier
SVZ	subventricular zone
SWI/SNF	switch/sucrose non-fermentable
TAP	transit-amplifying progenitor
Tbr2	T-box brain protein 2 (see *Eomes*)
Tcf3	HMG box transcription factor 3 (see *Tcf7l1*)
Tcf7l1	transcription factor 7 like 1 (see *Tcf3*)
TF	transcription factor
TierSchB	Tierschutzbeauftragte/r (animal welfare officer)
TierSchG	Tierschutzgesetz (animal welfare law)
Tlx	Tailless homolog (see *Nr2e1*)
TR	terminal repeat
TSL	transcript support level
TSS	transcription start site
tv	transcript variant
UL	upper-layer
UPR	unfolded protein response
UTR	untranslated region
V	Volt
VPR	VP64-p65-Rta tripartite activator
vs.	versus
VZ	ventricular zone
Wnt	Wingless-related integration site protein
Zfp423	zinc finger protein 423
Zfp536	zinc finger protein 536
Znf	zinc finger

LIST OF FIGURES

LIST OF TABLES

DECLARATION OF AUTHOR CONTRIBUTIONS

Dr. Pawel Smialowski (ISF-N, Helmholtz Center Munich, Munich, Germany) performed quality control and processing of the RNA-Seq data and created the lists of regulated genes upon which further analyses were based. He also provided the analyses for most characteristic genes regulated and the upstream factor ranking based on these data.

Dr. Christopher Breunig (Epigenetic Engineering, ISF, Helmholtz Center Munich, Munich, Germany; now at ISAR Bioscience GmbH, Planegg, Germany) designed all gRNA sequences and led in the design of the *piggyBac-CAG-dCas9-VPR-P2A-GFP* and *piggyBac-CAG-mScarlet-15xgRNA* plasmids. gRNA cassettes were subcloned into the *piggyBac-CAG-dCas9-VPR-P2A-GFP* vector in collaboration with Manpreet Kaur (student).

Other plasmids were provided by the following contributors: *pCAG-emGFP-miRNAcontrol*, Dr. Adam O'Neill (ISF-N, Helmholtz Center Munich, Munich, Germany; now at Stats NZ, Christchurch, New Zealand); *pCAG-PBase*, Dr. Germán Camargo Ortega (ISF-N, Helmholtz Center Munich, Munich, Germany; now at Dept. Biosystems and Engineering, ETH Zürich, Basel, Switzerland); *pCMV-mPB*, Rebeca Sánchez González (Dept. Molecular, Cellular and Developmental Neurobiology, Cajal Institute, Madrid, Spain); *piggyBac-GFP*, Dr. Miriam Esgleas Izquierdo (ISF-N, Helmholtz Center Munich, Munich, Germany; now at ViGeneron GmbH, Planegg, Germany); *piggyBac-dCas9-GFP*, Dr. Anna Köferle (Epigenetic Engineering, ISF, Helmholtz Center Munich, Munich, Germany; now at Boehringer Ingelheim RCV GmbH & Co KG, Vienna, Austria); *pcDNA-CMV-GFP-CMV-dCas9-VPR*, Dr. Christopher Breunig (see above).

Primers for qRT-PCR were provided by the following contributors: UPR genes (*Atf4*, *BiP*, *Chop*, *Edem*, *Grp94*, *total/us/sXBP1*), Dr. Sonia Najas Sales (ISF-N, Helmholtz Center Munich, Munich, Germany; now at IMIHGOM B.V., Leiden, Netherlands); selected neurogenesis candidates (*Emx1*, *Neurog1*, *Nfia*, *Nr2e1*, *Otx1*, *Pou3f4*, *Sox3*, *Zfp423*), Dr. Stefan Stricker (Epigenetic Engineering, ISF, Helmholtz Center Munich, Munich, Germany); housekeeping gene *Rpl27*, Dr. Germán Camargo Ortega (see above).

Cultures of mNPC were provided by Andrea Neuner (Epigenetic Engineering, ISF, Helmholtz Center Munich, Munich, Germany).